Systems-Based Analysis of a Ship Borne Approach for the Detection of Fissile Material Concealed in Cargo Containers

by

Brett P. Broderick

B.S. Electrical Engineering (2001)
Texas A&M University

Submitted to the Department of Nuclear Engineering
in Partial Fulfillment of the Requirements for the Degree of
Master of Science in Nuclear Engineering

at the

Massachusetts Institute of Technology

September 2004

Signature of Author .....
Department of Nuclear Engineering
August 31, 2004

Certified by .....
Richard C. Lanza
Senior Research Scientist in Nuclear Engineering
Thesis Supervisor

Read by .....
Michael J. Driscoll
Professor Emeritus of Nuclear Engineering
Thesis Reader

Accepted by .....
Jeffery A. Coderre
Chairman, Department Committee on Graduate Students

Systems-Based Analysis of a Ship Borne Approach for the Detection of Fissile Material Concealed in Cargo Containers

By

Brett P. Broderick

Submitted to the Department of Nuclear Engineering On August 31, 2004 in Partial Fulfillment of the Requirements for the Degree of Master of Science in Nuclear Engineering

Abstract

The international maritime container trade, which imports an average of 19,000 largely uninspected cargo containers to United States ports each day, has been identified as a potential avenue of attack for nuclear terrorism. Currently envisioned and deployed defensive measures that seek to detect and interdict concealed fissile material once containers have already reached a U.S. port do not adequately protect against nuclear threats due to the unique power and range of nuclear weapon effects. This thesis describes and examines a novel "ship-based" approach to container-borne fissile material detection where suites of radiation detectors with imaging capabilities are enclosed in standard, non-descript cargo containers and shipped in limited numbers aboard commercial containerships. Outfitted with communication hardware, these dedicated containerized units could provide crucial advance detection and notification of an inbound nuclear threat while the danger is still safely removed from U.S. shores.

Attributes of the container shipping trade that would impact the performance and viability of the proposed ship-based approach were identified and investigated. Average available count times, based on the duration of shipping voyages, for container imports to representative ports on the east and west coasts of the U.S. where found to be 19.2 days and 13.3. days, respectively. These long count times will enhance the ability of the ship-based approach to confidently detect heavily shielded and well-concealed fissile material. A distribution for the average distributed density of commercial cargo, which affects radiation attenuation between the source and detectors, was also derived and found to have a favorably low mean value of 0.198 g/cm^3.

The coverage efficiency (i.e. the number of containerized units required to provide detection coverage over a given percentage of a reference vessel) variations associated with prospective modes of deployment were also investigated using Matlab-based computer simulations. Evaluated deployment strategies ranged from fully random placement of detection units to completely constrained optimal placement. Despite holding important advantages in terms of stealth, random deployment was found to require an average of between 2.2 to 3.3 times more detectors than optimal deployment, depending on the desired level of detection coverage. This result suggests that some combination of random and constrained deployment might yield an optimized balance between stealth and coverage efficiency. This analysis also identified significant efficiency and deployment flexibility benefits associated with units that could detect sources at ranges equal to, or greater than, 70 ft (21.3 m).

Overall, no results were obtained that seriously challenged the potential efficacy and viability of the proposed ship-based approach.

Thesis Supervisor: Richard C. Lanza
Title: Senior Research Scientist in Nuclear Engineering

Acknowledgments

I would first like to thank my research advisor, Dr. Richard Lanza. His patient guidance and continuous stream of ideas were extremely helpful throughout this effort. I would also like to thank Professor Emeritus Michael Driscoll for agreeing to serve as my thesis reader. His insightful comments were invaluable to this thesis.

I owe an enormous debt of gratitude to Shawn Gallagher who first conceived of the topic about which I wrote. Without his selfless collaboration and intellectual ingenuity this thesis literally would not have been possible.

I would also like to thank Dr. Richard Wagner for his valuable feedback and continued support.

The Federal government and the fine people at the U.S. Defense Nuclear Facilities Safety Board provided financial support for this academic enterprise.

Rachel Batista was very helpful in making this thesis sound more like English, in addition to generally making life more pleasant around the office.

Antonio Damato was gracious enough to share his cultural sophistication and his Matlab expertise with an ugly American.

Finally, I'd like to thank Michael Pope for his many contributions and for sharing his proficiency in a number of areas, not the least of which was his extensive knowledge and appreciation of scientific jargon.

Table of Contents

Table of Figures

List of Tables

[This page left blank intentionally.]

Chapter 1: Nuclear Terrorism Threat

1.1 Objectives and Organization of Thesis

The objective of this thesis is to describe and analyze a novel "ship-based" approach, proposed by Gallagher at the Massachusetts Institute of Technology (MIT), for the detection of fissile material concealed in waterborne cargo containers. The need for new thinking will be established by investigating the nature of the threat posed by unconventional nuclear attack and nuclear terrorism and then highlighting the critical shortcomings of currently deployed approaches that seek to address this threat. The attributes and advantages of the ship-based approach will then be examined in the context of the threat and compared to existing detection and interdiction methodologies. Once a case for the promise and utility of the proposed approach has been presented, analysis will be performed to remove or constrain important remaining uncertainties related the to potential efficacy and viability of a ship-based fissile material detection regime.

1.2 Introduction

The specter of nuclear weapons has loomed large over the Earth since their dramatic introduction to the world in 1945. The nature of the threat that these weapons pose to the United States, however, has evolved over time. The end of the Cold War brought with it a relaxation of the conventional nuclear threat stemming from blast hardened silos dotting the land, strategic bombers roaming the skies, and ballistic missile submarines prowling the seas. Yet, the dissolution of the Soviet Union and the ascendance of transnational terrorism has brought with it a new challenge for the nuclear age, that of devising and implementing effective strategies to prevent the acquisition and deployment of nuclear weapons by individuals and organizations who are not restrained by the same means that had deterred nuclear catastrophes for more than half a century. Although the dynamics of the threat have changed, what remains constant is the understanding that the detonation of a single nuclear device on American soil would have

profound and lasting impacts on this country and the world, the scale and breadth of which are difficult to comprehend.

1.3 Threat Dynamics

The September 11th attacks clearly demonstrated that transnational terrorist organizations have supplanted state-based actors as the primary (or at least most immediate) threat to the security of the United States. To strengthen our homeland security posture and develop more effective strategies to defend against attack, including those involving unconventional weapons, we must seek to understand how the emergence of this new adversary alters the nature of threats faced by the United States. The transnational terrorist organizations we must combat today are not only fundamentally different than the state-based adversary faced during the Cold War, they are also markedly different from terrorist organizations that have been encountered in decades past. Some critical differences, at least as they pertain to the threat of nuclear attack, can be generally described in terms of deterability, material access, and motivation.

Nuclear aggression during the Cold War was deterred through the doctrine of mutually assured destruction. This conventional means of deterrence was effective because the primary belligerents were state-based actors having well-defined borders with citizens and national assets to protect. Both the United States and the Soviet Union developed nuclear arsenals massive enough, and deployment platforms and delivery systems diverse enough, that any offensive nuclear strike was sure to be met with a devastating retaliatory counterattack [Knorr, 1985]. Therefore, the motivation to unleash nuclear weapons to destroy the enemy was checked by the understanding that a decisive blow could not be struck without the assurance of a crippling reprisal. However, unlike states, transnational terrorist organizations, in general, are highly mobile, have no delineated territorial borders, and no populace to defend. Without fixed targets to be held in jeopardy of counter-attack, a terrorist organization can hope to deliver a devastating blow without the prospect (or at least the assurance) of immediate annihilation.

Therefore, a transnational terrorist adversary contemplating a nuclear attack remains undeterred by conventional means.

Unlike a large state-based actor, a terrorist organization is unlikely to have open access to a military-industrial infrastructure dedicated to the production of fissile material and the design and assembly of nuclear weapons. Numerous barriers, both physical and political, have been erected by international institutions to inhibit the flow of fissile material from established nuclear states, which are susceptible to conventional means of deterrence, to undeterred terrorist organizations [Bunn et. al, 2003]. As such, even highly motivated, well financed terrorist groups will likely find gaining access to fissile material the most difficult and daunting aspect of initiating a nuclear attack. The difficulty associated with the procurement or acquisition of fissile material, and the resulting scarcity of the commodity, has important implications for how an attack might be planned and executed.

In the past, terrorist organizations used attacks primarily in an attempt to achieve political objectives [NCT, 2000]. With this political motivation, it was thought that terrorist organizations would eschew attacks that claimed large numbers of civilian lives, because such an act would promote public outcry, inspire widespread condemnation of the perpetrators and ultimately weaken support for their cause [Hoffman, 1995]. The transnational terrorist organizations threatening the United States today, however, are increasingly found to have at their core fanatical religious and ideological, rather than purely political, motivations [Laqueur, 1998]. With radical religious ideology serving as the basis, attacks are no longer carried out with the express purpose of meeting political ends. Instead, they are executed to destroy infidels and punish the enemies of God/Allah. As such, religiously inspired terrorist organizations now tend to view attacks that cause mass casualties as desirable rather than taboo [Morgan, 2004]. This motivational shift was summed up succinctly by former CIA director James Woolsey who said, "Today's terrorists don't want a seat at the table, they want to destroy the table and everyone sitting at it." [NCT, 2000]

Another key to understanding the threat posed by unconventional nuclear attack is to appreciate the unique destructive capabilities of nuclear weapons. Although they are often grouped alongside chemical and biological weapons under the generic banner of weapons of mass destruction (WMD), nuclear weapons stand markedly apart even from their other WMD brethren. The totality of destruction that can be wrought, together with the massive spatial and instantaneous temporal scales over which their effects are unleashed, combine to make the gravity of threats posed by nuclear weapons wholly unique. Unlike chemical and biological agents that inflict harm by specifically targeting and damaging human biological functions, nuclear weapons destroy in a much more indiscriminate manner. With their combined thermal, blast, and radiation effects, nuclear weapons inflict their damage on all forms of matter in their vicinity, including people, buildings, and economically vital infrastructure. These effects can be devastating even at distances far removed from the location of the actual detonation. Finally, the primary effects of a nuclear detonation are all experienced more or less instantaneously and simultaneously, and without warning. As such, there is no time for affected populations to evacuate or seek refuge once a nuclear weapon has been actuated.

Given the destructive potential of nuclear weapons, the motivation and stated desire of transnational terrorist organizations to obtain and use these weapons, and the ineffectiveness of conventional means to deter terrorist-mounted nuclear attacks, it is unacceptable to rely solely on existing barriers meant to prevent unauthorized parties from gaining access to fissile material or assembled weapons. Realizing that no individual barrier or safeguard is going to provide perfectly reliable protection, we must develop multiple, redundant and diverse layers of protection that can impede or disrupt all phases of attack from fissile material procurement to final operational deployment. One important step in effectively implementing this type of defense-in-depth protection philosophy is to identify and assess potential avenues of attack that could be used by a terrorist adversary that had somehow managed to obtain fissile material. The vulnerabilities of each potential avenue of attack should then be evaluated so that deficiencies can be identified and remediated.

1.4 Container Scenario Development

One potentially vulnerable avenue of attack flows through US seaports where an average of just over 19,000 cargo containers arrive by ship each day [MARAD(1), 2004], any one of which could be used by an adversary to conceal fissile material or an assembled nuclear device. Only about 4% of these incoming cargo containers currently undergo any type of physical inspection [Lok, 2004]. The vulnerability associated with thousands of opaque, largely uninspected, and loosely controlled cargo containers arriving on U.S. shores everyday is compounded by the proximity of major seaports to large metropolitan population centers. As a result of this collocation, a weapon arriving in a major U.S. port is often already in range to cause massive casualties, regardless of the intended ultimate target of the device. Despite security concerns, seaports and the international container shipping trade are critical to sustaining modern global commerce and to maintaining a healthy U.S. economy. The transaction of international commerce requires an open architecture, where containerized goods can move freely and efficiently between countries and across borders. Therefore a critical and urgent challenge remains to develop and implement protective measures that can enhance the U.S. security posture with respect to seaports and incoming containers of foreign origin, without unduly burdening the free flow of commerce.

As a first step in meeting the challenge of successfully addressing port and cargo container related vulnerabilities, a conservative threat scenario will be developed based on carefully chosen and logically defended assumptions. Scenario development will frame the problem, allowing helpful insights to be drawn. The resulting product will then provide a means to evaluate the efficacy and highlight weaknesses of potential solutions.

The overarching assumption used in scenario development is that a rational, determined adversary would always seek to maximize the probability of a successful attack. (Despite fanatical religious ideologies, transnational terrorist organizations have repeatedly proven themselves rational in the context of operational planning, coordination and execution.) As discussed later, in detail, the following propositions are

some logical implications of the "rational enemy assumption" as applied to a transnational terrorist adversary: 1) if an enemy somehow procures fissile material, they will seek to weaponize it (if not already in the form of a functional nuclear weapon) and use it; 2) an enemy will seek to weaponize unassembled fissile material prior to container shipment to the U.S.; and 3) an enemy may provide some means (e.g. booby-trapping or remote detonation capability) to thwart the successful interdiction and neutralization of a deployed (i.e. shipped) weapon.

The assertion that a transnational terrorist organization, having obtained fissile material, will weaponize it and attempt to use it is perhaps the most easily justified of the preceding discussion. A number of leading figures in transnational terrorist organizations (including al Qaeda) have openly professed their desire to obtain nuclear weapons and there have been several well-documented attempts to purchase fissile material [Lee, 2003]. Additionally, these groups have demonstrated the motivation and ability to carry out well planned, large-scale attacks that result in mass civilian casualties. Finally, as noted previously, highly mobile, borderless terrorist organizations are not stymied by conventional means of deterrence based on the threat of massive retaliation. Given the vigor with which fissile material procurement has been pursued, the repeatedly demonstrated willingness to employ ever more lethal tactics to carry out high-casualty attacks, and the undeterred nature of the adversary, it is reasonable, and certainly conservative, to posit that if a sufficient quantity of fissile material is obtained, a terrorist organization would seek to assemble it into a weapon and use it for an attack.

The belief that an enemy would seek to ship a functional weapon to the U.S., as opposed to unassembled fissile material, follows from the rational enemy assumption for the following two reasons. First, to maximize the probability of a successful attack, an adversary that had obtained unassembled fissile material would clearly want to avoid disruption or detection during the device assembly process. Unfettered weapon assembly and preparation would presumably be far easier to achieve abroad, in a location of the terrorists' choosing, where they could enjoy a substantially stronger and more secure support network, in addition to a less menacing intelligence gathering and law

enforcement presence than would be encountered in the United States. Second, a rational adversary would seek to ship a functioning weapon rather than attempt to smuggle unassembled fissile material into the U.S. to create the possibility that some degree of operational success (i.e. a nuclear detonation causing significant casualties and physical damage) could still be achieved even in the event that the device was somehow detected or discovered prior to reaching its intended target. There is no such possibility of limited success if the fissile material has not been weaponized prior to shipment.

The assertion that an adversary would seek to implement countermeasures such as "booby traps" or remote detonation provisions to guard against interdiction and disarmament prior to detonation can also be defended using the rational enemy assumption. "Booby-traps" are defined here as a feature or features intended to trigger detonation of the device if certain perturbations, such as mechanical or radiation probing, are experienced. A remote detonation capability would give an adversary the opportunity to detonate a detected weapon before it could be isolated and rendered safe. Despite the technological difficulty of implementing such features, the presence of countermeasures to guard against interdiction cannot be ruled out since the rational-enemy assumption dictates that an adversary would aggressively seek to ensure detonation once the weapon was deployed. The desire to ensure detonation, using any available means, would only be amplified by the extremely limited availability of fissile material and the extraordinary efforts that were likely required to obtain it. Even if the device did not reach its intended target, a nuclear explosion impacting any Western port or territory would presumably be a marginally successful outcome for a terrorist organization.

Finally, to accept the rational enemy assumption but to reject the possibility of countermeasures being present requires the assumption that an enemy is not capable, for whatever reason, of implementing them. However, the fact that we concern ourselves with screening cargo containers for fissile material in the first place implies that we are willing to accept that an enemy possesses a level of sophistication high enough to procure, transport, (possibly) assemble and deploy a nuclear weapon, all without being detected or exposed by any military, law enforcement or intelligence gathering

organization. It seems, therefore, wholly irrational to then assume that the same enemy is not sophisticated enough to devise and implement effective countermeasures.

Consistent with the assumptions discussed in the previous paragraphs, we now postulate a scenario in which a functional nuclear weapon is concealed in a standard, full sized (40' long, 8' wide and 8.5' high) cargo container and deployed from a foreign location aboard a transoceanic container vessel that is due to call on a major United States seaport that is in or adjacent to a large urban population center (e.g. New York City or Los Angeles). We conservatively assume that the weapon is surrounded with some level of shielding appropriate for the fissile material used in the weapon (i.e. high atomic number material for uranium or both low and high atomic number material for plutonium). We further assume that the device has been outfitted with counter-interdiction features, including a remote detonation capability and booby-traps that trigger the weapon in the event that certain mechanical or radiation insults are experienced.

We consider the above scenario (referred to hereafter as "the container scenario") to be conservative and bounding. As such, it is assumed that an approach that can defeat this extremely challenging scenario can similarly defeat any number of less conservative, less challenging scenarios. We further believe that the highly conservative nature of the container scenario is appropriate considering the extraordinarily dire consequences of a successful nuclear attack on U.S. soil and the fact that none of the (admittedly) improbable elements of the scenario can be confidently excluded as incredible.

Using the postulated container scenario we can now make a number of useful observations regarding the capabilities that will be required to successfully address the specific vulnerabilities associated with the commercial maritime container trade as an avenue for nuclear attack. First, it is clear that the only way to ensure adequate protection from this threat is to keep the weapon (or the container concealing the weapon) from ever reaching U.S. shores. To do this, not only must the weapon be detected prior to the threat-bearing vessel reaching a U.S. port of call, but the presence of this threat must also

be communicated to appropriate parties in time for an effective response to be mobilized prior to port entry. Additionally, the initial threat detection must be made in a manner that accounts for the possibility that countermeasures may be present, which could function the weapon if intrusive perturbations are experienced.

The ultimate success criterion for any defensive measure (or measures) in defeating the container scenario or any other postulated nuclear attack is not the detection of the device; it is the ability to prevent a nuclear detonation that physically impacts the United States. Detecting the weapon is a necessary but not sufficient step toward defeating this threat. Stated differently, the deployment of a defensive measure that detects incoming fissile material with perfect effectiveness and reliability (even if this were possible) fails to adequately protect against the threat of nuclear attack if the weapon isn't detected until it is already in range to impact the United States (e.g. in a U.S. port).

Chapter 2: Fissile Material Detection

2.1 Fissile Material Characteristics

It is clear both intuitively and from the earlier discussion of the container scenario that no nuclear attack will be thwarted if the concealed weapon is never detected. As such, it is useful to investigate the common properties of fissile material and the various ways in which these properties can be exploited to remotely detect the presence of this material without the luxury of having physical access to the inside of each cargo container.

In the current context, a nuclide is defined as fissile if it can undergo neutron-induced fission with the absorption of a neutron of any energy. The ability to fission readily when interacting with neutrons of any energy regime makes fissile isotopes critically important in producing and sustaining the fission chain reactions that give nuclear weapons their explosive power. For the purposes of this analysis, fissile materials will be generally defined as materials containing fissile isotopes in sufficient quantities to make them suitable for use in nuclear weapons. Although nuclear weapons can theoretically be constructed using more exotic materials, such as neptunium or americium [Albright et. al, 1999], the following discussion will focus on materials that contain the fissile isotopes ^{239}Pu, ^{235}U, and ^{233}U.

Natural uranium has an isotopic composition of 99.28% (by weight) ^{238}U, 0.72% ^{235}U, and 0.0055% ^{234}U. Uranium is considered enriched if the abundance of the fissile ^{235}U constituent is artificially increased above its naturally occurring level. Uranium that is greater than 20% ^{235}U is classified as highly enriched. The 20% cutoff corresponds to the minimum enrichment, as identified by the International Atomic Energy Agency (IAEA), required for materials that can be used in nuclear weapons [IAEA, 2001]. Unlike the fissile ^{235}U isotope, ^{238}U can only be made to fission with neutrons exceeding a threshold energy of approximately 1 MeV [Krane, 1988]. This threshold makes

uranium with a high ^{238}U content unsuitable for creating and sustaining chain reactions because not all neutrons produced during a given generation of fissions will exceed the ^{238}U energy threshold and be available to create subsequent fission events. The population of neutrons energetic enough to fission ^{238}U would be further decreased as neutrons undergo inelastic scattering events that transfer some of their energy to the nuclei with which they interact. As a result, the highly enriched uranium (HEU) used in nuclear weapons typically has an enrichment of greater than 90% ^{235}U [Bunn et. al, 1997].

Plutonium, unlike uranium, is not a naturally occurring element and must be produced artificially. Fissile ^{239}Pu is typically bred in a nuclear reactor through the following transmutation chain and then chemically separated.

$$^{238}U \xrightarrow{(n,\gamma)} {}^{239}U \xrightarrow[23.5m]{\beta^-} {}^{239}Np \xrightarrow[56.5h]{\beta^-} {}^{239}Pu$$

Weapons grade plutonium is rich in the fissile ^{239}Pu isotope (again above 90%) and is defined as containing less than 7% of the ^{240}Pu isotope [DOE, 1994], which is considered a contaminant by weapons designers. Reactor grade plutonium also contains ^{239}Pu, but is defined as containing greater than 7% ^{240}Pu[1]. Each type of plutonium also contains varying amounts of other plutonium isotopes including ^{238}Pu, ^{241}Pu, and ^{242}Pu. Although weapons grade plutonium (as the name implies) is vastly preferable for use in fabricating a nuclear weapon, reactor grade plutonium can also be used to produce an explosive that delivers a nuclear yield[2] [Mark et. al, 1987]. For this reason, and because a terrorist organization is unlikely to be picky if an opportunity to obtain this material avails itself, reactor grade plutonium has been included in the discussion, despite the added weapon design and assembly difficulties associated with its use.

[1] Plutonium containing between 7 and 18% ^{240}Pu is sometimes referred to as fuel grade.
[2] In 1977 the United States declassified the existence of an underground test conducted in 1962 where a nuclear device fabricated with reactor grade plutonium was successfully detonated.

^{233}U is not a constituent of naturally occurring uranium and, like plutonium, must be produced artificially. This fissile nuclide is bred from thorium in nuclear reactors through the following transmutation chain.

$$^{232}Th \xrightarrow{(n,\gamma)} {}^{233}Th \xrightarrow[22.3\,m]{\beta^-} {}^{233}Pa \xrightarrow[27.0\,d]{\beta^-} {}^{233}U$$

Uranium bred and chemically separated from thorium blankets is contaminated with varying amounts of ^{232}U. ^{233}U is not nearly as popular as ^{235}U and ^{239}Pu for use in nuclear weapons (no country is publicly known to have produced weapons using ^{233}U [NTI, 2003]) because of radiation dose concerns arising from the ^{232}U contaminant. However, this material is very capable of producing a nuclear explosion, evidenced by a bare sphere critical mass[3] smaller than that of ^{235}U [NERAC, 2000]. Currently, the worldwide availability of ^{233}U is rather small compared to other fissile materials that are likely being coveted by terrorist organizations. However, a number of countries, most notably India (already a nuclear weapon state), are considering the use of a ^{233}U-producing thorium fuel cycle for nuclear power generation [Gopalakrishnan, 2002].

Despite their many physical, chemical, and metallurgical differences, fissile materials have a number of common traits that can be used as a basis for detection. One characteristic that is obviously shared by all fissile materials is that they can be made to fission. When fissile materials are bombarded with neutrons of any energy or gamma rays above a threshold energy[4], fission (or so-called photo-fission in the case of gamma bombardment) will occur and neutrons and prompt gamma rays will be released immediately as a result of the fission event, followed by delayed gamma rays (and occasionally delayed neutrons) emitted by subsequent decay and de-excitation of the fission products. Unlike the heavy ionized fragments created during fission and the beta particles that are typically emitted as these fission products decay toward stability, neutrons and gammas are uncharged. Due to their lack of electronic charge, these particles do not undergo Coulomb interactions with the atomic electrons of the matter

[3] The bare sphere critical masses of ^{233}U and ^{235}U are 16.4 kg and 47.9 kg, respectively.
[4] For ^{235}U and ^{239}Pu, the photo-fission threshold energy is about 5.3 MeV [Fetter(1), 1990]

through which they pass so they can travel a relatively long distance before and between interactions. The long-range nature (relative to other forms of nuclear radiation) of neutrons and gammas makes them particularly well suited to the task of detecting fissile material at a distance using conventional equipment and well-understood methods.

Another useful characteristic shared by all fissile materials is that they have high densities, and are able to readily absorb gamma rays and neutrons. Densities of some common weapons-grade fissile materials are shown in Table 2-1 [Mark et. al, 1987].

Table 2-1: Densities of common weapons-grade fissile materials

HEU	Weapons Grade Pu	
(94% U-235)	alpha phase	delta phase
18.7 g/cm^3	19.86 g/cm^3	15.6 g/cm^3

One way to quantify how effectively a material can absorb a particular type of radiation is to define the mean free path of that radiation in the material. The mean free path is the average distance traveled between interactions. Since each interaction creates the opportunity for scattering or absorption, a short mean free path, or equivalently, more average interactions per unit length, indicates that the material is effective in absorbing or shielding that particular radiation. Table 2-1 below shows the mean free path ratios between HEU and a number of other materials for neutrons and gamma rays of several different energy regimes [Fetter(1), 1990].

Table 2-2: Ratios of MFPs in selected materials to HEU

	Energy	Ratio of MFP in element to that in HEU				
	MeV	C	Al	Fe	W	Pb
	0.4	22	19	6.7	1.4	2.0
Gamma Rays	10	23	16	4.3	1.1	1.8
	100	56	27	5.5	1.1	1.7
	thermal	50	240	24	40	70
Neutrons	0.001	3.0	16	2.2	1.6	4.1
	10	2.2	2.4	1.5	0.94	1.5

Ratios in Table 2-1 greater than unity indicate a larger mean free path in the reference material than in HEU. Plutonium with its similar density, atomic number, and ability to

fission (even with thermal neutrons) would produce comparably small mean free paths for gamma rays and neutrons at energies tabulated above.

Fissile materials are also radioactive. However, since each type of fissile material has a distinct isotopic composition, which in turn gives rise to distinct populations of decay progeny, each of the materials produce intrinsic radiation signatures that can differ in terms of character and intensity. The characteristic emission signatures for each type of fissile material will now be identified and discussed separately in the context of how they can be used to facilitate remote detection.

2.1.1 HEU Radiation Signature

The isotopic composition of a radioactive material determines both the nature and energy of the radiation emitted. Therefore to begin discussing the radiation signature of HEU, the general composition of this material must first be revisited in greater detail. The primary constituents of HEU are the naturally occurring ^{238}U, ^{235}U, and ^{234}U isotopes. To produce weapons-usable material, some means of enrichment (e.g. gaseous diffusion or centrifuge enrichment) must be employed to artificially raise the relative abundance of the fissile ^{235}U isotope to well above its natural level of 0.72%. Because most means of enrichment exploit the fractional mass differences between isotopes, the trace amount of ^{234}U found in natural uranium is also preferentially enriched along with ^{235}U due to its comparatively low atomic mass. If none of the material used as input, or feedstock, to the enrichment process had ever been irradiated in a nuclear reactor, than the naturally occurring nuclides listed above would be the only uranium isotopes present in the resulting HEU. However, if even a minute fraction of the enrichment feedstock had been irradiated (and subsequently reprocessed), the HEU output would likely be contaminated with small amounts of the non-naturally occurring ^{232}U, ^{236}U, and ^{237}U isotopes [Peurrung, 1998].

As the ^{235}U, ^{238}U, and ^{234}U isotopes (as well as the ^{232}U, ^{236}U, and ^{237}U contaminants that may be present) begin down their long decay chains toward stable

nuclides, alpha and beta particles are emitted as individual nuclei decay. While these short-range, charged particles are generally unhelpful for remote detection, the long-range characteristic photons that often accompany these decays can be usefully exploited. The gamma rays emitted as the excited daughter nuclei created during alpha or beta decay transition to lower excited states or their ground states, give rise to a rich and complex spectrum of photons that can penetrate surrounding material and be detected at a physically removed location. Since gamma ray energies are determined by the characteristics of the emitting nucleus, peaks in the measured spectrum can be used to unambiguously identify the presence of specific isotopes. The HEU spectrum, as measured using a high resolution, high purity germanium (HPGe) detector, is shown in Figure 2-1 [Gosnell, 2000].

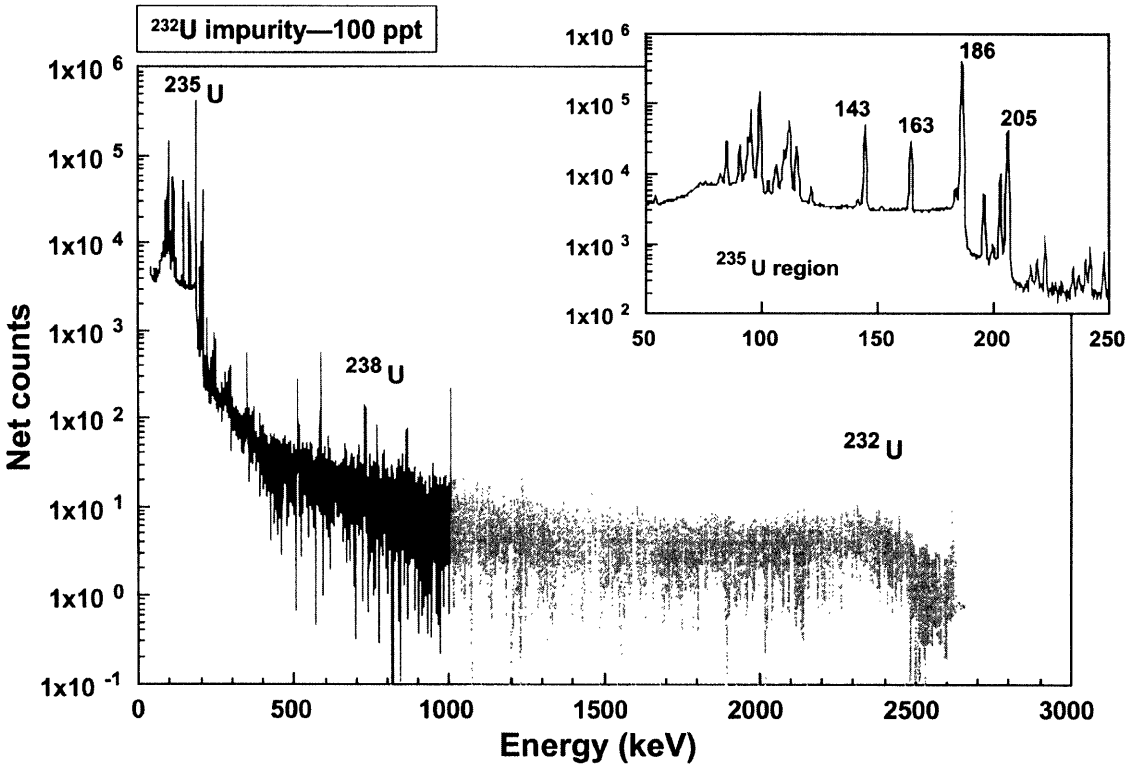

Figure 2-1: High resolution HEU spectrum

As indicated by the magnified region of Figure 2-1, the characteristic gamma lines emitted by ^{235}U are concentrated at the low energy end of the spectrum. The most intense of the 59 discrete lines emitted by ^{235}U is at 186 keV and the most energetic line emitted with a reasonably high intensity is at 205 keV. Unfortunately, these photons are

not highly penetrating because most types of matter have large linear attenuation coefficients in this energy regime, with a particularly large contribution from the photon-absorbing photoelectric process. Figure 2-2 shows the dominant regions for various types of photon interactions as functions of the atomic number of the transmission medium [Evans, 1955].

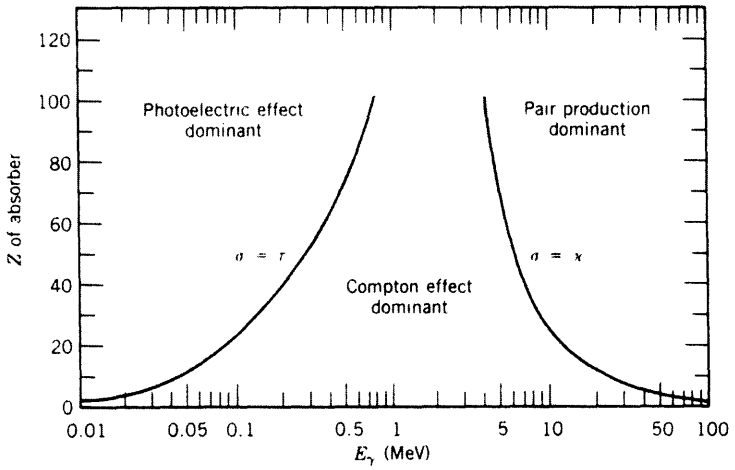

Figure 2-2: Dominant regions for different photon interactions

As a result of the high probability of photoelectric interaction, which results in the loss of the photon in the process, dense matter shields low energy gamma lines emitted by ^{235}U very efficiently. In uranium the mean free path of 200 keV gamma rays is 0.5 mm, so a significant fraction of these low energy photons are subject to self-absorption within the HEU from with they originate [Fetter(2), 1990].

The most notable contribution to the HEU spectrum stemming from residual ^{238}U is the 1001 keV line arising from the isomeric transition of ^{234m}Pa that is created through the following series of decays.

$$^{238}U \xrightarrow[4.5Gy]{\alpha} {}^{234}Th \xrightarrow[24.1d]{\beta^-} {}^{234m}Pa$$

Although this line is highly penetrating and emitted with reasonably high intensity, the use of gamma rays that arise from ^{238}U (or its daughters) for fissile material detection

purposes is inherently problematic. This is due in part to the fact that the presence of ^{238}U doesn't necessarily indicate the presence of HEU. Additionally, the ubiquitous nature of the ^{238}U isotope, particularly in terrestrial settings, produces a significant amount of nuisance background that can confound detection efforts.

Because gamma lines emitted by ^{235}U are intense but not highly penetrating and lines emitted by ^{238}U (and its daughters) are less than ideal for fissile material detection, gamma emissions stemming from the decay of ^{232}U and its daughter products can prove extremely useful for remote detection applications. ^{232}U is produced primarily through the following reactions in a nuclear reactor [Peurrung, 1998].

(1) $$^{235}U \xrightarrow[704\,My]{\alpha} {}^{231}Th \xrightarrow[25.5\,h]{\beta^-} {}^{231}Pa \xrightarrow{(n,\gamma)} {}^{232}Pa \xrightarrow[31.4\,h]{\beta^-} {}^{232}U$$

(2) $$^{234}U \xrightarrow[246\,ky]{\alpha} {}^{230}Th \xrightarrow{(n,\gamma)} {}^{231}Th \xrightarrow[25.5\,h]{\beta^-} {}^{231}Pa \xrightarrow{(n,\gamma)} {}^{232}Pa \xrightarrow[31.4\,h]{\beta^-} {}^{232}U$$

(3) $$^{235}U \xrightarrow{(n,\gamma)} {}^{236}U \xrightarrow{(n,\gamma)} {}^{237}U \xrightarrow[6.8\,d]{\beta^-} {}^{237}Np \xrightarrow{(n,2n)} {}^{236m}Np \xrightarrow[22.5\,h]{\beta^-} {}^{236}Pu \xrightarrow[2.9\,y]{\alpha} {}^{232}U$$

(4) $$^{238}U \xrightarrow{(n,2n)} {}^{237}U \xrightarrow[6.8\,d]{\beta^-} {}^{237}Np \xrightarrow{(n,2n)} {}^{236m}Np \xrightarrow[22.5\,h]{\beta^-} {}^{236}Pu \xrightarrow[2.9\,y]{\alpha} {}^{232}U$$

The reactions shown above (particularly the first two listed) are the most significant pathways by which ^{232}U is produced in a reactor, provided that actinide impurities arising from previous irradiations have been removed from the initial fuel prior to loading [Perrung, 1998]. If present in HEU, ^{232}U will decay through a long chain of successive alpha and beta decays through the so-called thorium series depicted below in Figure 2-3 [Krane, 1988].

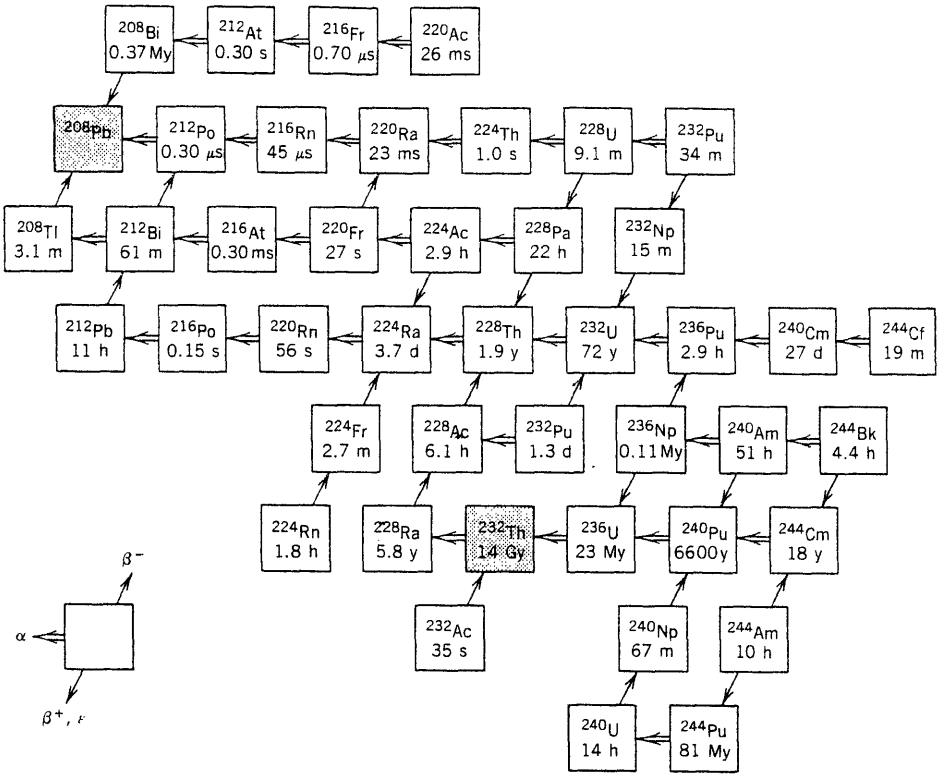

Figure 2-3: Thorium series

The thorium series is shown in detail because several of the distant daughter products of ^{232}U emit high energy, highly penetrating gamma lines that can significantly enhance the distance at which HEU can be remotely detected. Of the daughter products found in the thorium series, the one with the most utility for detection is ^{208}Tl. The beta decay of ^{208}Tl to stable ^{208}Pb is accompanied by one or more high-energy photons emitted as the daughter nucleus de-excites. Table 2-2 shows the energies of the most intense gamma ray lines produced by ^{208}Tl decay, as well as the branching ratios of these lines [Fetter(3), 1990].

Table 2-3: ^{208}Tl gamma lines and branching ratios

Gamma Energy (keV)	Branching Ratio (% per decay)
583.0	86.0
860.3	12.0
1620.7	1.51
2614.4	99.79

Because of their significant branching ratios and highly penetrating nature, the 583 and 2615 keV ^{208}Tl gamma lines can be particularly useful in detecting HEU that is contaminated with the ^{232}U parent nuclide, even if ^{232}U is found in concentrations less than 1 ppb [Fetter(1), 1990]. The prominence of these two peaks in the HEU spectrum can be seen in Figure 2-1. The 2615 keV photon is especially noteworthy because photon interaction cross-sections at this energy are generally quite low, which allows this gamma line to be powerfully penetrating and quite long range. Also, as shown in Figure 2-2 the Compton scattering process dominates the overall interaction cross-section at 2615 keV, so even when an interaction does take place, the photon will most likely be scattered (albeit losing some energy in the process) instead of absorbed. Additionally, in general, the background rate in this high-energy region of the spectrum is fairly low, so a source that emits gammas in this regime can usually be detected more easily than a low energy gamma emitter. Unfortunately, as the thorium series in Figure 2-3 demonstrates, ^{232}U is not the only potential source of ^{208}Tl and its 2615 keV decay photon. ^{232}Th, an isotope that represents greater than 99% of naturally occurring thorium and is 3 times more abundant in the earth's crust than natural uranium [WNA, 2003], also decays down to ^{208}Tl and can produce a very strong background signal, which inhibits confident detection of HEU.

Like many other extremely heavy isotopes, ^{238}U and ^{234}U can undergo spontaneous fission. In general, spontaneous fission is more likely in nuclides with even numbers of protons and neutrons and becomes increasingly important as atomic number increases. However, it does not seriously compete with alpha emission as the dominant decay process until atomic mass increases above about 250 [Krane, 1988]. As a result, ^{238}U and ^{234}U both have partial half-lives for spontaneous fission that are significantly longer than their total half-lives. (Partial half-lives are defined as the time necessary for half of the nuclei in a given sample to decay if only a single specified decay process were allowed to occur.) ^{238}U has a partial half life for spontaneous fission of 8.20×10^{15} yr versus a total half life of 4.468×10^{9} yr and ^{234}U has a spontaneous fission half life of 2.04×10^{16} yr versus a total half life of 2.455×10^{5} yr [Fetter(4), 1990].

Several other processes contribute to neutron generation in HEU. One is the production of neutrons through (α,n) reactions that can occur when light element impurities (e.g. carbon and oxygen) in the material interact with alpha particles emitted by the uranium nuclides and their daughter products [Fetter(2), 1990]. The other process influencing the neutron population in HEU is the multiplication that occurs when an existing neutron induces fission in the fissile material thereby releasing additional neutrons. The degree of multiplication is strongly dependant on the geometry of the material.

Despite the effects of multiplication and the neutron production that could occur due to (α,n) reactions in light element contaminated material, spontaneous fission events in ^{238}U and ^{234}U occur infrequently enough that the intrinsic neutron signature of HEU is very small and essentially undetectable for the remote detection application of interest.

2.1.2 Plutonium Radiation Signature

Both weapons grade and reactor grade plutonium contain essentially the same plutonium isotopes (^{238}Pu, ^{239}Pu, ^{240}Pu, ^{241}Pu and ^{242}Pu) but in different concentrations. Weapons grade plutonium is typically composed of greater than 93% ^{239}Pu, around 6% ^{240}Pu, and small quantities (less than 1%) of ^{238}Pu, ^{241}Pu, and ^{242}Pu [Fetter(1), 1990]. Reactor grade plutonium, a material that does not have uniquely specified isotopics, has been produced and separated from higher burnup fuel than weapons grade plutonium, giving it a lower concentration of ^{239}Pu and higher relative concentrations of the ^{238}Pu, ^{240}Pu, ^{241}Pu, and ^{242}Pu isotopes [Mark, 1990].

All of the plutonium isotopes identified above are radioactive, and just as in the case with HEU, the alpha and beta decays undergone by these isotopes and their daughter products are accompanied by the emission of one or more characteristic photons. The most prominent gamma lines in the plutonium spectrum arise from the decay of ^{239}Pu, and the decay of the ^{241}Pu isotope's daughter product. ^{239}Pu is an alpha emitter with a half-life of 2.411×10^5 yr. The two most intense gamma lines arising from the ^{239}Pu alpha

decay are at 375 and 414 keV with branching ratios (% per decay) of 0.00158 and 0.00151 respectively [Fetter(3), 1990]. The most energetic line emitted by ^{239}Pu with a useful intensity is at 769 keV, and has a branching ratio of 0.000011. ^{241}Pu has a half-life of 14.35 yr and beta decays to ^{241}Am 99.9976% of the time [Oetting, 1968]. The ^{241}Am daughter then alpha decays with a 432.2 yr half-life emitting gammas at 662, 721.96 and 722.70 keV with respective branching ratios of 0.00036, 0.00006 and 0.00013 [Fetter(3), 1990]. The peak energies of the later two photons are exceedingly difficult to resolve, using even high-quality semiconductor detectors, because the peak energies are so close together. As such, the counts from these two photons can be aggregated into one peak centered at approximately 722.5 keV, with a combined branching ratio of 0.00019. Table 2-4 shows the decay rates of the gamma emissions discussed above[5] [Fetter(3), 1990].

Table 2-4: Decay rates for selected gamma emissions from plutonium and its daughters

Parent Isotope	Gamma Energy (keV)	Decay Rate (g x s)^-1
Pu-239	375	36300
Pu-239	414	34600
Pu-239	769	252
Pu-241	662	174000
Pu-241	722.5	92000

In the case of weapons grade plutonium, the ^{239}Pu and ^{241}Am gamma lines identified above can be fairly helpful for remote detection due to their reasonable intensity and good penetrating power in most materials. Since reactor grade plutonium has a significantly higher concentration of both ^{241}Pu and ^{241}Am, the highly penetrating 662 and (averaged) 722.5 keV can become quite intense. Consequently these gamma lines can be extremely helpful in remotely detecting reactor grade material.

It should also be noted that because ^{239}Pu and ^{241}Am are not naturally occurring isotopes, the detection of plutonium using the gamma lines discussed above does not suffer from the same problems associated with natural background that can complicate HEU detection. However, ^{241}Am is used in commercial products such as smoke detectors

[5] Decay rates in Table 2-4 assume 10-year-old plutonium (i.e. 10 years of decay time starting with 1 g of the pure parent nuclides).

and the popular radiation source ^{137}Cs, emits a gamma ray at 661 keV, which is essentially indistinguishable from the 662 keV line emitted by ^{241}Am. Although the spectral peak overlap with ^{137}Cs could frustrate unambiguous identification of ^{241}Am, the unexpected detection of this line emanating from a cargo container would still presumably be of intense interest due to the potential use of ^{137}Cs (particularly in its powdery chloride form [Stone, 2002]) in a radiological dispersion device.

A potentially more important aspect of plutonium's intrinsic radiation signature, in terms of remote detection, is neutron emission. Plutonium has a high rate of internal neutron generation due largely to the spontaneous fissioning of its nuclei. All of the plutonium nuclides present in weapons grade and reactor grade materials undergo spontaneous fission more readily (i.e. they have shorter spontaneous fission partial half lives) than ^{238}U [Fetter(4), 1990]. The ^{238}Pu, ^{240}Pu, and ^{242}Pu nuclides, with their even number of protons and neutrons, are particularly active contributors to the neutron population with relatively short spontaneous fission partial half lives of 4.77×10^{10}, 1.31×10^{11}, and 6.84×10^{10} years respectively [Fetter(4), 1990].

As is the case with HEU, alpha particles interacting with light element impurities can cause (α,n) reactions, giving rise to another potentially important neutron production mechanism. However, reactions of the (α,n) variety are more significant in plutonium than HEU because the dramatically higher alpha activity in plutonium creates more opportunity for these reactions to occur. Likewise, neutron multiplication can also play a more significant role in plutonium because more spontaneous fission and (α,n) neutrons are present to begin the multiplication process by inducing fission.

There is also some evidence to suggest that a significantly enhanced high-energy (above 1.6 MeV) gamma flux can be observed in the vicinity of plutonium-based nuclear weapons [Baryshevsky et. al, 1994]. These energetic photons would most likely be the result of radiative capture reactions occurring as materials in the surrounding chemical high explosive absorb neutrons emitted by the plutonium. Due to the low natural

background flux in this energy regime, these highly penetrating gamma rays could prove quite useful for remote detection.

2.1.3 ^{233}U Radiation Signature

The isotopic composition of uranium that is chemically separated from thorium targets irradiated in a reactor varies depending on the reactor type and burnup. Although the relative concentrations may vary, all uranium produced from thorium irradiation will be contaminated with ^{232}U produced primarily through the following reaction chains.

$$^{232}Th \xrightarrow{(n,2n)} {}^{231}Th \xrightarrow[25.5h]{\beta^-} {}^{231}Pa \xrightarrow{(n,\gamma)} {}^{232}Pa \xrightarrow[31.4h]{\beta^-} {}^{232}U$$

$$^{232}Th \xrightarrow{(n,\gamma)} {}^{233}Th \xrightarrow[22.3m]{\beta^-} {}^{233}Pa \xrightarrow[27.0d]{\beta^-} {}^{233}U \xrightarrow{(n,2n)} {}^{232}U$$

The limiting reactions for both ^{232}U production mechanisms are the (n,2n) reactions that have threshold neutron energies of around 6 MeV. As a result, uranium bred in reactors with relatively large neutron populations in the high-energy (i.e. > 6 MeV) portion of the spectrum will typically be contaminated with higher levels of ^{232}U. ^{232}U contamination also increases with burnup [Kang, 2001].

As noted above for HEU, ^{232}U, with its 69.8 yr half-life and its ^{208}Tl progeny can be very helpful for remote detection even at ^{232}U contamination levels on the order of 100 ppt. In contrast to the minute concentrations of ^{232}U that can be found in contaminated HEU, ^{233}U is considered to be "clean" if it has levels of ^{232}U contamination less than 1 ppm. [Kang, 2001]. The intense radiation field given off by the ^{232}U decay chain is the root of radiation protection concerns that have kept ^{233}U from being pursued by states as the basis for nuclear weapons production. This intense, high-energy radiation will also help to facilitate fairly straightforward remote detection of concealed ^{233}U.

2.2 Detection Techniques

Detection techniques that seek to exploit the common properties of fissile material discussed in the previous section can be generally categorized as either active or passive. Active methods involve the application of external radiation sources to induce fission events in fissile material that may be present or to take photon transmission measurements that can indicate the presence and location of dense materials. Passive techniques do not probe with radiation, but instead measure the intrinsic radiation emitted by the fissile material to achieve detection. Methods using both active and passive techniques will now be discussed in additional detail and their applicability to the postulated container scenario will be assessed.

2.2.1 Active Detection

There are a number of disparate detection methods that fall under the category of active techniques. The commonality between these methods is that they all employ some dedicated photon or neutron source to bombard an object or material with intense radiation to measure its response. In some cases the response of interest is the induced radiation emitted by the object or material being interrogated and in other cases the measured response is the amount of radiation that is effectively transmitted through (or absorbed in) the test object. Methods concerned with stimulating radiation in fissile material using external radiation sources will be referred to here as induced fission techniques and methods that measure radiation transmission will be referred to as radiography.

2.2.1.1 Induced Fission

As discussed earlier, fissile materials can be made to fission with neutrons of any energy and by gamma rays above certain nuclide-specific threshold energies. Fission events are accompanied by the emission of about 7 prompt gamma rays and anywhere between 2 to 5 prompt neutrons depending on the isotope undergoing fission and the type

and energy of the particle that induced the event [Fetter(4), 1990]. Induced fission techniques interrogate an object with intense beams of radiation and detect evidence of induced fission in the form of prompt neutrons and/or gammas.

Induced fission techniques have a number of attractive attributes. The intense probing radiation can penetrate significant amounts of intervening material such that even well-shielded fissile material can normally be detected. Additionally, by artificially inducing a strong signal that is unique to the class of materials that are being screened for, induced fission techniques require a much smaller detection time than other methods, particularly those that are passive in nature. Disadvantages associated with this method include radiation protection concerns for workers and bystanders stemming from the use of intense and energetic radiation sources. An additional concern for methods that would employ neutrons as probing radiation arises from the possible activation of benign materials in the test object.

In terms of suitability to the container scenario, induced fission techniques are not a particularly desirable option. Although the ability to detect fissile material despite shielding is an important virtue of this method, the insult to the device arising from the bombardment of probing radiation is a critical drawback. A booby-trap provision, such as the one postulated by the container scenario, could be triggered by intense radiation resulting in detonation of the weapon.

2.2.1.2 Radiography

As photons pass through material they can interact with surrounding matter through a number of different processes. The most notable of these photon interactions are photoelectric absorption, Compton scattering, and (if the photon has an energy greater than 1.022 MeV) pair production. Examples of photon interaction cross-sections for aluminum and lead, illustrating the energy dependence of the three primary interaction processes, are shown in Figure 2-4 [Krane, 1988].

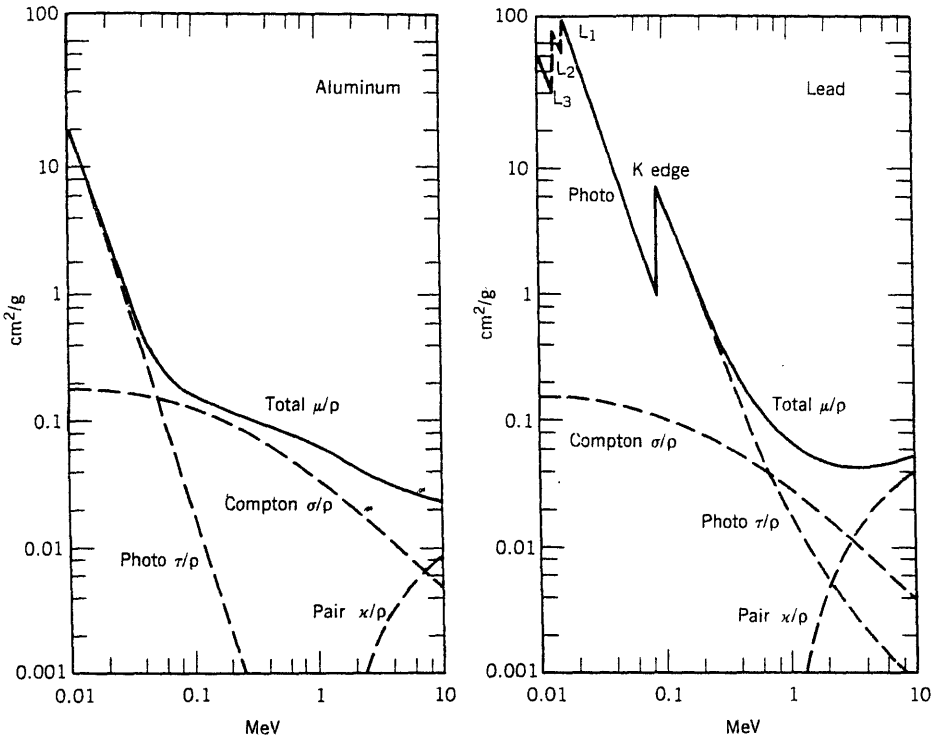

Figure 2-4: Photon interaction cross-sections for aluminum and lead

The denser the material being traversed by a photon, the more matter is available to cause these interactions per unit length traveled. As such, a test object with unknown contents can be exposed to a beam of photons with a known intensity and transmission measurements can be carried out to detect the presence of particularly dense material, which could indicate the presence of either fissile material or shielding. Sophisticated radiographic techniques can image the contents of an unknown test object using the contrast provided by the varying linear attenuation coefficients of different materials. These contrast images can be used to indicate both the presence and geometry of suspicious dense material.

An advantage of radiography is that it can provide visual insights into the contents of sealed, opaque containers without requiring them to be physically opened. The sensitivity to very dense materials could also easily detect the presence of engineered shielding. However, high densities are not unique to fissile materials or shielding that is being used to conceal a nuclear weapon. As such, this method (and other more exotic

radiographic methods including those using muons) could be prone to high false alarm rates that could create a potentially costly commercial choke point. Additionally, the bombardment of high-energy photons can damage some radiation-sensitive types of commercial cargo, such as photographic film.

Evaluated in terms of the container scenario, radiography warrants an assessment similar to that of induced fission techniques. The ability to readily detect the presence of material that could be used as shielding is desirable (although unlike induced fission methods, radiography cannot unambiguously detect the presence of fissile material behind potential shielding). However, the overall desirability of this technique, at least with respect to the postulated container scenario, is severely limited by the fact that the bombardment of a booby-trapped nuclear device with intense external radiation could trigger the weapon.

2.2.2 Passive Detection

Whereas active techniques use externally applied radiation to exploit common properties of fissile material related to fissionability and density, passive techniques focus on the intrinsic radiation that is emitted in varying forms by all fissile material as a means of detection. Using large static arrays of gamma and neutron detectors to obtain gross count measurements can identify the presence of a radiation source. This technique cannot, however, discriminate between fissile material and any other type of radiation emitting material. More advanced techniques using gamma spectroscopy can be used to detect and identify individual types of fissile material.

By relying on intrinsic radiation emitted by fissile material instead of radiation induced by powerful external sources, passive techniques are non-invasive and do not present radiation protection concerns. However, the intrinsic signal emitted by fissile material is significantly less intense than the signal that can be artificially induced using active methods. In general, the number of counts detected from an isotropic point source can be expressed as follows,

$$C = \frac{SA\varepsilon t}{4\pi r^2} e^{-\sum_i \mu_i \tau_i} \quad (1)$$

where S is the intensity of a point source, A is the detector area normal to the incident radiation, ε is the detector efficiency, t is count time, r is the linear distance between the source and the detector, μ is the linear attenuation coefficient of a given intervening material, and τ is the thickness of a given intervening material. The situation described by Eq. (1) is shown schematically in Figure 2-5.

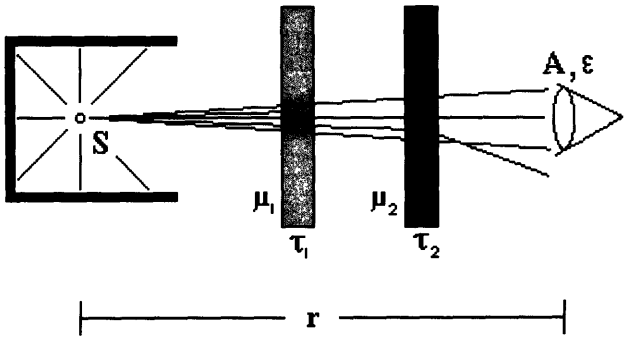

Figure 2-5: Schematic representation of source detection through intervening material

Assuming that the detector or detectors will be placed as close to the source as the situation permits and that detectors with efficiencies as high as feasible were employed, Eq. (1) shows that the only remaining options for increasing the magnitude of the detected signal are to increase the effective detector area or increase the count time. As a result, either large detectors, arrays of detectors, long count times or some combination thereof are likely to be required to make a confident detection of fissile material using passive techniques. An additional difficulty encountered using passive detection methods arises from the relative ease with which the low energy characteristic gamma emissions from some types of fissile material (most notably HEU with very limited or no ^{232}U contamination) can be shielded by dense materials. Shielding can cause already weak intrinsic signals to become even weaker and can be a serious obstacle to confident detection.

Assessed against the container scenario, passive techniques have the critical advantage of not perturbing radiation-sensitive booby-traps in the course of detection. The trade-off for this desirable attribute is the potential for significantly longer count times if the weakly penetrating intrinsic radiation from fissile material is to be detected despite the presence of intentional shielding. Increased count times may or may not be tolerable.

Chapter 3: Detection Schemes

3.1 Current Approaches

The preceding section discussed general methods for detecting concealed fissile material without consideration for how and where within the international container shipping architecture these techniques could be implemented. Identifying suitable deployment strategies for selected detection techniques is often complicated by the potentially competing interests of enhancing security and preserving the free flow of commerce. A number of deployment approaches seeking to strike a balance between security and commerce have been envisioned or even implemented. Some of the more prominent approaches that have been proposed or realized to date will now be discussed in terms of their abilities to address the conservative postulated threat.

3.1.1 Customs-Based Approach

The vast majority of detection schemes that are currently deployed or slated for deployment, can be generally characterized as customs-based approaches. These approaches strive to integrate detection systems using either active or passive techniques into existing infrastructure elements at U.S. ports. Examples include outfitting cranes that transfer containers from cargo vessels onto shore with passive large-area detectors, processing incoming containers through inspection facilities where they are subjected to active interrogation, or using mobile detection units to scan containers with photons for signs of fissile material. The development of in-port detection regimes, such as the examples cited above, represents a natural extension of conventional strategies based on the customs model for finding and seizing contraband as the material is coming into the country. Nuclear weapons, however, are utterly unlike conventional forms of contraband due to the power and range of their effects. As such, when an attack is mounted by a rational and determined adversary, the discovery of a nuclear weapon in a major U.S. port simply cannot ensure protection from the device's destructive power and reach.

3.1.2 "Smart" Containers

Another approach that has been vigorously discussed recently is the deployment of so-called "smart" containers. This approach would retrofit containers used for maritime commerce with small radiation detectors to sense the presence of concealed fissile material. Aside from the extremely daunting logistical challenges that would be presented by installing, maintaining, and mentoring detection equipment in the approximately 11 million [WSC, 2003] cargo containers in circulation worldwide, there are a number of critical limitations associated with this approach. First, the detectors employed in "smart" containers would be very susceptible to tampering. It is the sender who loads and seals the cargo container prior to shipment, so if a "smart container" approach was adopted and it was well known that each container was outfitted with a small detector or detectors, the enemy would have ample opportunity to disable or defeat the detection devices given their unlimited access to the container prior to shipment. Even if an enemy did not successfully defeat the detector or if sensors in neighboring containers detected radiation, the presence of a threat would still not be known until the container entered port unless the alarm could be communicated in a quasi-real time fashion. Equipping all containers with detectors that can transmit alarm information would most likely render the "smart" container approach cost prohibitive. Therefore, like customs-based approaches, "smart" containers would not identify the presence of a nuclear weapon until it has already reached a U.S. port, which is not adequately protective when faced with a sophisticated and determined adversary.

These and other current approaches that subscribe to the conventional notion that threats can be successfully detected and interdicted as they enter the country (in this case when the threat has come ashore in port) are critically flawed because they do not take into account the unique destructive dimensions of the nuclear threat they seek to address. Even if they make detections with perfectly reliability, these approaches and any others that propose to look for fissile material in containers that have already entered port cannot ensure that a nuclear detonation that physically impacts the United States can be

prevented. Therefore, with respect to the challenges posed by the threat of container-borne nuclear attack, these approaches do not meet the ultimate success criterion.

3.2 Ship-Based Approach

3.2.1 Attributes

The primary drawbacks of the approaches discussed above relate to the critical issue of how and where defensive measures are to be deployed. For conventional contraband, shipping ports are logical locations to field inspection and detection capabilities because they represent choke points where many elements (i.e. containers) of a generally diffuse threat (i.e. container borne contraband) come together. Domestic ports are also convenient deployment nodes because, unlike foreign ports and commercially owned property, the U.S. government has wide access to the facilities and infrastructure. To ensure protection from the effects of nuclear weapons, however, the threat must be interdicted prior to reaching, or even coming into range of, U.S. shores.

Large ocean-going container vessels represent another choke point where many cargo containers, each representing a potential threat, come together en route to the United States. If the presence of a concealed nuclear weapon could be detected and communicated while the ship carrying it was still at sea, a defensive response could be mounted while the threat was still safely removed from U.S. shores. The U.S. government cannot unilaterally deploy and maintain control over detection equipment deployed on the actual vessels themselves since they are the property and dominion of private concerns. However, akin to the terrorists who may seek to exploit it as an avenue of attack, the U.S. government does have access to the open architecture of international maritime commerce that allows any party to ship containers to and from just about any destination aboard these ships.

Therefore, Gallagher at MIT has proposed an approach whereby suites of commercial off the shelf (COTS) gamma and neutron detectors are mounted inside

standard, non-descript cargo containers. These dedicated units could then be shipped clandestinely using existing commercial channels where they would be deployed alongside potentially threat-bearing containers aboard vessels sailing for U.S. ports. On board the container ship, the detection units will be able to utilize passive neutron counting and imaging-enhanced gamma spectroscopy techniques to detect and potentially identify any threat-related nuclear signature being emitted from nearby containers with a count time constrained only by the duration of the voyage. The containerized detection units would also be outfitted with a transmission capability such that the presence of potential threats could be communicated as they were detected and prior to entering U.S. ports. The primary advantages of this "ship-based approach" can be summarized as sensitivity, stealth, and most importantly, standoff.

3.2.1.1 Sensitivity

Characteristics of the ship-based deployment environment and the containerized detection units themselves combine to promote good detection sensitivity. Standard full-sized cargo containers, which would be used to house detectors, have dimensions measuring 40' in length, 8' in width and 8.5' in height. The 2720 ft^3 interior volume of these containers provides ample space to mount neutron detection equipment and arrays of gamma detectors that can be configured to present a large effective area when viewed from any incident direction. Additionally, the long transoceanic voyages required to ship containers from many foreign ports of call to U.S. shores provide extremely long count times. From most foreign ports, count times of a week or more would be available.

Referring back to Eq. (1), it is clear that a large detector area and very long count times will enhance signal strength and help to offset the unknown and variable distance to the fissile source. However, the signal strength defined in Eq. (1) is not the only relevant factor in confidently detecting the presence of fissile material. Background radiation being emitted by benign sources can mimic or obscure the emissions from a genuine threat. Two particularly problematic contributors of background radiation are cosmic ray induced neutrons and naturally occurring radionuclides. Cosmic rays, composed

primarily of energetic protons and alpha particles, produce neutrons predominantly through spallation interactions with matter [Frank et. al, 2000]. The distributed neutron background flux at an interface between air and iron (e.g. on the deck of a containership) has been found to be approximately 12 times greater than the background flux at an interface between air and ground [O'Brien, et. al, 1978]. This distributed neutron background enhancement, sometimes referred to as the "Ship Effect", is the result of a massive object composed of dense material (e.g. iron) serving as an effective medium for the production of cosmic ray-induced neutrons. Naturally occurring uranium and thorium can also frustrate detection efforts because these radioactive materials and their daughter products produce characteristic gamma emissions that are identical in energy to those emitted by some fissile materials of interest. Unlike many terrestrial settings, the uranium and thorium concentrations of seawater are small at 3.3 μg/L [Turekian, 1976] and 9.2 ng/L [Emsley, 1998] respectively, and these concentrations are not expected to fluctuate substantially. Therefore the background sources likely to interfere with ship-based fissile material detection are diffuse uranium and thorium impurities in the ship's structural steel and distributed benign sources in commercial containers. Imaging techniques provide a means for identifying localization of incident radiation. As a result, threatening point-like sources can be distinguished from the benign distributed background sources described above.

3.2.1.2 Stealth

The nondescript nature of the containerized ship-based detection systems allows these units to operate surreptitiously. The stealth afforded by these sealed, containerized units will frustrate attempts by adversaries to disable or defeat the embedded detection equipment. Additionally, while the exact number and location of the detection units would not be obvious to an enemy, the knowledge that they are operationally deployed may produce sufficient uncertainty regarding mission success to dissuade the enemy from using this means of delivery. This could achieve an important degree of deterrence.

3.2.1.3 Standoff

The most important advantage of the ship-based approach is the physical location of the material when a positive detection is made and communicated. Instead of identifying the presence of concealed fissile material once it has already entered the country, a ship-based approach could detect the presence of a threat while the container was still safely removed from American shores. The warning time provided by a transmitter equipped, ship-based detection system would allow protective measures to be taken to ensure that a minimum level of standoff distance between the container vessel and the United States coastline could be established and maintained. Not only would early warning prevent a concealed weapon from ever becoming a threat to the American homeland, it would also ensure that responders had the greatest possible degree of flexibility in how to safely contain and neutralize the threat.

3.2.2 External Uncertainties

It is difficult to overstate the critical advantages of a system that uses COTS equipment and well understood techniques to provide advance detection and notification of an incoming container borne nuclear threat. However, before the effectiveness, reliability, and practicality of this conceptual approach can be persuasively demonstrated, a number of important remaining uncertainties must be investigated and resolved. Some of these uncertainties involve aspects of design and performance verification concerned with elements internal to the containerized detection units. Other uncertainties are external to the detection units and relate to facets of the international shipping trade and characteristics of the deployment environment. A concerted effort is underway to remove or constrain these uncertainties and to produce defensible assessments of the efficacy and viability of the ship-based approach. Research and development activities supporting this effort have been roughly divided along the lines of whether they address uncertainties that are internal or external to the detection units. The remainder of this thesis will address some of the more pressing external uncertainties. These uncertainties include the count times available on container voyages originating from different regions of the world, the number of detection units needed to adequately cover a vessel of a given

size, and the number of detection units needed for a fully deployed system. Internal uncertainties are being investigated by Gallagher at MIT and are outside the scope of this thesis. Some important internal issues that are explicitly excluded are detection suite design and quantification of internal performance parameters such as the expected maximum distance (or range) at which a detection unit will be able to confidently and reliably detect fissile sources under realistic conditions. Although concerns internal to the detection unit will not be addressed here, there is an extremely high degree of coordination and collaboration between the two functional areas and as work is produced on one track it is immediately fed into ongoing activities on the parallel track.

Chapter 4: Container Shipping and Cargo Analysis

Some important uncertainties associated with a ship-based detection regime cannot be meaningfully addressed and resolved outside the context of the international container trade and its attendant infrastructure, equipment, and cargo diversity. The following analysis seeks to gain insights into relevant external uncertainties by examining the imported container traffic at U.S. ports and deconstructing it terms of where the containers came from, how far containers traveled to get here, what kinds of vessels (with respect to container capacity and speed) were used to transport them, and what are the relevant material properties of the cargo found within them.

4.1 Container Shipping Overview

In 2003, commercial vessels of all types, including tankers, bulk material carriers, vehicle transports, and containerships, made 56,759 calls at U.S. ports [MARAD(1), 2004]. Containerships accounted for 17,271 (31.7%) of these calls with 1,025 separate vessels importing over 13,900,000 containers, measured in twenty-foot equivalent units[6] (TEUs). In the same year, containerships averaged about 17 calls per vessel and had an average nominal capacity of 3,144 TEU. Table 4-1 shows the volume of imported and exported containers that are processed through the top 30 U.S. ports in 2003 [MARAD(2), 2004].

[6] Cargo containers come in lengths of 20', 40', and 45'. For the sake of normalization, TEU is the standard measure for container statistics even though 40' containers are the most commonly used. A TEU is nominally defined as a 20' x 8' x 8' container. A standard 40' container therefore counts as 2 TEU.

Table 4-1: Containerized cargo volume by U.S. port (CY 2003)

Rank	Port	Total (TEU x 1000)	Export (TEU x 1000)	Import (TEU x 1000)
1	Los Angeles	4664	1022	3642
2	Long Beach	3091	723	2368
3	New York	2803	838	1965
4	Charleston SC	1250	529	721
5	Savannah	1124	529	595
6	Norfolk	1093	460	633
7	Oakland	1064	548	517
8	Houston	933	483	450
9	Tacoma	931	337	594
10	Seattle	815	329	486
11	Miami	764	336	428
12	Port Everglades	423	236	187
13	Baltimore	307	115	192
14	New Orleans	237	139	98
15	Portland OR	210	147	63
16	Wilmington DE	195	29	166
17	San Juan	185	39	147
18	Gulfport MS	179	71	108
19	West Palm Beach	140	106	34
20	Jacksonville	113	72	42
21	Philadelphia	103	9	95
22	Boston	93	34	58
23	Newport News	80	32	48
24	Chester PA	72	28	44
25	Wilmington NC	72	28	44
26	San Diego	53	9	44
27	Freeport TX	50	23	28
28	Richmond VA	41	20	21
29	Honolulu	37	18	19
30	Port Bienville MS	25	23	2
	Total (Top 30)	21148	7312	13837
	All Other Ports	141	77	62
	Grand Total	21289	7389	13899

Table 4-2 shows the origin and volume of containers imported in 2003 from the top 25 U.S. containerized cargo trading partners [MARAD(3), 2004].

Table 4-2: Foreign container import data (CY 2003)

Country of Origin	Imports (TEU x 1000)	Total Trade (TEU x 1000)
China	4447	5656
Hong Kong	1292	1619
Japan	722	1603
Taiwan	651	946
Korea	469	898
Germany	467	650
Italy	473	602
Brazil	388	533
Thailand	378	496
United Kingdom	206	429
Belgium	156	392
Indonesia	261	391
Netherlands	225	390
India	253	389
Malaysia	239	299
France	195	280
Honduras	152	275
Guatemala	156	268
Spain	158	246
Costa Rica	166	245
Philippines	141	221
Dominican Republic	98	216
Australia	78	210
Turkey	114	196
Chile	135	190
Total	12019	17637
All Others	1880	3650
Grand Total	13899	21287

4.2 Count Time

The amount of available count time is a critical factor in determining the efficacy of the proposed ship-based approach. Count times for ship-based detection are constrained only by the duration of the containership voyage. The voyage time between any two ports is determined primarily by the total nautical distance between the ports of interest and the average speed of the vessel. The following focuses on nautical distances between ports and vessel speeds separately and then combines the results of these analyses to derive defensible count time estimates for container shipments originating anywhere in the world.

4.2.1 Distance Between Ports

The nautical distance a vessel travels between a foreign port and a given U.S. port is dominated by the location of the originating port and world geography (i.e. intervening land masses). This distance, however, can also be heavily influenced by the number of intermediate calls made between the ports of interest and by the size of the containership. Many international shipping lines offer regularly scheduled service routes that call on multiple ports en route to the United States. These additional port calls add distance to the overall voyage and each call results in some idle time while the ship is berthed during the container discharge and loading process. The size of containerships is relevant to the travel distance because some important navigational short cuts have physical dimensions that limit the size of vessels that can safely access them. The most important of these size-limited navigational conveniences for containerships is the Panama Canal, which has a 32.2 m maximum width restriction [Ircha, 2002]. Vessels with a beam width exceeding this dimension (i.e. vessels that can fit more than 13 containers across the weather deck) cannot transit the canal and must instead sail around the tip of South America. Despite the additional voyage distances, economies of scale associated with larger, higher capacity vessels drove many international shipping companies to build containerships with deck widths that exceed 32.2 m [Wijnolst, 1999]. These so-called "Post-Panamax" vessels, with capacities greater than 4,000 TEU, now account for 30% of the worldwide containership fleet, by capacity [Tozer, 2003].

Several important assumptions were made prior to carrying out distance to port calculations that would ultimately serve as input to count time estimates. First, New York was selected as a representative destination for the east coast of the United States and Los Angeles was chosen as a representative west coast destination port. In addition to being the largest U.S. ports on their respective coasts, these ports were chosen because their proximity to large urban population centers with vast cultural and economic significance presumably makes them especially attractive targets for attack. Another assumption was that all voyages made from foreign ports to the reference ports (i.e. New

York and Los Angeles) were direct, with no intermediate calls. This assumption was made to ensure conservatism, since intervening port calls add time and distance to the voyage. Finally, it was assumed that the originating port used in a nuclear attack (i.e. the port from which a fully functional device is operationally deployed to the United States) could be anywhere in the world.

A total of 133 foreign ports were included in the distance analysis. An effort was made to select a set of foreign ports that provided reasonably comprehensive coverage of the world's navigable coastlines when taken as a whole. Therefore, some ports were selected for inclusion because of their prominence in the international container trade (e.g. Singapore and Hong Kong), and others were chosen to fill in geographical gaps. By providing quasi-continuous coastal coverage, the distance from any port not included in this analysis can be reasonably approximated by interpolation. Figures 4-1 through 4-8 show the geographic locations [Hammond, 1999] of the selected ports by region.

North America

Map Number	Port	Country
1	Halifax	Canada
2	Prince Rupert	Canada

Figure 4-1: Map of upper North America showing selected ports

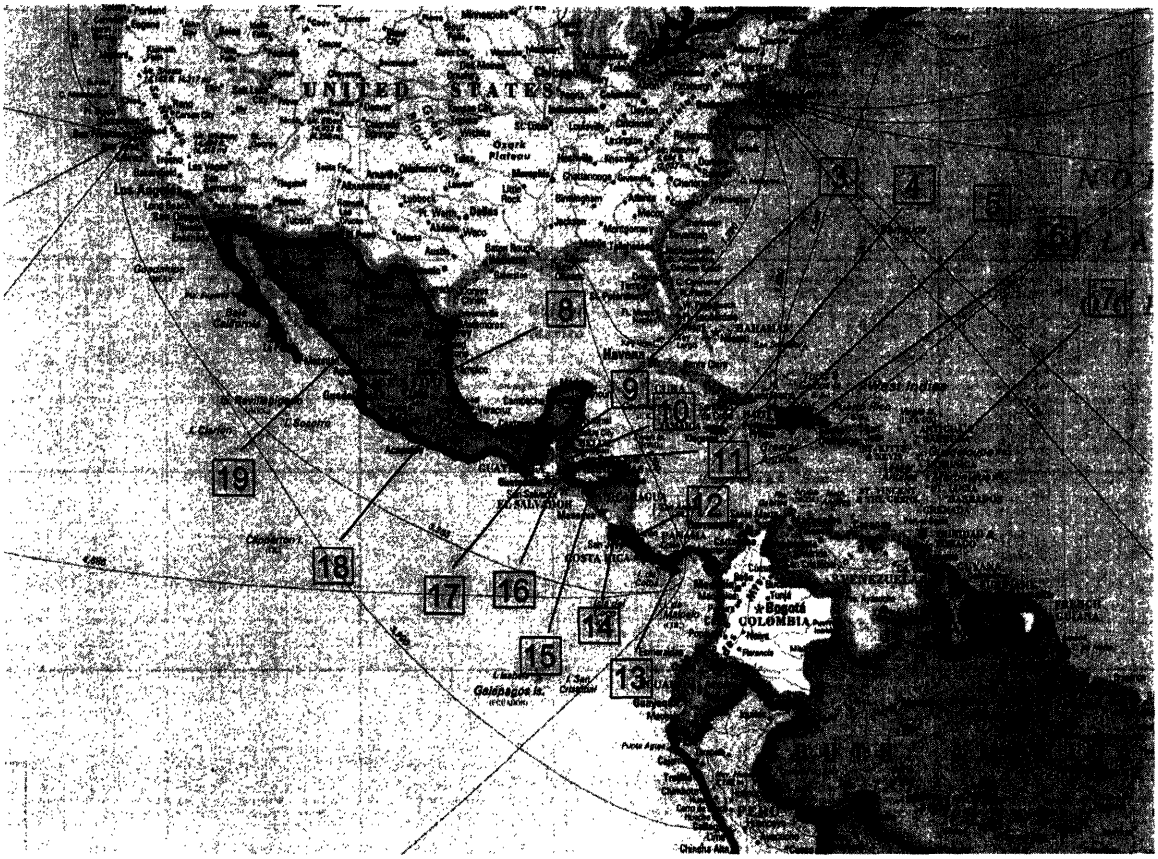

Central America / Caribbean

Map Number	Port	Country	Map Number	Port	Country
3	Havana	Cuba	22	Georgetown	French Guyana
4	Kingston	Jamaica	23	Paramaribo	Suriname
5	Port au Prince	Haiti	24	Natal	Brazil
6	Santo Domingo	Dom. Rep.	25	Salvador	Brazil
7	Fort de France	Martinique	26	Rio de Janeiro	Brazil
8	Tampico	Mexico	27	Porto Alegre	Brazil
9	Belize City	Belize	28	Monte Video	Uruguay
10	Puerto Barrios	Guatemala	29	Buenos Aires	Argentina
11	Puerto Cortes	Honduras	30	Bahia Blanca	Argentina
12	Limon	Costa Rica	31	Comodoro Rivadavia	Argentina
13	Panama	Panama	32	Puenta Arenas	Chile
14	Puntarenas	Costa Rica	33	Puerto Montt	Chile
15	Corinto	Nicaragua	34	Valparaiso	Chile
16	Acajutla	El Salvador	35	Antofagasta	Chile
17	Champerico	Guatemala	36	Mollendo	Peru
18	Acapulco	Mexico	37	Callao	Peru
19	Mazatlan	Mexico	38	Guayaquil	Ecuador
20	Cartagena	Colombia	39	Esmeraldes	Ecuador
21	Maracaibo	Venezuela	40	Buenaventura	Colombia

Figure 4-2: Map of the United States, Central America and the Caribbean showing selected ports

Africa

Map Number	Port	Country
41	Port Said	Eygpt
42	Tunis	Tunisia
43	Banghazi	Libya
44	Algiers	Algeria
45	Casablanca	Morocco
46	Las Palmas	Canary Islands
47	Dakar	Senegal
48	Freetown	Sierra Leone
49	Lagos	Nigeria
50	Boma	Congo
51	Luanda	Angola
52	Cape Town	South Africa
53	Durban	South Africa
54	Beira	Mozambique
55	Dar Es Salaam	Tanzania
56	Mombasa	Kenya
57	Mogadishu	Somalia
58	Djibouti	Djibouti
59	Tamatave	Madagascar

Figure 4-3: Map of Africa showing selected ports

Europe

Map Number	Port	Country	Map Number	Port	Country
60	Batumi	Georgia	77	Zeebrugge	Belgium
61	Odessa	Ukraine	78	Antwerp	Belgium
62	Constanza	Romania	79	Rotterdam	Netherlands
63	Varna	Bulgaria	80	Hamburg	Germany
64	Istanbul	Turkey	81	Copenhagen	Denmark
65	Piraeus	Greece	82	Gdynia	Poland
66	Durres	Albania	83	Klaipeda	Lithuania
67	Split	Croatia	84	Oslo	Norway
68	Koper	Slovenia	85	Stockholm	Sweden
69	La Spezia	Italy	86	Helsinki	Finland
70	Barcelona	Spain	87	St. Petersburg	Russia
71	Lisbon	Portugal	88	Riga	Latvia
72	Coruna	Spain	89	Tallinn	Estonia
73	Bordeaux	France	90	Murmansk	Russia
74	Le Havre	France	91	Arkhangelsk	Russia
75	Southampton	England	92	Reykjavik	Iceland
76	Dublin	Ireland			

Figure 4-4: Map of Europe showing selected ports

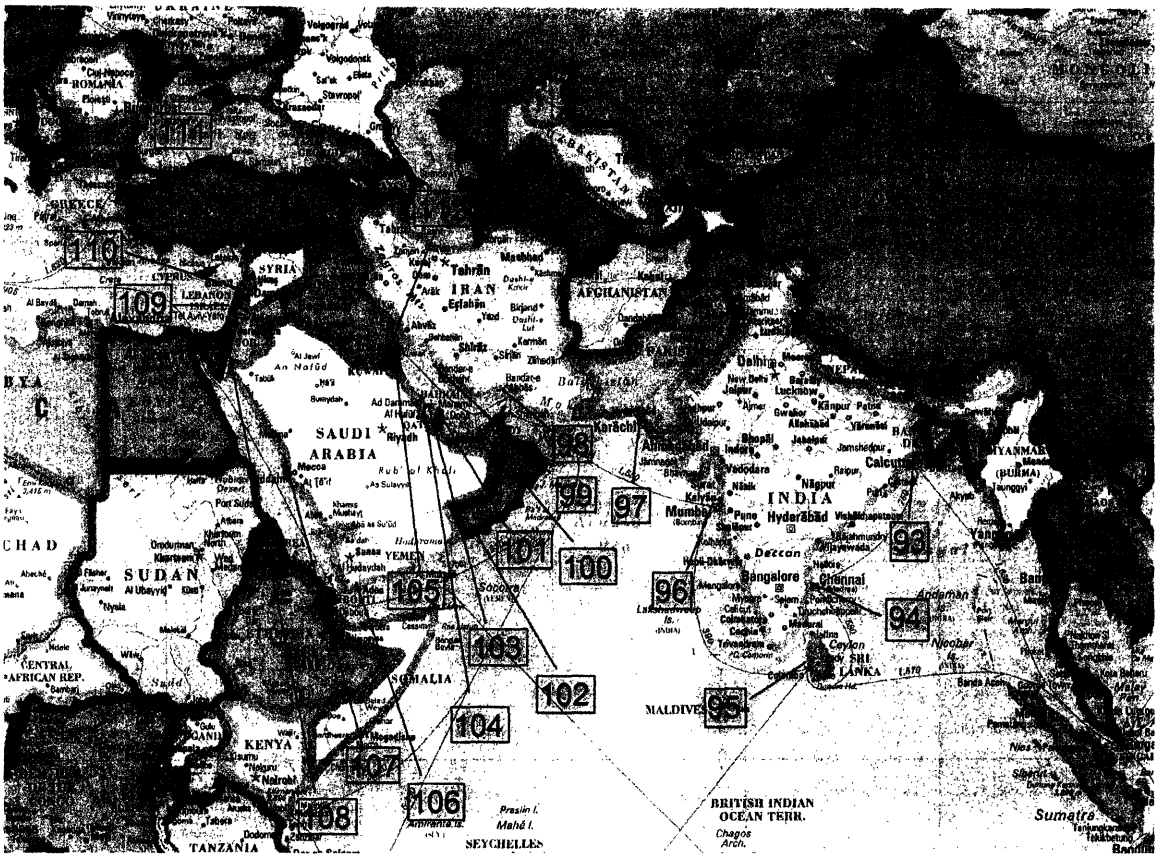

Middle East / India

Map Number	Port	Country
93	Calcutta	India
94	Madras	India
95	Colombo	Sri Lanka
96	Bombay	India
97	Karachi	Pakistan
98	Bandar Abbas	Iran
99	Bushehr	Iran
100	Abu Dhabi	U.A.E.
101	Umm Said	Qatar
102	Mina Raysut	Oman
103	Manama	Bahrain
104	Ad Damman	Saudi Arabia
105	Mina al Ahmadi	Kuwait
106	Aden	Yemen
107	Rabigh	Saudi Arabia
108	Eilat	Israel
109	Haifa	Israel
110	Beirut	Lebanon
111	Al Latakia	Syria
112	Al Basrah	Iraq

Figure 4-5: Map of the Middle East and India showing selected ports

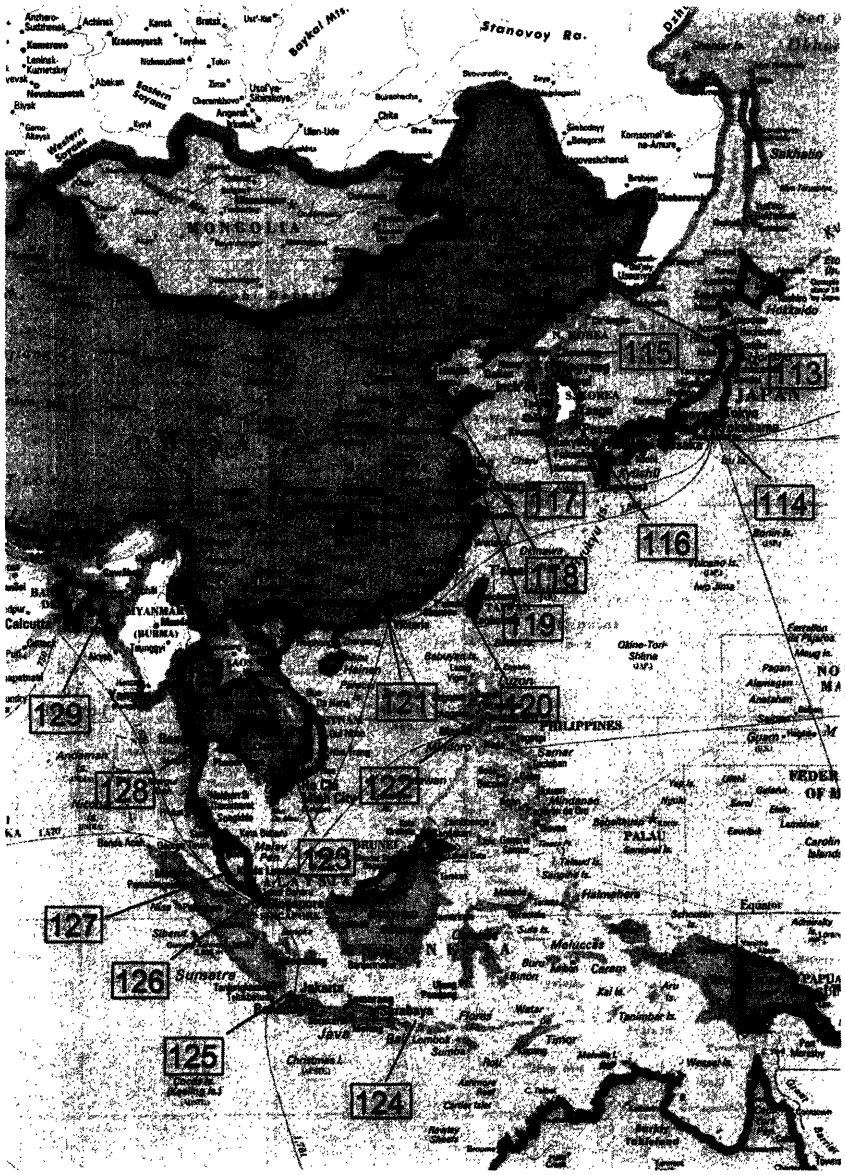

Far East

Map Number	Port	Country
113	Vladivostok	Russia
114	Yokohama	Japan
115	Weonsan	North Korea
116	Busan	South Korea
117	Nampo	North Korea
118	Tianjin	China
119	Shanghai	China
120	Kaohsiung	Tiawan
121	Hong Kong	China
122	Manilla	Philippines
123	Ho Chi Minh	Vietnam
124	Selat Lombok	Indonesia
125	Jakarta	Indonesia
126	Singapore	Singapore
127	Port Kelang	Malaysia
128	Bangkok	Thailand
129	Chittagong	Bangladesh

Figure 4-6: Map of the Far East showing selected ports

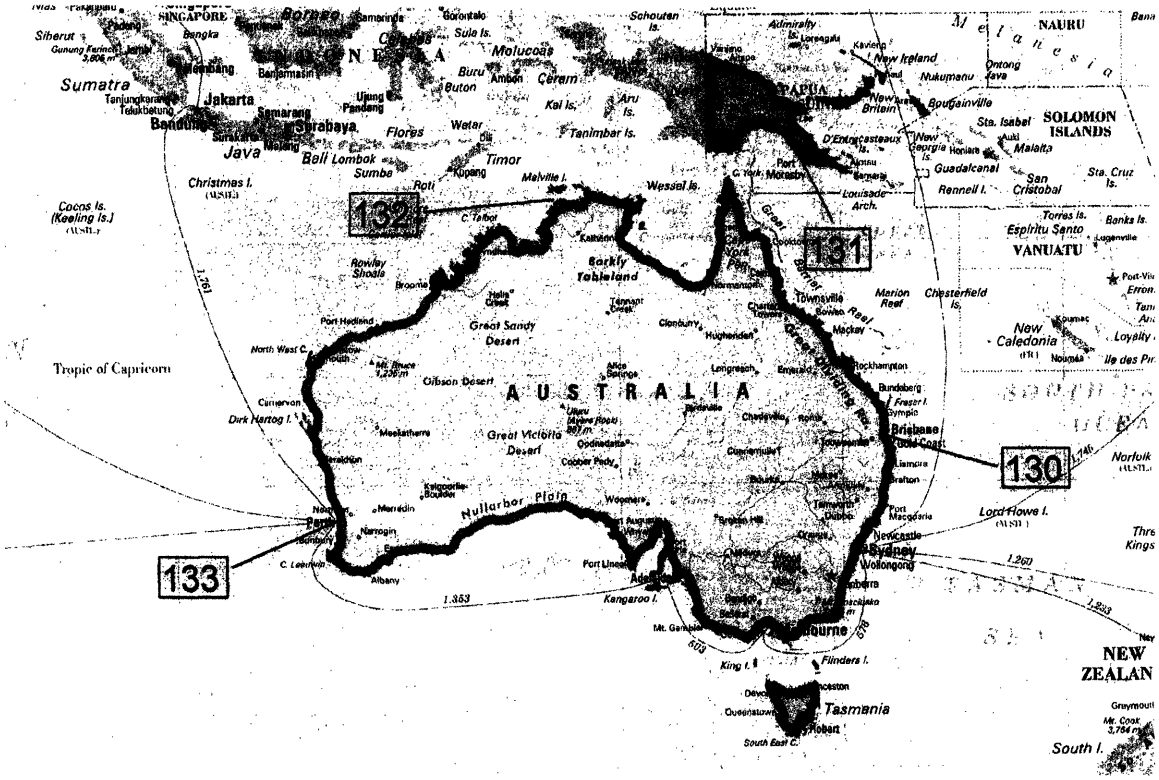

Australia

Map Number	Port	Country
130	Brisbane	Australia
131	Port Moresby	Papua New Guinea
132	Port Darwin	Australia
133	Freemantle	Australia

Figure 4-7: Map of Australia showing selected ports

The nautical distances between the two U.S. reference ports and the 133 selected foreign ports shown above were calculated using information tabulated in "Publication 151 – Distance Between Ports" (referred to hereafter as DBP) prepared by the National Imagery and Mapping Agency [NIMA, 2001]. Information on over 1400 worldwide ports is compiled in this document and all published distances are based on accepted maritime routes and charted nautical sailing lanes. Because of the impracticality of listing distances between every possible combination of these ports, distance calculations using this document typically have to be carried out in several intermediate steps using specified "junction points". The DBP identifies 25 junction points where international shipping routes converge and through which ships pass when sailing from one major maritime area to another (e.g. the Strait of Gibraltar or the Cape of Good Hope). Distances between any two tabulated world ports can then be calculated by summing the distances to, and between, these junction points. Some voyage distances vary considerably depending on whether the Panama Canal can be transited. Because a significant fraction of the international containership fleet is Post-Panamax, distances between a given foreign port and the two U.S. reference ports were calculated with and without access to the Panama Canal. When the two distances differed depending on canal access, the following expression was used to calculate a weighted average,

$$D_{avg} = 0.3D_{Post\_Panamax} + 0.7D_{Panamax} \quad (2)$$

where $D_{Post\_Panamax}$ is the voyage distance without access to the Panama Canal and $D_{Panamax}$ is the distance with access. The weighting factors were chosen because 30% of the current fleet (by capacity) is Post-Panamax and the balance is not. Therefore, a container heading to the U.S. should have a 0.3 probability of being on a ship that can't gain access to the Panama Canal and a 0.7 probability of being on a ship that can.

Distances from the 133 foreign ports to New York and Los Angeles in nautical miles[7] are shown in Table 4-3. The Panamax, Post-Panamax and weighted average

[7] 1 nautical mile = 1.15 statute miles = 1.85 km

distances are captured for each foreign port to the 2 U.S. reference ports. Highlighted cells illustrate the shorter of the voyage distances between the two reference ports.

Table 4-3: Nautical distances from selected foreign ports to New York and Los Angeles

Map Number	Port	Country	Distance to New York (n.m.)			Distance to Los Angeles (n.m.)		
			Panamax	Post-Panamax	Weighted Avg.	Panamax	Post-Panamax	Weighted Avg.
1	Halifax	Canada	600	600	600	5251	12670	7477
2	Prince Rupert	Canada	6321	14181	8679	1432	1432	1432
3	Havana	Cuba	1199	1199	1199	3954	12671	6569
4	Kingston	Jamaica	1474	1474	1474	3507	11934	6035
5	Port au Prince	Haiti	1372	1372	1372	3730	12587	6387
6	Santo Domingo	Dom. Rep.	1489	1489	1489	3759	12194	6290
7	Fort de France	Martinique	1717	1717	1717	4115	11321	6277
8	Tampico	Mexico	2029	2029	2029	4441	13381	7123
9	Belize City	Belize	1699	1699	1699	3772	13520	6696
10	Puerto Barrios	Guatemala	1804	1804	1804	3736	13104	6546
11	Puerto Cortes	Honduras	1764	1764	1764	3689	13174	6535
12	Limon	Costa Rica	2047	2047	2047	3147	12614	5987
13	Panama	Panama	2018	2018	2018	2913	2913	2913
14	Puntarenas	Costa Rica	2489	10944	5026	2499	2499	2499
15	Corinto	Nicaragua	2701	10114	4925	2281	2281	2281
16	Acajutla	El Salvador	2851	11243	5369	1932	1932	1932
17	Champerico	Guatemala	2972	11022	5387	1995	1995	1995
18	Acapulco	Mexico	3444	11516	5866	1501	1501	1501
19	Mazatlan	Mexico	4024	12111	6450	1011	1011	1011
20	Cartagena	Colombia	2018	2018	2018	2913	2913	2913
21	Maracaibo	Venezuela	2489	10944	5026	2499	2499	2499
22	Georgetown	French Guyana	2217	2217	2217	4471	10901	6400
23	Paramaribo	Suriname	2334	2334	2334	4604	11078	6546
24	Natal	Brazil	3532	3532	3532	6101	9271	7052
25	Salvador	Brazil	4089	4089	4089	6654	8791	7295
26	Rio de Janeiro	Brazil	4762	4762	4762	7324	8109	7560
27	Porto Alegre	Brazil	5267	5267	5267	7556	7556	7556
28	Monte Video	Uruguay	5749	5749	5749	7171	7171	7171
29	Buenos Aires	Argentina	5871	5871	5871	7265	7265	7265
30	Bahia Blanca	Argentina	6154	6154	6154	6875	6875	6875
31	Comodoro Rivadavia	Argentina	6349	6349	6349	6456	6456	6456
32	Puenta Arenas	Chile	6934	6934	6934	5871	5871	5871
33	Puerto Montt	Chile	5195	7926	6014	5431	5431	5431

34	Valparaiso	Chile	4634	8366	5754	4808	4808	4808
35	Antofagasta	Chile	4158	8930	5590	4430	4430	4430
36	Mollendo	Peru	3235	8873	4926	4144	4144	4144
37	Callao	Peru	3368	9605	5239	3655	3655	3655
38	Guayaquil	Ecuador	2842	10241	5062	3218	3218	3218
39	Esmeraldes	Ecuador	2492	10420	4870	3010	3010	3010
40	Buenaventura	Colombia	2360	10731	4871	3051	3051	3051
41	Port Said	Eygpt	5119	5119	5119	9207	12902	10316
42	Tunis	Tunisia	3996	3996	3996	8084	13043	9572
43	Banghazi	Libya	4532	4532	4532	8620	13579	10108
44	Algiers	Algeria	3613	3613	3613	7701	12660	9189
45	Casablanca	Morocco	3210	3210	3210	7098	12057	8586
46	Las Palmas	Canary Islands	2965	2965	2965	7673	11576	8844
47	Dakar	Senegal	3335	3335	3335	6651	10799	7895
48	Freetown	Sierra Leone	3757	3757	3757	6889	10602	8003
49	Lagos	Nigeria	4883	4883	4883	7963	11696	9083
50	Boma	Congo	5567	5567	5567	8583	10869	9269
51	Luanda	Angola	5670	5670	5670	11760	11760	11760
52	Cape Town	South Africa	6801	6801	6801	9379	10133	9605
53	Durban	South Africa	7565	7565	7565	10143	10897	10369
54	Beira	Mozambique	8255	8255	8255	10833	11587	11059
55	Dar Es Salaam	Tanzania	9131	9131	9131	11909	11909	11909
56	Mombasa	Kenya	9273	9273	9273	11854	11854	11854
57	Mogadishu	Somalia	9656	9656	9656	11478	11478	11478
58	Djibouti	Djibouti	6493	6493	6493	10581	14196	11666
59	Tamatave	Madagascar	8856	8856	8856	11434	11542	11466
60	Batumi	Georgia	5584	5584	5584	9672	14293	11058
61	Odessa	Ukraine	5345	5345	5345	9433	14054	10819
62	Constanza	Romania	5194	5194	5194	9282	13902	10668
63	Varna	Bulgaria	5162	5162	5162	9250	13854	10631
64	Istanbul	Turkey	4997	4997	4997	9085	13706	10471
65	Piraeus	Greece	4627	4627	4627	8715	13674	10203
66	Durres	Albania	4525	4525	4525	8613	13853	10185
67	Split	Croatia	4683	4683	4683	8771	14035	10350
68	Koper	Slovenia	4858	4858	4858	8946	14212	10526
69	La Spezia	Italy	4067	4067	4067	8155	13114	9643
70	Barcelona	Spain	3710	3710	3710	7798	13391	9476

71	Lisbon	Portugal	2980	2980	2980	7065	12269	8626
72	Coruna	Spain	2917	2917	2917	7140	12973	8890
73	Bordeaux	France	3241	3241	3241	7510	12915	9132
74	Le Havre	France	3180	3180	3180	7530	13100	9201
75	Southampton	England	3169	3169	3169	7510	13080	9181
76	Dublin	Ireland	3028	3028	3028	7383	13145	9112
77	Zeebrugge	Belgium	3330	3330	3330	7657	13237	9331
78	Antwerp	Belgium	3386	3386	3386	7728	13298	9399
79	Rotterdam	Netherlands	3391	3391	3391	7731	13301	9402
80	Hamburg	Germany	3654	3654	3654	7990	13560	9661
81	Copenhagen	Denmark	3826	3826	3826	8165	13735	9836
82	Gdynia	Poland	4003	4003	4003	8342	13912	10013
83	Klaipeda	Lithuania	4064	4064	4064	8403	13973	10074
84	Oslo	Norway	3884	3884	3884	8233	13803	9904
85	Stockholm	Sweden	4167	4167	4167	8506	14076	10177
86	Helsinki	Finland	4289	4289	4289	8628	14198	10299
87	St. Petersburg	Russia	4443	4443	4443	8782	14352	10453
88	Riga	Latvia	4219	4219	4219	8558	14128	10229
89	Tallinn	Estonia	4267	4267	4267	8606	14176	10277
90	Murmansk	Russia	3844	3844	3844	8512	15626	10646
91	Arkhangelsk	Russia	4734	4734	4734	9170	15097	10948
92	Reykjavik	Iceland	2495	2495	2495	7021	16187	9771
93	Calcutta	India	12245	12245	12245	9516	9516	9516
94	Madras	India	11591	11591	11591	9450	9450	9450
95	Colombo	Sri Lanka	11118	11118	11118	9448	9448	9448
96	Bombay	India	11355	11355	11355	10308	10308	10308
97	Karachi	Pakistan	11459	11459	11459	10749	10749	10749
98	Bandar Abbas	Iran	7961	7961	7961	11248	11248	11248
99	Bushehr	Iran	11833	11833	11833	11604	11604	11604
100	Abu Dhabi	U.A.E.	8063	8063	8063	11384	11384	11384
101	Umm Said	Qatar	8218	8218	8218	11497	11497	11497
102	Mina Raysut	Oman	7098	7098	7098	11045	11045	11045
103	Manama	Bahrain	8251	8251	8251	11519	11519	11519
104	Ad Damman	Saudi Arabia	8261	8261	8261	11548	11548	11548
105	Mina al Ahmadi	Kuwait	8405	8405	8405	11692	11692	11692
106	Aden	Yemen	6519	6519	6519	10607	11498	10874
107	Rabigh	Saudi Arabia	5769	5769	5769	9857	12241	10572

108	Eilat	Israel	5500	5500	5500	9588	12735	10532
109	Haifa	Israel	5207	5207	5207	9295	13073	10428
110	Beirut	Lebanon	5210	5210	5210	9298	13132	10448
111	Al Latakia	Syria	5205	5205	5205	7574	13212	9265
112	Al Basrah	Iraq	12033	12033	12033	11783	11783	11783
113	Vladivostok	Russia	9757	16873	11892	4981	4981	4981
114	Yokohama	Japan	9700	15269	11371	4839	4839	4839
115	Weonsan	North Korea	10056	15188	11596	5181	5181	5181
116	Busan	South Korea	10365	14882	11720	5229	5229	5229
117	Nampo	North Korea	10708	15001	11996	5711	5711	5711
118	Tianjin	China	10909	15203	12197	6304	6304	6304
119	Shanghai	China	10584	14587	11785	5810	5810	5810
120	Koashuing	Tiawan	10695	14290	11774	6011	6011	6011
121	Hong Kong	China	11213	13772	11981	6380	6380	6380
122	Manilla	Philippines	13543	13543	13543	6530	6530	6530
123	Ho Chi Minh	Vietnam	13029	13029	13029	7403	7403	7403
124	Selat Lombok	Indonesia	12262	12262	12262	7519	7519	7519
125	Jakarta	Indonesia	12042	12042	12042	8392	8392	8392
126	Singapore	Singapore	12380	12380	12380	7867	7867	7867
127	Port Kelang	Malaysia	12160	12160	12160	8087	8087	8087
128	Bangkok	Thailand	13257	13257	13257	7775	7775	7775
129	Chittagong	Bangladesh	12293	12293	12293	9374	9374	9374
130	Brisbane	Australia	9705	12997	10693	6274	6274	6274
131	Port Moresby	Papua N. G.	10310	13831	11366	5901	5901	5901
132	Port Darwin	Australia	11204	12901	11713	6954	6954	6954
133	Freemantle	Australia	11556	11556	11556	8584	8584	8584

4.2.2 *Vessel Speed*

The diverse fleet of international containerships has a broad spectrum of nominal cruising speeds. Although point estimates, such as mean values, can be used to convey information about large and diverse data sets, the character of a wide spectrum of values is better and more completely captured by a statistical distribution. To develop an appropriate and representative distribution, a containership database was created using publicly available Lloyd's Register information provided online by large commercial shipping lines and U.S. ports. This database was populated with nominal speed (in knots[8]) and/or container capacity (in TEU) data for 1,734 commercial container vessels. Information on both capacity and speed could not be found for every vessel included in the database so there are 1,184 vessel speed entries and 1,706 vessel capacity entries. The full database can be found in Appendix A. No size threshold was initially imposed to exclude any vessel from the database, however, since the subject of interest is international shipping, some screening criterion had to be devised to bar small domestic feeder ships from further consideration. In its annual breakdown of commercial shipping statistics the Maritime Administration (MARAD) of the Department of Transportation imposes a vessel size threshold of 10,000 deadweight tons[9] [MARAD(1), 2004]. This threshold was adopted as a screening criterion for the containership database to facilitate fair comparison with the MARAD statistical abstract and was found heuristically to correspond to vessels with a capacity of roughly 715 TEU. The screened database contained speed information for 910 vessels and capacity data for 1,313 vessels. For comparison, MARAD reported that 1,025 containerships called on U.S. ports in 2003.

The speed and capacity information contained in the database were assumed to be reasonably representative of vessels importing containers to U.S. ports for the following reasons. All information used to populate the database was available through U.S. ports or major container shipping lines that service the U.S. Additionally, the size of the data sets for speed and capacity are comparable to, or exceed, the total number of

[8] 1 knot = 1 nautical mile/hour = 1.85 km/hour

[9] Deadweight tonnage is the amount of cargo, fuels, water, stores, and crew that a vessel can carry when fully loaded. It is measured in long tons (1 long ton = 2,240 lbs.).

containerships that called on U.S. ports in all of 2003. However, to obtain some benchmark of how well the vessel information in the database comported with the containership fleet that actually serviced U.S. ports in 2003, the mean capacity of (screened) database vessels was compared to the actual mean capacity reported by MARAD. The results are shown in Table 4-4 below.

Table 4-4: Vessel database capacity benchmark results

Mean Capacity (TEU)		
Database	**MARAD**	**Error (%)**
3047	3144	3.085

Although this benchmark used only a single parameter (because it was the only value that invited straightforward comparison), the excellent agreement between the database and the MARAD data suggests that conclusions drawn using the vessel database will be reasonably representative of the actual containership fleet servicing the U.S.

To extract meaningful statistical information from the 910 nominal vessel speeds tabulated in the containership database, a cumulative distribution function (CDF) was constructed. A CDF is a statistical distribution that relates the value of a parameter to the probability that the given parameter value, or a lesser value, will be observed. In this case, the CDF gives the probability that a containership calling on a U.S. port will have a nominal speed equal to or less than any given value.

To construct a CDF, the raw vessel speed data from the screened containership database was first sorted into ascending order. Then the frequency of each distinct nominal speed was computed by simply counting how many times a given speed was observed in the database. The probability, or relative frequency, of each nominal speed was then calculated using the following general expression,

$$P_i = \frac{n_i}{\sum n_i} \tag{3}$$

where P_i is the probability of the i_{th} value, and n_i is the frequency of the i_{th} value. The CDF was then found using the following general formula,

$$F[x_i] = \sum_{0}^{i} P_i \tag{4}$$

where $F[x_i]$ is the discrete CDF value for the i_{th} element. In this case, x_i represents each distinct nominal vessel speed. Figure 4-9 is a plot of the vessel speed CDF with the 25th, 50th, 75th, 95th, and 99th percentile values identified graphically.

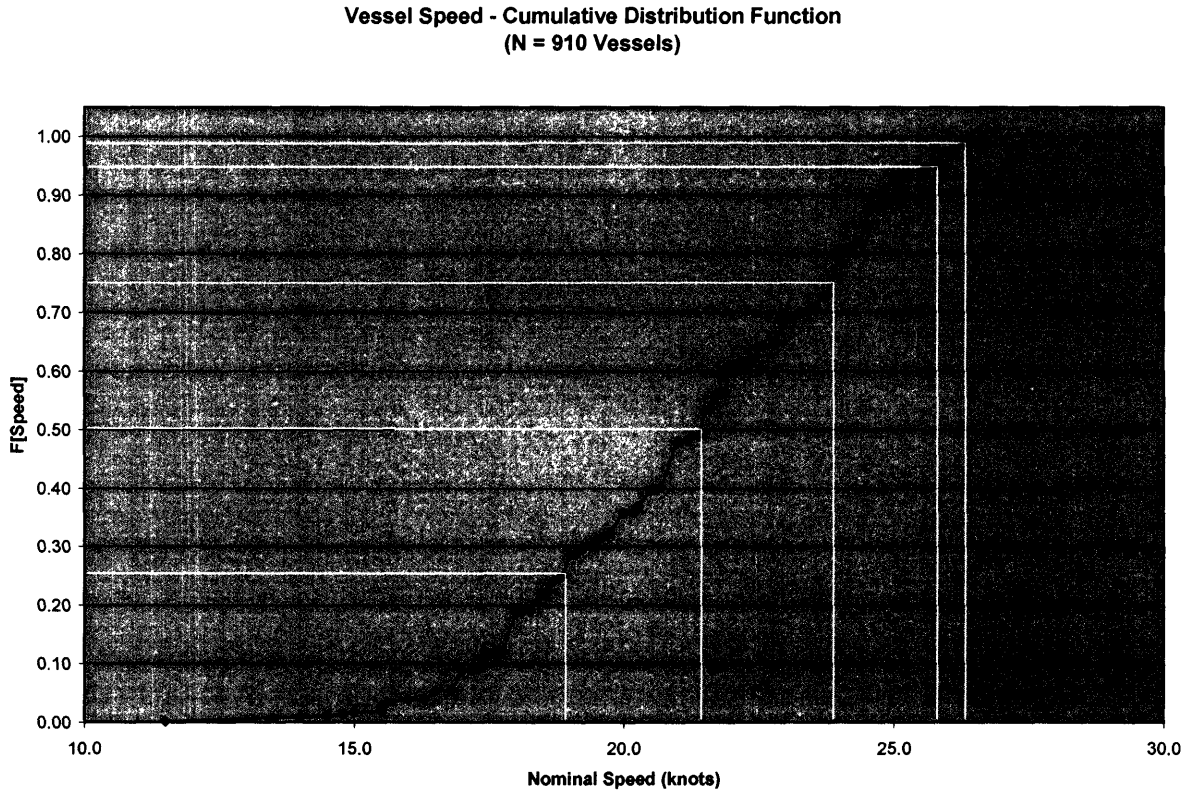

Figure 4-8: Vessel speed CDF

The mean, median, and mode values of the nominal speed from the screened containership database are shown in Table 4-5 along with interpolated numerical values of the 25th, 75th, 95th, and 99th percentiles.

Table 4-5: Vessel speed statistics

	Speed (knots)
MEDIAN	21.43
MEAN	21.29
MODE	21.00
25TH	18.88
75TH	23.86
95TH	25.77
99TH	26.33

4.2.3 Voyage Times

The distance and speed analyses performed in the previous sections can now be used to generate estimated non-stop voyage times for the 133 foreign ports. Weighted average distances between foreign ports and the U.S. reference ports were used to calculate voyage times to account for the additional expanse that must be traveled by Post-Panamax vessels on some routes. Also, acknowledging the inherent variability of vessel speeds, voyage times were calculated using both the expected, or mean, value of 21.29 knots and the conservative 95th percentile value of 25.77 knots. Voyage times, in days, were found using the following expression,

$$T_{voyage} = \frac{D_{avg}}{24 * v_x} \tag{5}$$

where T_{voyage} is the voyage time (in days), D_{avg} is the weighted average distance between the ports of interest (in n.m.) and v_x is the mean or 95th percentile vessel speed (in knots). Table 4-6 shows calculated voyage times, by region.

Table 4-6: Voyage times from selected foreign ports to New York and Los Angeles

Map	Map Number	Port	New York			Los Angeles		
			Weighted Distance (n.m.)	Time [Mean] (days)	Time [95th] (days)	Weighted Distance (n.m.)	Time [Mean] (days)	Time [95th] (days)
North America	1	Halifax (Canada)	600	1.2	1.0	5251	10.3	8.5
North America	2	Prince Rupert (Canada)	8679	17.0	14.0	1432	2.8	2.3
C. America/Carib.	3	Havana (Cuba)	1199	2.3	1.9	3954	7.7	6.4
C. America/Carib.	4	Kingston (Jamaica)	1474	2.9	2.4	3507	6.9	5.7
C. America/Carib.	5	Port au Prince (Haiti)	1372	2.7	2.2	3730	7.3	6.0
C. America/Carib.	6	Santo Domingo (Dom. Rep.)	1489	2.9	2.4	3759	7.4	6.1
C. America/Carib.	7	Fort de France (Martinique)	1717	3.4	2.8	4115	8.1	6.7
C. America/Carib.	8	Tampica (Mexico)	2029	4.0	3.3	4441	8.7	7.2
C. America/Carib.	9	Belize City (Belize)	1699	3.3	2.7	3772	7.4	6.1
C. America/Carib.	10	Puerto Barrios (Guatemala)	1804	3.5	2.9	3736	7.3	6.0
C. America/Carib.	11	Puerto Cortes (Honduras)	1764	3.5	2.9	3689	7.2	6.0
C. America/Carib.	12	Limon (Costa Rica)	2047	4.0	3.3	3147	6.2	5.1
C. America/Carib.	13	Panama (Panama)	2018	3.9	3.3	2913	5.7	4.7
C. America/Carib.	14	Puntarenas (Costa Rica)	5026	9.8	8.1	2499	4.9	4.0
C. America/Carib.	15	Corinto (Nicaragua)	4925	9.6	8.0	2281	4.5	3.7
C. America/Carib.	16	Acajutla (El Salvador)	5369	10.5	8.7	1932	3.8	3.1
C. America/Carib.	17	Champerico (Guatemala)	5387	10.5	8.7	1995	3.9	3.2
C. America/Carib.	18	Acapulco (Mexico)	5866	11.5	9.5	1501	2.9	2.4
C. America/Carib.	19	Mazatlan (Mexico)	6450	12.6	10.4	1011	2.0	1.6
C. America/Carib.	20	Cartagena (Colombia)	2018	3.9	3.3	2913	5.7	4.7
C. America/Carib.	21	Maracaibo (Venezuela)	5026	9.8	8.1	2499	4.9	4.0
C. America/Carib.	22	Georgetown (Fren. Guyana)	2217	4.3	3.6	4471	8.8	7.2
C. America/Carib.	23	Paramaribo (Suriname)	2334	4.6	3.8	4604	9.0	7.4
C. America/Carib.	24	Natal (Brazil)	3532	6.9	5.7	6101	11.9	9.9
C. America/Carib.	25	Salvador (Brazil)	4089	8.0	6.6	6654	13.0	10.8
C. America/Carib.	26	Rio de Janeiro (Brazil)	4762	9.3	7.7	7324	14.3	11.8
C. America/Carib.	27	Porto Alegre (Brazil)	5267	10.3	8.5	7556	14.8	12.2
C. America/Carib.	28	Monte Video (Uruguay)	5749	11.3	9.3	7171	14.0	11.6
C. America/Carib.	29	Buenos Aires (Argentina)	5871	11.5	9.5	7265	14.2	11.7
C. America/Carib.	30	Bahia Blanca (Argentina)	6154	12.0	10.0	6875	13.5	11.1
C. America/Carib.	31	Comodoro Rivadavia (Arg.)	6349	12.4	10.3	6456	12.6	10.4
C. America/Carib.	32	Puenta Arenas (Chile)	6934	13.6	11.2	5871	11.5	9.5

C. America/Carib.	33	Puerto Montt (Chile)	6014	11.8	9.7	5431	10.6	8.8
C. America/Carib.	34	Valparaiso (Chile)	5754	11.3	9.3	4808	9.4	7.8
C. America/Carib.	35	Antofagasta (Chile)	5590	10.9	9.0	4430	8.7	7.2
C. America/Carib.	36	Mollendo (Peru)	4926	9.6	8.0	4144	8.1	6.7
C. America/Carib.	37	Callao (Peru)	5239	10.3	8.5	3655	7.2	5.9
C. America/Carib.	38	Guayaquil (Ecuador)	5062	9.9	8.2	3218	6.8	5.2
C. America/Carib.	39	Esmeraldes (Ecuador)	4870	9.5	7.9	3010	5.9	4.9
C. America/Carib.	40	Buenaventura (Colombia)	4871	9.5	7.9	3051	6.0	4.9
Africa	41	Port Said (Eygpt)	5119	10.0	8.3	9207	18.0	14.9
Africa	42	Tunis (Tunisia)	3996	7.8	6.5	8084	15.8	13.1
Africa	43	Banghazi (Libya)	4532	8.9	7.3	8620	16.9	13.9
Africa	44	Algiers (Algeria)	3613	7.1	5.8	7701	15.1	12.5
Africa	45	Casablanca (Morocco)	3210	6.3	5.2	7098	13.9	11.5
Africa	46	Las Palmas (Canary Is.)	2965	5.8	4.8	7673	15.0	12.4
Africa	47	Dakar (Senegal)	3335	6.5	5.4	6651	13.0	10.8
Africa	48	Freetown (Sierra Leone)	3757	7.4	6.1	6889	13.5	11.1
Africa	49	Lagos (Nigeria)	4883	9.6	7.9	7963	15.6	12.9
Africa	50	Boma (Congo)	5567	10.9	9.0	8583	16.8	13.9
Africa	51	Luanda (Angola)	5670	11.1	9.2	11760	23.0	19.0
Africa	52	Cape Town (South Africa)	6801	13.3	11.0	9379	18.4	15.2
Africa	53	Durban (South Africa)	7565	14.8	12.2	10143	19.9	16.4
Africa	54	Beira (Mozambique)	8255	16.2	13.3	10833	21.2	17.5
Africa	55	Dar Es Salaam (Tanzania)	9131	17.9	14.8	11909	23.3	19.3
Africa	56	Mombasa (Kenya)	9273	18.1	15.0	11854	23.2	19.2
Africa	57	Mogadishu (Somalia)	9656	18.9	15.6	11478	22.5	18.6
Africa	58	Djibouti (Djibouti)	6493	12.7	10.5	10581	20.7	17.1
Africa	59	Tamatave (Madagascar)	8856	17.3	14.3	11434	22.4	18.5
Europe	60	Batumi (Georgia)	5584	10.9	9.0	9672	18.9	15.6
Europe	61	Odessa (Ukraine)	5345	10.5	8.6	9433	18.5	15.3
Europe	62	Constanza (Romania)	5194	10.2	8.4	9282	18.2	15.0
Europe	63	Varna (Bulgaria)	5162	10.1	8.3	9250	18.1	15.0
Europe	64	Istanbul (Turkey)	4997	9.8	8.1	9085	17.8	14.7
Europe	65	Piraeus (Greece)	4627	9.1	7.5	8715	17.1	14.1
Europe	66	Durres (Albania)	4525	8.9	7.3	8613	16.9	13.9
Europe	67	Split (Croatia)	4683	9.2	7.6	8771	17.2	14.2
Europe	68	Koper (Slovenia)	4858	9.5	7.9	8946	17.5	14.5
Europe	69	La Spezia (Italy)	4067	8.0	6.6	8155	16.0	13.2

Europe	70	Barcelona (Spain)	3710	7.3	6.0	7798	15.3	12.6
Europe	71	Lisbon (Portugal)	2980	5.8	4.8	7065	13.8	11.4
Europe	72	Coruna (Spain)	2917	5.7	4.7	7140	14.0	11.5
Europe	73	Bordeaux (French)	3241	6.3	5.2	7510	14.7	12.1
Europe	74	Le Havre (French)	3180	6.2	5.1	7530	14.7	12.2
Europe	75	Southampton (England)	3169	6.2	5.1	7510	14.7	12.1
Europe	76	Dublin (Ireland)	3028	5.9	4.9	7383	14.4	11.9
Europe	77	Zeebrugge (Belgium)	3330	6.5	5.4	7657	15.0	12.4
Europe	78	Antwerp (Belgium)	3386	6.6	5.5	7728	15.1	12.5
Europe	79	Rotterdam (Netherlands)	3391	6.6	5.5	7731	15.1	12.5
Europe	80	Hamburg (Germany)	3654	7.2	5.9	7990	15.6	12.9
Europe	81	Copenhagen (Denmark)	3826	7.5	6.2	8165	16.0	13.2
Europe	82	Gdynia (Poland)	4003	7.8	6.5	8342	16.3	13.5
Europe	83	Klaipeda (Lithuania)	4064	8.0	6.6	8403	16.4	13.6
Europe	84	Oslo (Norway)	3884	7.6	6.3	8233	16.1	13.3
Europe	85	Stockholm (Sweden)	4167	8.2	6.7	8506	16.6	13.8
Europe	86	Helsinki (Finland)	4289	8.4	6.9	8628	16.9	14.0
Europe	87	St. Petersburg (Russia)	4443	8.7	7.2	8782	17.2	14.2
Europe	88	Riga (Latvia)	4219	8.3	6.8	8558	16.7	13.8
Europe	89	Tallinn (Estonia)	4267	8.4	6.9	8606	16.8	13.9
Europe	90	Murmansk (Russia)	3844	7.5	6.2	8512	16.7	13.8
Europe	91	Arkhangelsk (Russia)	4734	9.3	7.7	9170	17.9	14.8
Europe	92	Reykjavik (Iceland)	2495	4.9	4.0	7021	13.7	11.4
Middle East/India	93	Calcutta (India)	12245	24.0	19.8	9516	18.6	15.4
Middle East/India	94	Madras (India)	11591	22.7	18.7	9450	18.5	15.3
Middle East/India	95	Colombo (Sri Lanka)	11118	21.8	18.0	9448	18.5	15.3
Middle East/India	96	Bombay (India)	11355	22.2	18.4	10308	20.2	16.7
Middle East/India	97	Karachi (Pakistan)	11459	22.4	18.5	10749	21.0	17.4
Middle East/India	98	Bandar Abbas (Iran)	7961	15.6	12.9	11248	22.0	18.2
Middle East/India	99	Bushehr (Iran)	11833	23.2	19.1	11604	22.7	18.8
Middle East/India	100	Abu Dhabi (U.A.E.)	8063	15.8	13.0	11384	22.3	18.4
Middle East/India	101	Umm Said (Qutar)	8218	16.1	13.3	11497	22.5	18.6
Middle East/India	102	Mina Raysut (Oman)	7098	13.9	11.5	11045	21.6	17.9
Middle East/India	103	Manama (Bahrain)	8251	16.1	13.3	11519	22.5	18.6
Middle East/India	104	Ad Damman (Saudi Arabia)	8261	16.2	13.4	11548	22.6	18.7
Middle East/India	105	Mina al Ahmadi (Kuwait)	8405	16.4	13.6	11692	22.9	18.9
Middle East/India	106	Aden (Yemen)	6519	12.8	10.5	10607	20.8	17.2

Middle East/India	107	Rabigh (Saudi Arabia)	5769	11.8	9.3	9857	19.3	15.9
Middle East/India	108	Eilat (Israel)	5500	10.8	8.9	9588	18.8	15.5
Middle East/India	109	Haifa (Israel)	5207	10.2	8.4	9295	18.2	15.0
Middle East/India	110	Beirut (Lebanon)	5210	10.2	8.4	9298	18.2	15.0
Middle East/India	111	Al Latakia (Syria)	5205	10.2	8.4	7574	14.8	12.2
Middle East/India	112	Al Basrah (Iraq)	12033	23.5	19.5	11783	23.1	19.1
Far East	113	Vladivostok (Russia)	11892	23.3	19.2	4981	9.7	8.1
Far East	114	Yokohama (Japan)	11371	22.3	18.4	4839	9.5	7.8
Far East	115	Weonsan (North Korea)	11596	22.7	18.7	5181	10.1	8.4
Far East	116	Busan (South Korea)	14882	29.1	24.1	5229	10.2	8.5
Far East	117	Nampo (North Korea)	11996	23.5	19.4	5711	11.2	9.2
Far East	118	Tianjin (China)	12197	23.9	19.7	6304	12.3	10.2
Far East	119	Shanghai (China)	11785	23.1	19.1	5810	11.4	9.4
Far East	120	Hua-Lien Kang (Tiawan)	11774	23.0	19.0	6011	11.8	9.7
Far East	121	Hong Kong (China)	11981	23.4	19.4	6380	12.5	10.3
Far East	122	Manilla (Phillapines)	13543	26.5	21.9	6530	12.8	10.6
Far East	123	Ho Chi Minh (Vietnam)	13029	25.5	21.1	7403	14.5	12.0
Far East	124	Selat Lombok (Indonesia)	12262	24.0	19.8	7519	14.7	12.2
Far East	125	Jakarta (Indonesia)	12042	23.6	19.5	8392	16.4	13.6
Far East	126	Singapore (Singapore)	12380	24.2	20.0	7867	15.4	12.7
Far East	127	Port Kelang (Malaysia)	12160	23.8	19.7	8087	15.8	13.1
Far East	128	Bangkok (Thailand)	13257	25.9	21.4	7775	15.2	12.6
Far East	129	Chittagong (Bangladesh)	12293	24.1	19.9	9374	18.3	15.2
Australia	130	Brisbane (Australia)	10693	20.9	17.3	6274	12.3	10.1
Australia	131	Pt. Moresby (Papua N. G.)	11366	22.2	18.4	5901	11.5	9.5
Australia	132	Port Darwin (Australia)	11713	22.9	18.9	6954	13.6	11.2
Australia	133	Freemantle (Australia)	11556	22.6	18.7	8584	16.8	13.9

Highlighted cells in Table 4-6 illustrate whether the voyage is shorter between the given foreign port and New York or Los Angeles. The highlighted 95th percentile voyage time represents a conservative lower bound for the amount of count time that will be available if an attack is mounted from this port. Count times for non-stop voyages from almost any port in the world to New York or Los Angeles can now be approximated by interpolating between the tabulated values shown in Table 4-6.

The information above is useful for determining the minimum count time available for a container shipment being deployed from a particular port or region of the world. However, it cannot be used directly to give an accurate measure of the expected, or average, count time that would be available on incoming containerships. This is because containers are not uniformly imported to the U.S. from all parts of the globe. To derive a reasonable estimate of how much count time will actually be available on average, the voyage times from ports that ship more containers to the U.S. must be given higher relative weightings. The information in Table 4-2 documenting the volume of container imports broken down by country can be used to assign weighting factors. Since the 25 countries listed in Table 4-2 make up 86.5% of the total containerized imports to the United States, using voyage times from ports located in these countries alone should yield a reasonable estimate. Using this approximation, weighting factors were then calculated as follows,

$$W_i = \frac{n_{TEU_i}}{\sum n_{TEU_i}} \tag{6}$$

where W_i is the weighting factor for the i_{th} country in Table 4-2 and n_{TEUi} is the number of imported containers from the i_{th} country (in TEU). Distances from the countries listed in Table 4-2 to the U.S. reference ports were obtained using information from the distance analysis presented above. Each country of interest has at least one port listed in Table 4-3. For countries with multiple ports listed in Table 4-3, the arithmetic mean of the port distances from that country was used to establish a single representative distance.

Voyage times from the countries in Table 4-2 were then calculated using the mean vessel speed of 21.29 knots (because an expected value was being sought). The appropriate weighting factors were then applied to the voyage times for each country to find expected count time values for ships calling on New York and Los Angeles. Results are shown in Table 4-7.

Table 4-7: Mean voyage times to New York and Los Angeles

Country	Imports	Weighting	New York		Los Angeles	
	(TEU x 1000)	Factor	Avg. Distance (n.m.)	Time [Mean] (days)	Avg. Distance (n.m.)	Time [Mean] (days)
China	4447	0.36997	11991	23.5	6057	11.9
Hong Kong	1292	0.10749	11981	23.4	6380	12.5
Japan	722	0.06007	11371	22.3	4839	9.5
Taiwan	651	0.05416	11774	23.0	6011	11.8
Italy	473	0.03935	4067	8.0	9643	18.9
Korea	469	0.03902	11771	23.0	5374	10.5
Germany	467	0.03885	3654	7.2	9661	18.9
Brazil	388	0.03228	4413	8.6	7366	14.4
Thailand	378	0.03145	13257	25.9	7775	15.2
Indonesia	261	0.02171	12042	23.6	8392	16.4
India	253	0.02105	11730	23.0	9758	19.1
Malaysia	239	0.01988	12160	23.8	8087	15.8
Netherlands	225	0.01872	3391	6.6	9402	18.4
United Kingdom	206	0.01714	3169	6.2	9181	18.0
France	195	0.01622	3211	6.3	9167	17.9
Costa Rica	166	0.01381	3537	6.9	4243	8.3
Spain	158	0.01314	3314	6.5	9183	18.0
Belgium	156	0.01298	3358	6.6	9365	18.3
Guatemala	156	0.01298	1804	3.5	6546	12.8
Honduras	152	0.01265	1764	3.5	6535	12.8
Philippines	141	0.01173	13543	26.5	6530	12.8
Chile	135	0.01123	6073	11.9	5135	10.0
Turkey	114	0.00948	4997	9.8	10471	20.5
Dominican Republic	98	0.00815	1489	2.9	6290	12.3
Australia	78	0.00649	11321	22.2	7271	14.2
Total	12020		Weighted Avg. =	19.2	Weighted Avg. =	13.3

The mean count times available for vessels calling on New York and Los Angeles are on the order of 2 weeks. This represents a significant amount of time to make a confident detection of fissile material. Finally, even though the average count times shown above were calculated using mean vessel speeds, the assumption that all voyages are non-stop still makes these numbers reasonably conservative.

4.3 Vessel Container Capacities

Modern containerships vary considerably in size, with the largest vessels in the current fleet able to carry over 8,000 TEU [MacGregor, 2003]. The number of detection units needed to provide adequate coverage of a given vessel will depend on the dimensions of that particular vessel's container array and the number of commercial containers being transported. Therefore, to gauge the number of containerized detections units that will be necessary to implement a comprehensive ship-based detection regime, a container capacity distribution must be derived for the commercial fleet.

Information from the containership database that was discussed in the vessel speed section was used to construct a similar CDF for container capacity. The screened database contained 1,313 capacity entries ranging from 724 TEU to 8,200 TEU. The CDF development process used for vessel speed was employed again for container capacity. The general formulae shown in Eqs. (3) and (4) were used, with the frequency of each distinct container capacity serving as n in Eq. (3) and container capacity (in TEU) being represented by x in Eq. (4). The resulting capacity CDF is shown in Figure 4-9, with the 25^{th}, 50^{th}, 75^{th}, 95^{th}, and 99^{th} percentile values illustrated graphically.

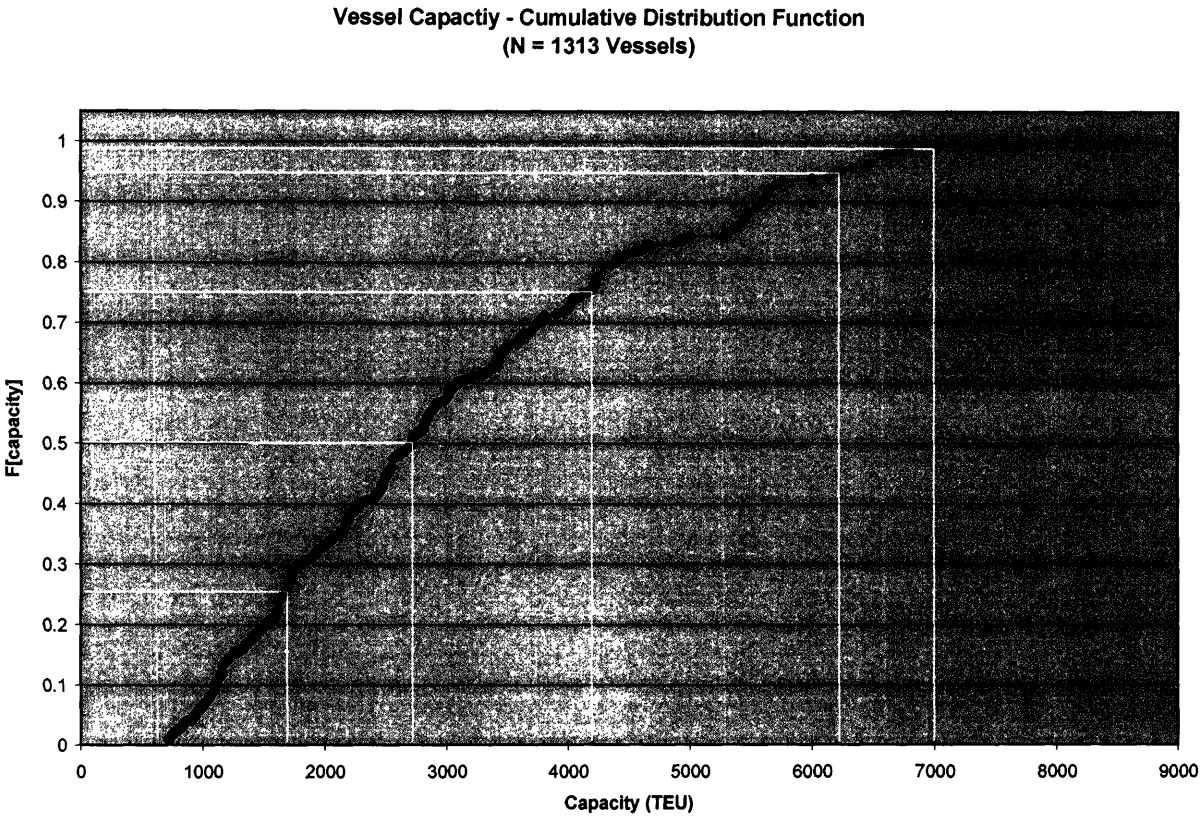

Figure 4-9: Vessel capacity CDF

The mean, median, and mode values of the container capacity from the screened containership database are shown in Table 4-8 along with interpolated numerical values of the 25th, 75th, 95th, and 99th percentiles.

Table 4-8: Vessel capacity statistics

	Capacity (TEU)
MEDIAN	2722
MEAN	3047
MODE	4300
25TH	1666
75TH	4173
95TH	6204
99TH	6782

The container capacity CDF generated here will be used in subsequent analysis to develop defensible estimates for the total number of containerized detection units that will be needed for a fully implemented system.

4.4 Cargo Density

For a ship-based approach to be effective, the signal emitted by concealed fissile material must be strong enough to be confidently distinguished from natural background fluctuations by a passive detection unit some distance removed from the source. The signal will be attenuated by intentional shielding that is likely to be present in the container bearing the weapon and by the commercial cargo in containers that are oriented between the source and detector. The maximum amount of intentional shielding is constrained by the physical dimensions of the container and the 32-ton weight restriction imposed by international shippers [Lok, 2004]. Although they still allow for a very substantial amount of intentional shielding, the space and weight constraints do bound the problem and worst-case signal attenuation can be calculated. What is less straightforward is the extent to which the intervening commercial cargo will attenuate the signal.

Density is a cargo parameter that is helpful when trying to accurately model radiation transport through intervening commercial material. One way to obtain a rough but useful measure of the density of imported cargo material is to assume that the contents of a container (and the mass of the contents) are equally distributed throughout the volume of the container. This "distributed density" (in g/cm^3) can then be found using the following expression,

$$\rho_{dist} = \frac{m}{Vol_{container}} \tag{7}$$

where m is the total mass of the cargo, $Vol_{container}$ is the interior volume of the container. Although the homogeneous distribution of mass throughout the container is clearly

unphysical, it can be a helpful measure for benchmarking computer simulations. When simulations are run where representative types of cargo (e.g. furniture, electronics, clothing, etc.) have been explicitly modeled, it is important to know how the aggregate distributed density of the modeled cargo compares with the average distributed density of actual imported cargo (i.e. is the model more, less, or similarly attenuating as actual cargo). A simple method for obtaining a point estimate of the average distributed density of actual imported cargo is given by,

$$\rho_{dist} = \frac{m_{tot}}{n_{TEU} * Vol_{TEU}} \tag{8}$$

where m_{tot} is the total tonnage of a large sample of imported containers, n_{TEU} is the number of imported containers, and Vol_{TEU} is the interior volume of a TEU. Using imported cargo data for calendar year 2001 (the most recent year for which MARAD reported total tonnage information) as the large container sample, m_{tot}, n_{TEU}, and Vol_{TEU} are 80,725 metric tons (MT), 11,268 TEU, and 1360 ft^2 respectively [MARAD, 2002]. Converting these values into appropriate units and plugging into Eq. (3) gives an average distributed density of 0.1977 g/cm^3. However, a single point estimate of the average distributed density is less instructive than a distribution that reflects the relative probabilities of a range of distributed densities.

The 2001 data for container imports at the top 25 U.S. ports was used construct an average distributed density CDF. Table 4-9 below shows m_{tot}, n_{TEU} and the calculated average densities for the top 25 ports [MARAD, 2002].

Table 4-9: Average distributed density, ρ_{dist}, values for imported cargo

Port	n_TEU (TEU x 1000)	m_tot (MT x 1000)	Avg Density (g/cc)
Los Angeles	2614	16221	0.1712
Long Beach	2376	14355	0.1667
New York	1588	12758	0.2217
Charleston	612	4890	0.2204
Seattle	500	2993	0.1652
Norfolk	454	3556	0.2161
Savannah	431	2998	0.1919
Oakland	419	3058	0.2014
Houston	381	3656	0.2647
Tacoma	356	2111	0.1636
Miami	347	3120	0.2481
Baltimore	178	1942	0.3010
PT Everglades	171	1235	0.1993
San Juan	108	1006	0.2570
Wilmington (DE)	103	965	0.2585
New Orleans	86	891	0.2858
Gulfport	74	599	0.2233
Philadelphia	71	913	0.3548
Boston	51	445	0.2407
Portland	47	350	0.2055
Wilmington (NC)	37	232	0.1730
Chester (PA)	31	316	0.2812
Ponce	30	332	0.3053
W Palm Beach	27	195	0.1993
Jacksonville	25	210	0.2318
All Other	153	1379	0.2487
Total	11268	80725	0.1977

By specifying m_{tot} and n_{TEU} for 26 separate sample populations (i.e. the top 25 ports and the lumped data for all others) this data can be used to construct an approximate CDF. The same CDF derivation procedure outlined earlier is used here with the tabulated values of n_{TEU} serving as the frequency of the given average distributed density value. The resulting CDF is plotted in Figure 4-10.

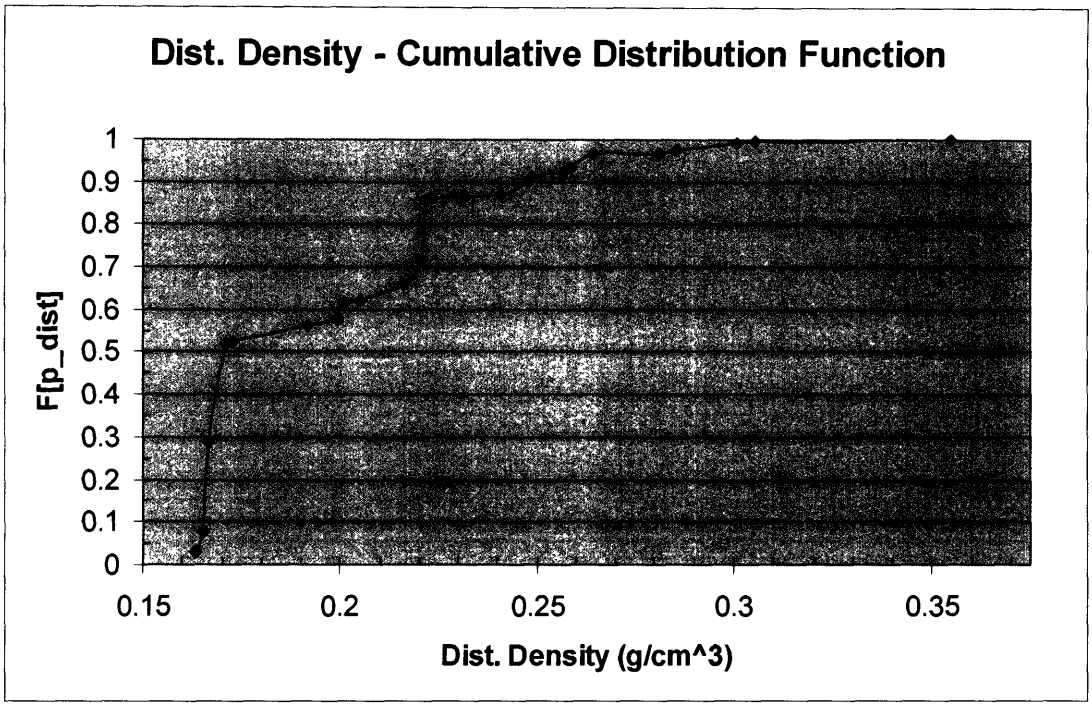

Figure 4-10: Cargo distributed density, $\rho_{dist,}$ CDF

Ideally the mass of every individual imported cargo container would be known so that an exact CDF for ρ_{dist} could be derived. In this case, however, the data points used to construct the CDF were themselves already point estimates of larger data sets. Although some useful information about the character of the original data is lost when a single point estimate is used to represent a population of data, these point estimates encapsulate the most important aggregated attributes of the original data. Therefore, even though it is based on aggregated point estimates instead of exhaustive raw data, the approximate average distributed density CDF is still a useful measure of the probability that the distributed density of a cargo container will exceed a given value.

Chapter 5: Deployment Simulation

5.1 Introduction

The fact that the proposed ship-based approach would deploy containerized detection units aboard commercial containerships has been discussed, but the manner in which these units would be deployed (i.e. how they are loaded onto the ship and distributed throughout the vessel's container array) has not been addressed. Ideally, the detection units could be loaded in a manner that simultaneously allowed completely clandestine deployment and maximum detection coverage with the minimum number of units. If this could be accomplished, total system costs would be minimized and adversaries would be kept utterly unaware of the number and location of deployed detection units that could interrupt or thwart their efforts. In reality, however, there is a trade-off between the precision with which one can dictate or predict the placement of the detection units and the covert nature of the deployment process. Specifying exactly where or how certain cargo containers are to be loaded into the container array can optimize the amount of the containership covered per detection unit, but it could also provide enemies with valuable information about the defensive measures being employed against them. This fundamental trade-off leads to a potential clash between coverage efficiency and stealth.

A computer-based deployment simulator was created using Matlab to help inform the process of striking an appropriate balance between coverage efficiency and stealth. This simulator was used to quantify the coverage efficiency gains that could be reaped by adopting increasingly constrained (and consequently less stealthy) deployment strategies. Three strategies were investigated, including a random deployment where units could be placed anywhere in the container array, a partially constrained deployment where units were randomly placed anywhere except a specified exclusion zone one container deep around the surface of the array, and a fully constrained deployment where units could only be placed along a row down the length of the array. Hereafter, these strategies are referred to as random, constrained, and centerline deployment, respectively.

An extremely important remaining uncertainty (that is outside the scope of this thesis) is the effective detection range of a deployed unit. The effective range is the maximum distance at which a unit is expected to reliably detect the presence of fissile material when deployed amongst commercial containers with realistic and representative cargo. Once a reasonable estimate for the effective range is obtained, it is a straightforward problem to determine the expected detection coverage provided by centerline deployment. The relative ease of calculating centerline coverage stems from the highly constrained nature of this deployment strategy, which uniquely determines the spatial distribution of detection units for any given container array. The spatial distributions arising from the other two strategies, however, are determined either totally or partially by chance. Mean attributes, such as expected detection coverage, of systems with this stochastic character are often difficult or impossible to derive analytically and instead lend themselves to Monte Carlo analysis.

Monte Carlo techniques use random numbers to sample distributions for parameters to be used in a calculation, or calculations, of interest. The calculation is then carried out a large number of times with each iteration using different randomly sampled parameter values. The large population of outputs from the calculation of interest can then be statically analyzed to gain meaningful insights. The speed with which modern digital computers can carry out large numbers of computations makes Monte Carlo analysis a very powerful tool for solving complex problems.

Detection coverage calculations for container arrays of arbitrary sizes were carried out using Monte Carlo methods for both random and constrained deployment. Random numbers were used to sample the uniform distributions representing Cartesian coordinates that determined the placement location of a given detection unit within the container array. Once a given number of detection units with a specified detection range were randomly distributed throughout a container array with known dimensions, the detection coverage calculation could be carried out for this geometry. The output was then logged and the entire detector placement and coverage calculation process was

carried out again until the output population was large enough to yield good statistics. Expected values, along with corresponding standard deviations, for random and constrained deployment could then be determined through statistical analysis.

5.2 Model Development

The deployment simulator was programmed in Matlab and takes advantage of the ease with which the Matlab environment can create and manipulate n-dimensional matrices. The entire container array of a hypothetical vessel is modeled in matrix space with each cubic foot of actual volume represented by an individual element in a 3-dimensional matrix. Detection units are then distributed through the container array in a manner consistent with the constraints of the scenario (i.e. random, constrained, or centerline) being studied. With the geometry of the problem now uniquely specified, the fractional volume of the actual container array that would be effectively covered by the detectors in the generated configuration can be calculated using a few simple matrix operations in Matlab. If Monte Carlo analysis were being used, as would be the case for random and constrained deployment, this process of detector placement and fractional coverage calculation would be repeated many times.

5.2.1 Assumptions

Key assumptions will be identified, and explained before a detailed treatment of the simulator's algorithm and mechanics is offered. First, it was assumed that all container arrays were continuous rectangular prisms. This is an approximation given that large vessels often have container arrays that taper below deck (to accommodate hull dimensions) and some discontinuity created by the ship's superstructure. These effects were not explicitly modeled because the degree of tapering and the location and magnitude of superstructure discontinuities vary depending on the size and design of the containership and cannot be meaningfully generalized.

Since the detection suite is not necessarily confined to the center of a containerized unit, it was also assumed that detectors could be centered at any (non-constrained) location in the container array and not limited solely to coordinates that corresponded to the midpoints of containers. This assumption simplifies calculation but was made primarily to conserve computation time. It was noted that this assumption could lead to the non-physical situation of two or more detectors being randomly assigned to the volume corresponding to a single container. The probability of any two detectors being randomly assigned to the same (TEU)[10] container volume is represented by the following expression,

$$P = \frac{1}{(xyz)^{(n-1)}} \prod_{i=1}^{n-1} (xyz - i) = \frac{(xyz-1)!}{xyz^{n-1}(xyz-n)!} \qquad (9)$$

where x, y, and z are the number of unconstrained TEUs arrayed in the respective x, y, and z directions and n is the number of detectors being deployed. In general, the probability of 2 detectors being assigned to the same container volume increases as n increases and as the total number of TEUs (i.e. $[xyz]$) decreases. The effects of this "double-assignment" will be examined in more detail in subsequent sections.

Another important assumption is that deployed units provide coverage of a perfectly spherical volume with a radius determined by the effective detection range. (Estimates for the effective detection range are being developed by Gallagher at MIT and are still evolving as design decisions and improvements are made, so a series of range values were assumed as part of a parameter study). This is an approximation of a real-world setting, where shielding effects manifested by the specific loading and cargo characteristics of surrounding commercial containers and the threat container itself would render the effective detection volume non-spherical. It is further assumed that fissile material located anywhere within the idealized coverage sphere will be detected with equal probability. In reality, a source close to the detector will be more easily detected

[10] The probability that any two detectors will be assigned to the same 40' container can also be found using Eq. (9) by substituting (xyz/2) for each (xyz) term.

than one at the outer edge of the sphere (along the same line of sight) as a result of shielding by intervening materials and the inverse square nature of detector solid angles. This assumption was deemed acceptable because the definition of the effective detection range is the expected maximum distance at which a source can be confidently and reliably detected with a given count time under realistic conditions. Also, by not considering or crediting the enhanced ease of detection afforded by source proximity and detection sphere overlap, the analysis gains a measure of conservatism.

5.2.2 Input/Output

The Matlab-based deployment simulator accepted user-defined inputs for container array dimensions (length, width, and height in TEUs), the number of detectors to be distributed through the array, the effective detection range (in ft.) and the number of runs to be completed for Monte Carlo analysis. Output for Monte Carlo calculations were statistics (mean, median, standard deviation, minimum, and maximum values) that described the set of fractional detection coverages calculated for each run, or iteration, of the simulation. Output for the deterministic centerline analysis consisted of a fractional detection coverage corresponding to the evaluated scenario.

5.2.3 Algorithm

The simulation of each deployment strategy (i.e. random, constrained, and centerline) used the same algorithm to generate a virtual container array and then calculate the fractional volume that was "covered" by deployed detectors. Differences in random, constrained, and centerline deployment simulation were limited primarily to the manner in which the detectors were placed into (or distributed through) the virtual array. For clarity, the algorithm will be explained in its entirety using random deployment as an example. Differences in the detector placement step for constrained and centerline deployment will then be identified and discussed. The actual Matlab codes used to simulate each type of deployment are found in Appendix B.

The simulation began by creating a matrix representation of the physical space to be modeled by employing user inputs that defined the desired container array dimensions. The inputs specify array dimensions in terms of how many (TEU) containers are to be aligned along the length, width, and height of the array. Figure 5-1 shows the assumed orientation of the containers along the 3 Cartesian axes.

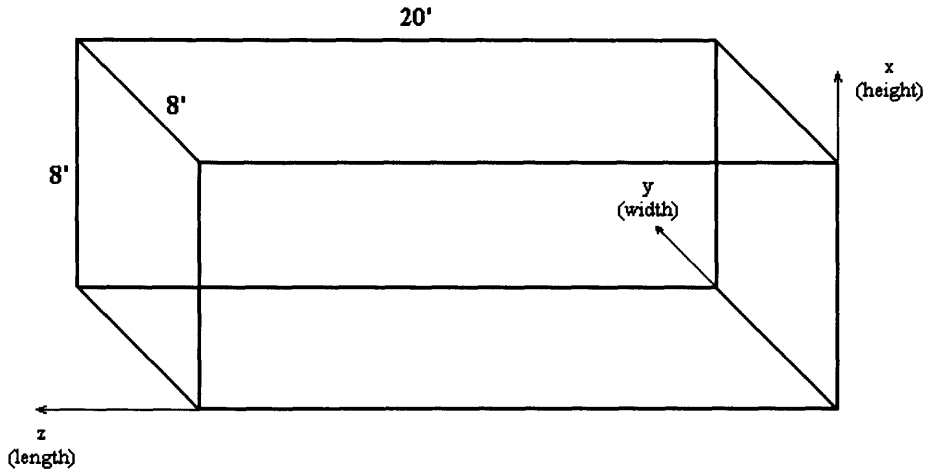

Figure 5-1: Container orientation for simulation

A 3-dimensional matrix was then constructed in which each cubic foot of physical space in the user-specified container array was represented by a matrix element with an initial value of 0. This "geometry matrix" had dimensions [(x*8),(y*8),(z*20)], where x, y, and z were the user inputs for the number of containers along the respective height, width, and length of the array and the scaler multipliers are the corresponding height, width, and length dimensions of (TEU) containers in feet.

Detector placement was the next step in simulation. For random deployment, Matlab's random number generator was used to assign arbitrary coordinates (referred to here as dx, dy, and dz) to fix the center-point of an emplaced detector. Once dx, dy, and dz had been identified, a new null matrix, referred to hereafter as the "detector matrix", was created. The detector matrix was of the same dimensions as the geometry matrix and the element at (dx,dy,dz) representing the emplaced detector was assigned a value of 1.

Next the coverage sphere associated with the emplaced detector was generated. An approximated sphere can be created within a 3-dimensional matrix by serially evaluating individual elements to determine the linear distance between the given element and the emplaced detector using the following expression,

$$D = \sqrt{(i - dx)^2 + (j - dy)^2 + (k - dz)^2} \tag{10}$$

where i, j, and k are the respective x, y, and z coordinates of the matrix element being evaluated. If this distance is greater than the effective detection radius, R, then the element under evaluation is outside the detection sphere and the value of that element remains 0. If the distance is less than or equal to R, the element in question is within the detection sphere and its value in the detector matrix is changed to 1. To save computation time, only matrix elements inside a cube centered at (dx, dy, dz) with sides measuring $2R$ were evaluated using Eq. (10). This cube bounding the detection sphere is shown (2-dimensionally) in Figure 5-2.

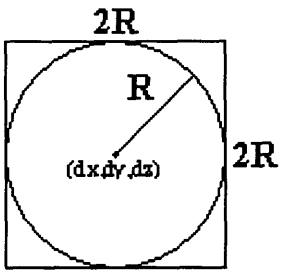

Figure 5-2: Cube bounding the detection sphere

Once the entire coverage sphere, represented by elements with a value of 1, had been generated, an element-by-element comparison of the detector matrix and the geometry matrix was performed using the logical OR operator, whose properties are shown in Table 5-1.

Table 5-1: Properties of the OR operator

X	Y	X (OR) Y
0	0	0
0	1	1
1	0	1
1	1	1

The matrix resulting from this operation becomes the updated geometry matrix. The process of detector placement is then repeated and a new detector matrix is created. The new detector matrix is then compared to the updated geometry matrix, again using the logical OR operator, and the result becomes the new geometry matrix. Each time the geometry matrix is updated, the OR operation imprints it with another coverage sphere. The OR operator is used in lieu of matrix addition to avoid overlapping coverage regions being double counted in the final fractional coverage calculation.

The process of emplacing detectors, creating detector matrices, and updating the geometry matrix continues until the user specified number of detectors has been deployed. At this point, the geometry matrix holds the placement and coverage information of every detector, in addition to information defining the overall dimensions of the simulated container array. An element of the geometry matrix with a value of 1 represents physical space that is within the effective detection range of an emplaced detector, and is therefore "covered". Matlab can then sum the values of all the elements in the geometry matrix to find the volume covered by deployed detectors. The coverage volume, represented by the summation of the geometry matrix, can then be divided by the total number of elements in the geometry matrix, which represents the total volume of the simulated container array, to find the fractional coverage volume. The fractional coverage volume calculation is shown symbolically as follows,

$$\Gamma = \frac{V_{cov}}{V_{total}} \tag{11}$$

where Γ is the fractional coverage volume, V_{cov} is the volume of the array that is "covered" by deployed detectors, and V_{total} is the total volume of the array.

This entire process is repeated until the user-defined number of fractional coverage volume outputs has been generated. At the end of each run, the calculated fractional coverage value is added to an output vector. Once the vector has been fully populated, Matlab performs statistical analysis on the output data and returns the mean, median, standard deviation, minimum and maximum values for the fractional coverage.

Detector placement for constrained and centerline deployment is the only major difference from the simulation process described above. Matlab's random number generator is also used to determine coordinates for detector placement in constrained deployment simulations. However, before a detector matrix is generated reflecting a given placement location, the coordinates are checked to ensure that the detector is not being placed in physical space that would be in a container that is along the surface of the array (i.e. the first or last [TEU] container in any row, column, or span of the array). If the prospective placement coordinates fall in this exclusion zone, then they are discarded and new sets of random numbers are generated until coordinates are obtained that satisfy the constraints. When coordinates are found that do not place the detector in the exclusion zone, a detector matrix is generated and the element representing the placement coordinates is given a value of 1. For deterministic centerline deployment calculations, detector placement is determined by the user inputs concerning the geometry of the container array and the number of detectors to be deployed.

5.2.4 Validation and Verification

During development, a 2-dimensional version of the each simulation code was created to facilitate validation and debugging. Once the 2-dimensional models were found to work as expected with high confidence, they were scaled up to the full 3-dimensional simulations of interest. Prior to actual data collection, the output from 3-dimensional test simulations, starting with small scale runs (i.e. modestly sized arrays

with a small number of deployed detectors) and concluding with a limited number of larger scale runs, were extensively checked against hand calculations.

This validation and verification process also sought to ensure that reality was being modeled with reasonable accuracy. One problem with representing physical space, and especially spherical regions of space, with elements of 3-dimensional matrices is the discretization error introduced by the non-continuous nature of matrix space. To provide reasonably high fidelity models of coverage spheres, each matrix element represented 1 cubic foot. For reference, at this resolution, it takes 2720 matrix elements to model the interior of one full sized 40' cargo container. To check the error introduced by discretization, the calculated volume values for spheres generated in matrix space were compared to the theoretical volume (in ft^3) given by the following formula,

$$V = \frac{4}{3}\pi r^3 \tag{12}$$

where r is the radius of the sphere (in ft). Table 5-2 shows the discretization error observed for spheres of varying radii.

Table 5-2: Spherical volume error

Radius (ft)	Simulation (ft^3)	Theoretical (ft^3)	Error (%)
45	381615	381703.5	0.0232
50	523305	523598.8	0.0561
55	696507	696910	0.0578
60	904089	904778.7	0.0762
65	1149651	1150346.5	0.0605
70	1436385	1436755	0.0258
75	1767063	1767145.9	0.0047
80	2143641	2144660.6	0.0475
85	2571711	2572440.8	0.0284

The errors tabulated above are quite small, so the volume underestimation caused by the discrete nature of matrix space will not significantly impact the accuracy of the fractional coverage values output by the simulations.

5.3 Random Deployment

A deployment methodology where containerized detection units are randomly loaded onto containerships is vastly preferable in terms of both logistics and stealth. By imposing no constraints on the placement of these units, there is no opportunity for an adversary to identify their presence due to abnormal or preferential treatment during the loading process. Therefore, the enemy is not afforded an opportunity to study and probe the defense posture prior to attack or the opportunity to take compensatory action during an attack. The logistics of random deployment are also favorable in that the detection units can be simply delivered to the embarkation port or commercial shipper and then monitored from afar without the need for further direct involvement.

Despite these important advantages, randomly placed detection units can lead to highly inefficient container array geometries due to spatial clustering of units or deployment on or near the fringes of the array. Due to the possibility of poor container array geometries, additional units must be deployed to ensure that an adequate level of detection coverage will be provided. Simulation was carried out in an attempt to better quantify the effects of placement randomization on coverage efficiency (i.e. the fractional coverage provided by a given number of detection units) and to estimate the number of

units that would be required for different levels of coverage for containerships of a given size.

The simulation explained in Section 5.2.3 calls for the specification of container array dimensions, effective detection range, number of deployed detectors, and number of runs as inputs. Five standard container array geometries were selected for use throughout this analysis to facilitate comparison between the deployment strategies. The dimensions of these "reference arrays" are shown in Table 5-3.

Table 5-3: Reference array dimensions

Reference Array Dimensions			Capacity
Height (cont)	Width (cont)	Length (cont)	(TEU)
8	9	20	1440
8	12	26	2496
10	12	30	3600
10	15	32	4800
10	17	38	6460

Reference arrays shown above were selected to provide a representative sample of the capacities and array geometries of the contemporary containership fleet.

Gallagher at MIT is currently investigating the effective detection range. Preliminary analysis and modeling suggests that the range may be somewhere around 65 ft. Using this uncertain estimate as a point of departure, detection ranges spanning from 45 ft. to 85 ft. (in 5 ft. increments) were studied.

To determine the appropriate number of iterations to obtain high confidence results with good statistics, a sample simulation was run using 1, 5, 10, 50, 100, 200, 500 and 1000 iterations. Results of the test, which used 15 detectors with 65 ft. ranges randomly deployed within the 4800 TEU reference array, are shown in Table 5-4.

Table 5-4: Mean fractional coverage results for variable run sizes

Runs	1	5	10	50	100	200	500	1000
Mean	0.7133	0.7308	0.7750	0.7577	0.7522	0.7523	0.7566	0.7553
Std Dev	0	0.0646	0.0922	0.0673	0.0566	0.0584	0.0583	0.0587

Table 5-4 shows that the mean fractional coverage begins to converge at around 50 iterations and the standard deviation has been reduced to the extent practicable by the 100th run. These results are similar to those obtained for cases using different test parameters. As a result, 200 was chosen to be the standard number of iterations used in the simulation of each scenario. This number of runs was large enough to provide high confidence results with good statistics, but small enough to make efficient use of limited computational resources.

Simulations were carried out as follows. Starting with the smallest reference array, the shortest effective detection range was held fixed and the number of deployed units was varied until a distribution of outputs with mean fractional detection coverage values having a nominal span of at least 0.75 to 0.95 was obtained. Then 5 ft. was added to the effective detection range input and the process was carried out again. Once this had been completed for each 5 ft. increment of effective detection range from 45 ft to 85 ft. the next reference array was selected and the entire process began anew. Inputs and output statistics for each simulated scenario are shown in Table 5-5.

Table 5-5: Random deployment simulation results

Capacity	Specific Geometry			Range (ft)	Detection	Coverage Statistics					Runs
(TEU)	width (cont)	height (cont)	length (cont)		Units	Mean	Median	Std. Dev.	Min	Max	
1440	9	8	20	45	10	0.6511	0.659	0.0683	0.4555	0.8262	200
1440	9	8	20	45	13	0.7475	0.7513	0.0634	0.5311	0.8946	200
1440	9	8	20	45	15	0.7878	0.789	0.0612	0.5194	0.9098	200
1440	9	8	20	45	18	0.843	0.8463	0.0494	0.6761	0.9497	200
1440	9	8	20	45	20	0.8707	0.8761	0.0463	0.681	0.9602	200
1440	9	8	20	45	23	0.898	0.9055	0.0409	0.7509	0.9742	200
1440	9	8	20	45	25	0.9159	0.9217	0.0325	0.8009	0.9839	200
1440	9	8	20	45	30	0.9456	0.9523	0.0308	0.7579	0.9876	200
1440	9	8	20	45	31	0.9477	0.9522	0.0283	0.806	0.9947	200
1440	9	8	20	45	35	0.9652	0.9697	0.02	0.8643	0.9949	200
1440	9	8	20	50	7	0.6238	0.6238	0.0778	0.4372	0.8008	200
1440	9	8	20	50	10	0.7371	0.74	0.0708	0.4554	0.8952	200
1440	9	8	20	50	11	0.7758	0.7811	0.0721	0.5508	0.9198	200
1440	9	8	20	50	13	0.8265	0.8349	0.0602	0.6497	0.9662	200
1440	9	8	20	50	14	0.8418	0.85	0.0626	0.5801	0.9569	200
1440	9	8	20	50	16	0.8854	0.8927	0.0515	0.7284	0.9701	200
1440	9	8	20	50	20	0.9251	0.9326	0.0408	0.7283	0.9888	200
1440	9	8	20	50	25	0.9554	0.964	0.0307	0.8434	0.9957	200
1440	9	8	20	55	7	0.6955	0.7033	0.0884	0.459	0.8883	200
1440	9	8	20	55	10	0.8232	0.8355	0.0742	0.5177	0.971	200
1440	9	8	20	55	11	0.8412	0.8472	0.0739	0.5759	0.9755	200
1440	9	8	20	55	13	0.8841	0.8931	0.0593	0.7113	0.9768	200
1440	9	8	20	55	14	0.906	0.9143	0.0496	0.7789	0.9826	200
1440	9	8	20	55	16	0.9299	0.9411	0.0459	0.7491	0.9959	200
1440	9	8	20	55	17	0.9361	0.9475	0.0458	0.7299	0.9945	200
1440	9	8	20	55	19	0.953	0.9673	0.0374	0.8156	0.9975	200
1440	9	8	20	60	5	0.6625	0.6608	0.0857	0.4472	0.9006	250
1440	9	8	20	60	7	0.7604	0.7708	0.1009	0.4673	0.9721	200
1440	9	8	20	60	10	0.8774	0.8902	0.0685	0.684	0.984	200
1440	9	8	20	60	12	0.9048	0.9269	0.069	0.6072	0.9937	200
1440	9	8	20	60	15	0.9513	0.9677	0.0464	0.7638	0.9982	200
1440	9	8	20	65	3	0.5262	0.5235	0.091	0.29	0.7096	200
1440	9	8	20	65	5	0.7105	0.7234	0.1081	0.3678	0.9658	200

1440	9	8	20	65	7	0.835	0.8492	0.0948	0.4819	0.9848	200
1440	9	8	20	65	9	0.887	0.9044	0.0803	0.605	0.9888	200
1440	9	8	20	65	12	0.942	0.9596	0.0592	0.6532	1	250
1440	9	8	20	65	15	0.965	0.9843	0.0466	0.7542	1	200
1440	9	8	20	70	3	0.5963	0.603	0.111	0.3003	0.857	200
1440	9	8	20	70	5	0.7601	0.7775	0.1177	0.3103	0.9651	200
1440	9	8	20	70	7	0.8653	0.883	0.0954	0.385	0.9908	200
1440	9	8	20	70	9	0.9204	0.9458	0.0698	0.6746	0.9999	200
1440	9	8	20	70	11	0.9529	0.9764	0.0579	0.5985	1	200
1440	9	8	20	75	3	0.6257	0.6306	0.1171	0.2244	0.8849	250
1440	9	8	20	75	5	0.7933	0.8047	0.1142	0.4303	0.9997	250
1440	9	8	20	75	7	0.9011	0.9203	0.0872	0.5793	0.9996	250
1440	9	8	20	75	9	0.9381	0.967	0.0686	0.6577	1	250
1440	9	8	20	75	11	0.964	0.9872	0.0535	0.6989	1	200
1440	9	8	20	80	3	0.664	0.6817	0.1332	0.286	0.9358	250
1440	9	8	20	80	5	0.8336	0.8595	0.1227	0.4072	0.999	250
1440	9	8	20	80	7	0.9111	0.9323	0.0868	0.5528	1	250
1440	9	8	20	80	9	0.9593	0.988	0.0639	0.6672	1	250
1440	9	8	20	85	3	0.7065	0.7178	0.1373	0.3039	0.9903	250
1440	9	8	20	85	5	0.8636	0.8789	0.1133	0.3763	0.9999	250
1440	9	8	20	85	7	0.9311	0.9698	0.0899	0.4725	1	250
1440	9	8	20	85	9	0.974	0.9956	0.0496	0.6904	1	250
2496	12	8	26	45	15	0.6295	0.6321	0.0514	0.468	0.7606	200
2496	12	8	26	45	23	0.7773	0.7786	0.0454	0.6168	0.8941	200
2496	12	8	26	45	31	0.8564	0.8606	0.0409	0.6724	0.9432	200
2496	12	8	26	45	39	0.9118	0.9141	0.0271	0.8313	0.9769	200
2496	12	8	26	45	47	0.9421	0.9445	0.0228	0.8517	0.9855	200
2496	12	8	26	45	52	0.958	0.9608	0.0175	0.8781	0.989	200
2496	12	8	26	50	10	0.5917	0.5927	0.0626	0.3884	0.7164	200
2496	12	8	26	50	15	0.7253	0.7277	0.0561	0.5616	0.8455	200
2496	12	8	26	50	23	0.8495	0.8596	0.0475	0.687	0.9336	200
2496	12	8	26	50	31	0.9182	0.9242	0.0374	0.7712	0.9759	200
2496	12	8	26	50	39	0.9497	0.9568	0.0272	0.8515	0.9925	200
2496	12	8	26	55	10	0.6592	0.6619	0.0714	0.4395	0.8121	200
2496	12	8	26	55	15	0.7979	0.7994	0.0597	0.6395	0.9123	200
2496	12	8	26	55	20	0.8672	0.874	0.0463	0.7253	0.9588	200
2496	12	8	26	55	25	0.9273	0.9352	0.0317	0.7987	0.9802	200

2496	12	8	26	55	30	0.9497	0.956	0.0306	0.7945	0.997	200
2496	12	8	26	60	5	0.5028	0.5008	0.075	0.2677	0.6953	250
2496	12	8	26	60	10	0.7265	0.738	0.0811	0.4198	0.8991	200
2496	12	8	26	60	15	0.8525	0.8619	0.0591	0.6549	0.9622	200
2496	12	8	26	60	20	0.9188	0.929	0.0451	0.7447	0.9867	200
2496	12	8	26	60	25	0.9543	0.9589	0.0273	0.8676	0.9977	200
2496	12	8	26	65	5	0.5508	0.5573	0.082	0.2885	0.7515	250
2496	12	8	26	65	10	0.7998	0.8131	0.0763	0.5377	0.9586	250
2496	12	8	26	65	15	0.8925	0.9034	0.0551	0.7231	0.982	250
2496	12	8	26	65	20	0.9485	0.9628	0.0394	0.7422	0.9964	200
2496	12	8	26	65	23	0.9637	0.9736	0.0329	0.7928	0.9986	200
2496	12	8	26	70	5	0.6098	0.6122	0.092	0.3735	0.8287	250
2496	12	8	26	70	7	0.7261	0.7217	0.0885	0.4913	0.9239	200
2496	12	8	26	70	10	0.8365	0.8572	0.0833	0.5875	0.9746	200
2496	12	8	26	70	15	0.9283	0.9427	0.0535	0.7208	0.996	200
2496	12	8	26	70	20	0.963	0.9746	0.0383	0.7314	0.9998	200
2496	12	8	26	70	25	0.9835	0.9914	0.0234	0.8382	0.9999	200
2496	12	8	26	75	5	0.6618	0.6635	0.1048	0.3062	0.9059	250
2496	12	8	26	75	7	0.7756	0.7837	0.0879	0.4947	0.967	200
2496	12	8	26	75	10	0.8829	0.8982	0.0708	0.6561	0.9898	200
2496	12	8	26	75	15	0.9541	0.9638	0.0422	0.7694	0.9985	200
2496	12	8	26	75	20	0.9806	0.9873	0.0253	0.794	1	200
2496	12	8	26	75	25	0.9936	0.9976	0.0106	0.9228	1	200
2496	12	8	26	80	3	0.5208	0.5218	0.1006	0.2068	0.7613	250
2496	12	8	26	80	5	0.7042	0.7091	0.1031	0.4239	0.9406	250
2496	12	8	26	80	7	0.8241	0.8345	0.0968	0.5171	0.9842	250
2496	12	8	26	80	9	0.88	0.8987	0.0787	0.6293	0.9905	250
2496	12	8	26	80	11	0.9287	0.9451	0.0639	0.6153	1	250
2496	12	8	26	80	13	0.9474	0.9682	0.0565	0.6902	1	200
2496	12	8	26	80	15	0.9637	0.9792	0.043	0.7769	1	200
2496	12	8	26	85	3	0.5576	0.5698	0.1106	0.2456	0.7994	250
2496	12	8	26	85	5	0.752	0.7673	0.1114	0.4371	0.9702	250
2496	12	8	26	85	7	0.8449	0.8634	0.0935	0.4935	0.9907	250
2496	12	8	26	85	9	0.915	0.9377	0.0715	0.6286	0.9998	250
2496	12	8	26	85	11	0.945	0.9682	0.0584	0.7205	1	250
2496	12	8	26	85	13	0.9639	0.9835	0.0445	0.7967	1	200
3600	12	10	30	45	20	0.6225	0.6216	0.0453	0.4921	0.7347	250

3600	12	10	30	45	30	0.7572	0.7585	0.0399	0.6497	0.8428	250
3600	12	10	30	45	40	0.8482	0.8488	0.031	0.7155	0.9229	250
3600	12	10	30	45	50	0.8964	0.8977	0.0247	0.8143	0.944	200
3600	12	10	30	45	60	0.9314	0.9343	0.0214	0.8455	0.9771	200
3600	12	10	30	45	70	0.9538	0.9553	0.016	0.9025	0.9816	200
3600	12	10	30	50	10	0.4767	0.4795	0.0472	0.3432	0.6048	200
3600	12	10	30	50	20	0.7137	0.7186	0.0501	0.5676	0.8296	250
3600	12	10	30	50	30	0.8424	0.8473	0.0383	0.7001	0.9151	250
3600	12	10	30	50	40	0.9075	0.9103	0.0303	0.7918	0.9614	250
3600	12	10	30	50	50	0.9449	0.9453	0.0201	0.8804	0.9853	200
3600	12	10	30	50	55	0.9584	0.9606	0.0174	0.8553	0.9915	200
3600	12	10	30	55	10	0.5598	0.5624	0.0545	0.3967	0.6932	200
3600	12	10	30	55	20	0.7947	0.7958	0.0496	0.5543	0.9014	250
3600	12	10	30	55	30	0.8935	0.8982	0.0372	0.7623	0.9599	250
3600	12	10	30	55	40	0.9478	0.9516	0.0242	0.8381	0.9843	250
3600	12	10	30	55	45	0.9607	0.9658	0.0203	0.8821	0.9926	200
3600	12	10	30	60	10	0.6324	0.6309	0.0633	0.4578	0.7809	200
3600	12	10	30	60	15	0.7693	0.7734	0.0585	0.593	0.8957	200
3600	12	10	30	60	20	0.8506	0.8533	0.0482	0.7169	0.9347	200
3600	12	10	30	60	25	0.9067	0.9128	0.0408	0.7542	0.9723	200
3600	12	10	30	60	30	0.9376	0.9453	0.0331	0.8314	0.9874	200
3600	12	10	30	60	35	0.9583	0.9625	0.0244	0.8515	0.9939	200
3600	12	10	30	65	5	0.4633	0.4735	0.0712	0.255	0.6289	200
3600	12	10	30	65	10	0.702	0.7074	0.07177	0.4525	0.8717	500
3600	12	10	30	65	15	0.827	0.8313	0.0591	0.6369	0.9626	500
3600	12	10	30	65	20	0.8988	0.9087	0.0487	0.7029	0.9789	200
3600	12	10	30	65	25	0.939	0.9484	0.0335	0.7999	0.9919	200
3600	12	10	30	65	30	0.9639	0.9697	0.0237	0.8659	0.9941	200
3600	12	10	30	70	5	0.5248	0.5248	0.0763	0.2873	0.7108	200
3600	12	10	30	70	7	0.6275	0.6304	0.0824	0.3919	0.8266	200
3600	12	10	30	70	10	0.7514	0.7551	0.0784	0.5012	0.9218	250
3600	12	10	30	70	15	0.8787	0.8899	0.097	0.6077	0.9791	200
3600	12	10	30	70	20	0.9332	0.9448	0.0432	0.751	0.9915	200
3600	12	10	30	70	25	0.9627	0.9712	0.0287	0.8323	0.9969	200
3600	12	10	30	70	30	0.9783	0.987	0.0216	0.8948	0.9995	200
3600	12	10	30	75	5	0.5706	0.5741	0.0897	0.2473	0.7678	200
3600	12	10	30	75	7	0.6913	0.6955	0.0827	0.4504	0.9024	200

3600	12	10	30	75	10	0.8024	0.8126	0.0792	0.5682	0.9317	200
3600	12	10	30	75	15	0.908	0.9226	0.0563	0.705	0.9953	200
3600	12	10	30	75	20	0.9599	0.9689	0.0332	0.7872	0.9973	200
3600	12	10	30	80	5	0.6283	0.6353	0.096	0.3307	0.8343	200
3600	12	10	30	80	7	0.7327	0.7436	0.0905	0.5193	0.9383	200
3600	12	10	30	80	10	0.8535	0.8677	0.0713	0.6325	0.9774	200
3600	12	10	30	80	15	0.937	0.9527	0.05	0.735	0.9981	200
3600	12	10	30	80	20	0.9749	0.9842	0.0278	0.8212	0.9999	200
3600	12	10	30	85	3	0.4846	0.487	0.0915	0.1938	0.7061	250
3600	12	10	30	85	6	0.7224	0.739	0.0927	0.4851	0.9329	200
3600	12	10	30	85	9	0.8605	0.8767	0.0834	0.5156	0.9907	200
3600	12	10	30	85	12	0.9213	0.9374	0.0639	0.6492	0.9992	200
3600	12	10	30	85	15	0.9574	0.9735	0.046	0.7684	0.9996	200
4800	15	10	32	45	30	0.679	0.6832	0.0408	0.5607	0.7698	200
4800	15	10	32	45	40	0.7782	0.7813	0.0305	0.6777	0.8761	200
4800	15	10	32	45	50	0.839	0.8403	0.0272	0.7527	0.9036	200
4800	15	10	32	45	60	0.8861	0.8859	0.0211	0.8289	0.9453	200
4800	15	10	32	45	70	0.9138	0.9156	0.021	0.8404	0.9589	200
4800	15	10	32	45	80	0.9381	0.9402	0.0172	0.8774	0.9747	200
4800	15	10	32	45	90	0.955	0.9557	0.0129	0.9045	0.9828	200
4800	15	10	32	50	20	0.6321	0.6314	0.0457	0.5204	0.7247	200
4800	15	10	32	50	30	0.7673	0.7739	0.0406	0.5997	0.8749	200
4800	15	10	32	50	40	0.8513	0.8542	0.0335	0.7304	0.9289	200
4800	15	10	32	50	50	0.9009	0.9042	0.0262	0.8209	0.9574	200
4800	15	10	32	50	60	0.9342	0.9368	0.0215	0.8525	0.9761	200
4800	15	10	32	50	70	0.9552	0.957	0.0166	0.8919	0.9912	200
4800	15	10	32	50	80	0.9699	0.9725	0.0135	0.9152	0.9944	200
4800	15	10	32	55	20	0.7161	0.72	0.0473	0.5522	0.8802	200
4800	15	10	32	55	30	0.8375	0.8423	0.0403	0.7229	0.9325	200
4800	15	10	32	55	40	0.908	0.9113	0.027	0.7929	0.9615	200
4800	15	10	32	55	50	0.9442	0.9472	0.0227	0.8442	0.9853	200
4800	15	10	32	55	55	0.957	0.9616	0.0202	0.8612	0.9865	200
4800	15	10	32	60	15	0.6875	0.6929	0.0553	0.5412	0.8236	200
4800	15	10	32	60	20	0.7794	0.7847	0.0511	0.6428	0.8981	200
4800	15	10	32	60	30	0.89	0.8946	0.0378	0.7518	0.9578	200
4800	15	10	32	60	40	0.9425	0.9467	0.026	0.8305	0.9891	200
4800	15	10	32	60	50	0.9697	0.9727	0.0153	0.9135	0.996	200

4800	15	10	32	65	10	0.6206	0.626	0.061	0.401	0.7788	500
4800	15	10	32	65	11	0.6544	0.6556	0.0641	0.4143	0.8057	500
4800	15	10	32	65	15	0.7551	0.7566	0.0583	0.5518	0.8971	500
4800	15	10	32	65	20	0.8479	0.8536	0.0479	0.6546	0.949	500
4800	15	10	32	65	25	0.8988	0.9057	0.0405	0.746	0.9767	200
4800	15	10	32	65	30	0.9358	0.9406	0.0319	0.7621	0.9796	200
4800	15	10	32	65	35	0.9539	0.9573	0.0251	0.8598	0.9899	200
4800	15	10	32	70	10	0.6772	0.6847	0.0707	0.4592	0.884	500
4800	15	10	32	70	12	0.74	0.7442	0.0683	0.5098	0.9028	200
4800	15	10	32	70	15	0.8107	0.8179	0.0603	0.6042	0.9399	500
4800	15	10	32	70	20	0.8861	0.895	0.0501	0.6833	0.9701	500
4800	15	10	32	70	25	0.9266	0.9329	0.0371	0.8156	0.9835	200
4800	15	10	32	70	30	0.9598	0.9641	0.024	0.8769	0.9935	200
4800	15	10	32	75	10	0.7346	0.7457	0.071	0.5096	0.9253	200
4800	15	10	32	75	12	0.7951	0.8065	0.0705	0.5141	0.9469	200
4800	15	10	32	75	15	0.8595	0.8655	0.0531	0.6856	0.9562	200
4800	15	10	32	75	20	0.9247	0.9329	0.0414	0.7553	0.9847	200
4800	15	10	32	75	25	0.9549	0.9624	0.0287	0.8491	0.9975	200
4800	15	10	32	80	5	0.5467	0.5525	0.0822	0.3195	0.7612	200
4800	15	10	32	80	10	0.7862	0.7926	0.0774	0.5192	0.9419	200
4800	15	10	32	80	15	0.8959	0.9056	0.056	0.6802	0.9829	200
4800	15	10	32	80	20	0.9449	0.9555	0.0409	0.7517	0.9944	200
4800	15	10	32	80	23	0.9602	0.9696	0.0313	0.8355	0.9982	200
4800	15	10	32	85	5	0.5895	0.5878	0.0844	0.3512	0.8104	200
4800	15	10	32	85	7	0.7152	0.724	0.0901	0.4585	0.9424	200
4800	15	10	32	85	10	0.827	0.8385	0.0764	0.4874	0.9725	200
4800	15	10	32	85	15	0.9184	0.9303	0.0542	0.687	0.989	200
4800	15	10	32	85	20	0.9592	0.9697	0.0365	0.7939	0.9988	200
4800	15	10	32	85	25	0.984	0.9896	0.0207	0.8213	0.9999	200
6460	17	10	38	45	30	0.5806	0.5815	0.0352	0.4824	0.678	200
6460	17	10	38	45	40	0.6846	0.6873	0.0304	0.5894	0.7667	200
6460	17	10	38	45	50	0.7594	0.7609	0.0283	0.6749	0.8469	200
6460	17	10	38	45	60	0.8152	0.8183	0.026	0.7322	0.8807	200
6460	17	10	38	45	70	0.8545	0.858	0.0243	0.7624	0.901	200
6460	17	10	38	45	80	0.8893	0.8933	0.0222	0.8257	0.9415	200
6460	17	10	38	45	90	0.9121	0.9121	0.0199	0.8534	0.9557	200
6460	17	10	38	45	100	0.9302	0.9326	0.0174	0.8733	0.9712	200

6460	17	10	38	45	110	0.9456	0.9464	0.0138	0.899	0.9719	200
6460	17	10	38	45	120	0.9553	0.9575	0.0125	0.9159	0.9824	200
6460	17	10	38	50	30	0.6749	0.6792	0.0367	0.5659	0.7545	200
6460	17	10	38	50	40	0.776	0.7796	0.0314	0.6929	0.8491	200
6460	17	10	38	50	50	0.8395	0.8397	0.029	0.7261	0.9065	200
6460	17	10	38	50	60	0.8842	0.8863	0.0266	0.8	0.9414	200
6460	17	10	38	50	70	0.9159	0.9164	0.0192	0.8632	0.9576	200
6460	17	10	38	50	80	0.9396	0.9405	0.0161	0.8905	0.9726	200
6460	17	10	38	50	90	0.9546	0.9567	0.0144	0.9011	0.9804	200
6460	17	10	38	55	20	0.6262	0.626	0.0403	0.5344	0.7294	200
6460	17	10	38	55	30	0.7579	0.7571	0.0408	0.6187	0.8403	200
6460	17	10	38	55	40	0.8452	0.8465	0.0323	0.7358	0.9162	200
6460	17	10	38	55	50	0.8953	0.8999	0.0305	0.7704	0.9656	200
6460	17	10	38	55	60	0.9313	0.9331	0.0203	0.8507	0.9758	200
6460	17	10	38	55	70	0.9526	0.9566	0.0175	0.8845	0.9824	200
6460	17	10	38	60	20	0.6971	0.6988	0.0487	0.5532	0.8081	200
6460	17	10	38	60	25	0.7731	0.7762	0.0431	0.6623	0.8773	200
6460	17	10	38	60	30	0.8262	0.826	0.0443	0.6313	0.9167	200
6460	17	10	38	60	40	0.8966	0.8994	0.0308	0.8028	0.9614	200
6460	17	10	38	60	50	0.9375	0.9406	0.0232	0.8304	0.9788	200
6460	17	10	38	60	60	0.9606	0.9644	0.0173	0.884	0.9878	200
6460	17	10	38	65	10	0.5262	0.5307	0.055	0.3922	0.6828	200
6460	17	10	38	65	20	0.7614	0.7602	0.0482	0.6125	0.908	200
6460	17	10	38	65	30	0.875	0.8777	0.0386	0.7175	0.9441	200
6460	17	10	38	65	40	0.9324	0.9372	0.0292	0.8021	0.986	200
6460	17	10	38	65	50	0.9639	0.9677	0.0197	0.8764	0.9917	200
6460	17	10	38	70	10	0.5886	0.5883	0.0634	0.3822	0.7454	200
6460	17	10	38	70	15	0.7247	0.7242	0.0588	0.5392	0.85	200
6460	17	10	38	70	20	0.8193	0.8259	0.0514	0.6795	0.9147	200
6460	17	10	38	70	25	0.8785	0.8857	0.0446	0.7236	0.9686	200
6460	17	10	38	70	30	0.9169	0.9236	0.036	0.7524	0.9788	200
6460	17	10	38	70	40	0.9602	0.9664	0.0233	0.8384	0.9918	200
6460	17	10	38	75	10	0.6477	0.6467	0.0661	0.4788	0.8185	200
6460	17	10	38	75	15	0.7803	0.7838	0.056	0.6139	0.9343	200
6460	17	10	38	75	20	0.8651	0.8743	0.0444	0.7094	0.9565	200
6460	17	10	38	75	25	0.915	0.9185	0.0367	0.7484	0.9847	200
6460	17	10	38	75	30	0.9466	0.9495	0.0264	0.8158	0.9948	200

6460	17	10	38	75	33	0.956	0.9596	0.0245	0.8858	0.9965	200
6460	17	10	38	80	10	0.6953	0.6993	0.0682	0.5124	0.8598	200
6460	17	10	38	80	12	0.7627	0.768	0.0659	0.5601	0.891	200
6460	17	10	38	80	15	0.8301	0.8344	0.061	0.592	0.9669	200
6460	17	10	38	80	20	0.8956	0.9057	0.0475	0.727	0.9832	200
6460	17	10	38	80	25	0.9343	0.9417	0.0396	0.752	0.9972	200
6460	17	10	38	80	30	0.9616	0.9703	0.0283	0.8485	0.9991	200
6460	17	10	38	85	5	0.4982	0.4989	0.0778	0.3106	0.7061	200
6460	17	10	38	85	10	0.7447	0.7471	0.071	0.5581	0.8866	200
6460	17	10	38	85	15	0.8591	0.8683	0.0641	0.601	0.9702	200
6460	17	10	38	85	20	0.9249	0.9386	0.0451	0.7239	0.9873	200
6460	17	10	38	85	25	0.9532	0.9652	0.0401	0.7122	0.9991	200
6460	17	10	38	85	30	0.976	0.9826	0.0224	0.8727	0.9994	200

To distill the information captured in Table 5-5 for easier inspection and analysis, Figures 5-2 through 5-6 show plots that relate the mean values of fractional coverage volume, as defined in Eq. (11), to the number of deployed detectors for each reference array.

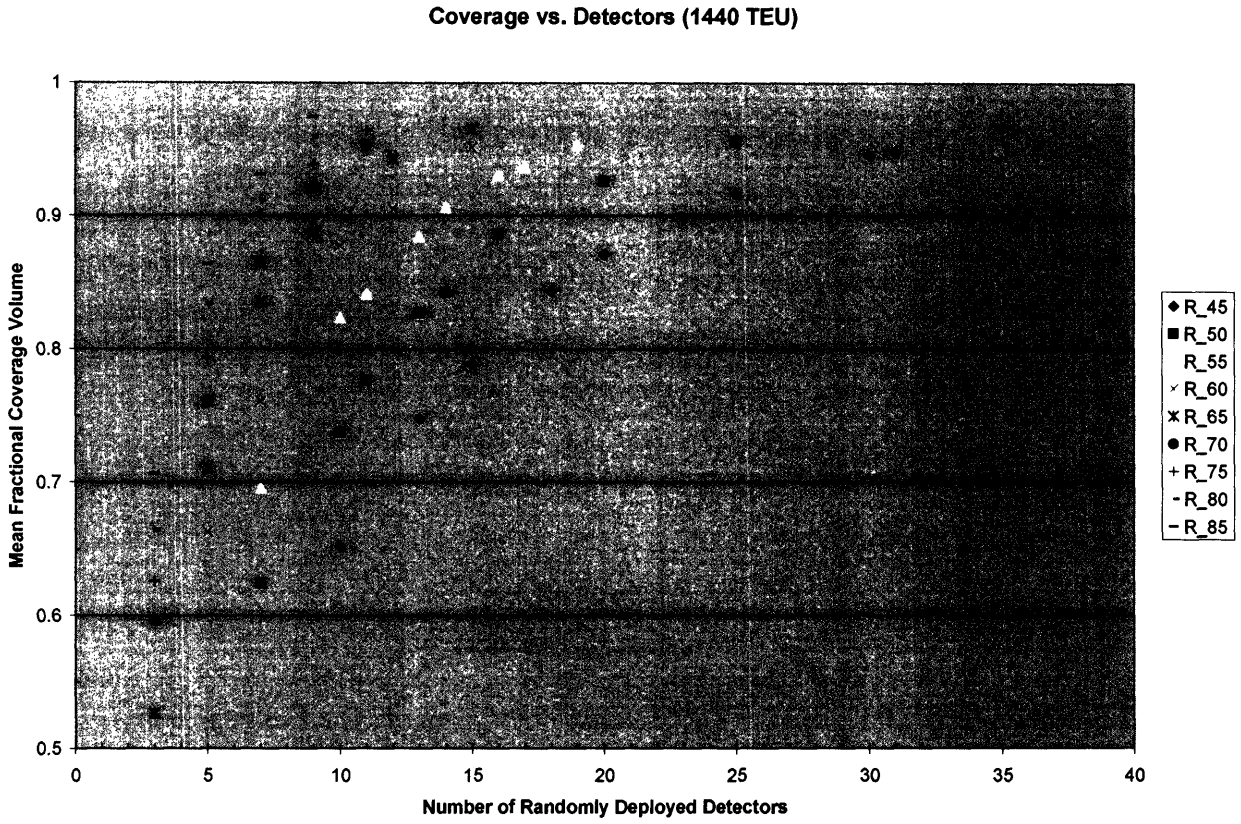

Figure 5-3: Coverage vs. Detectors plot for the 1440 TEU array [Random]

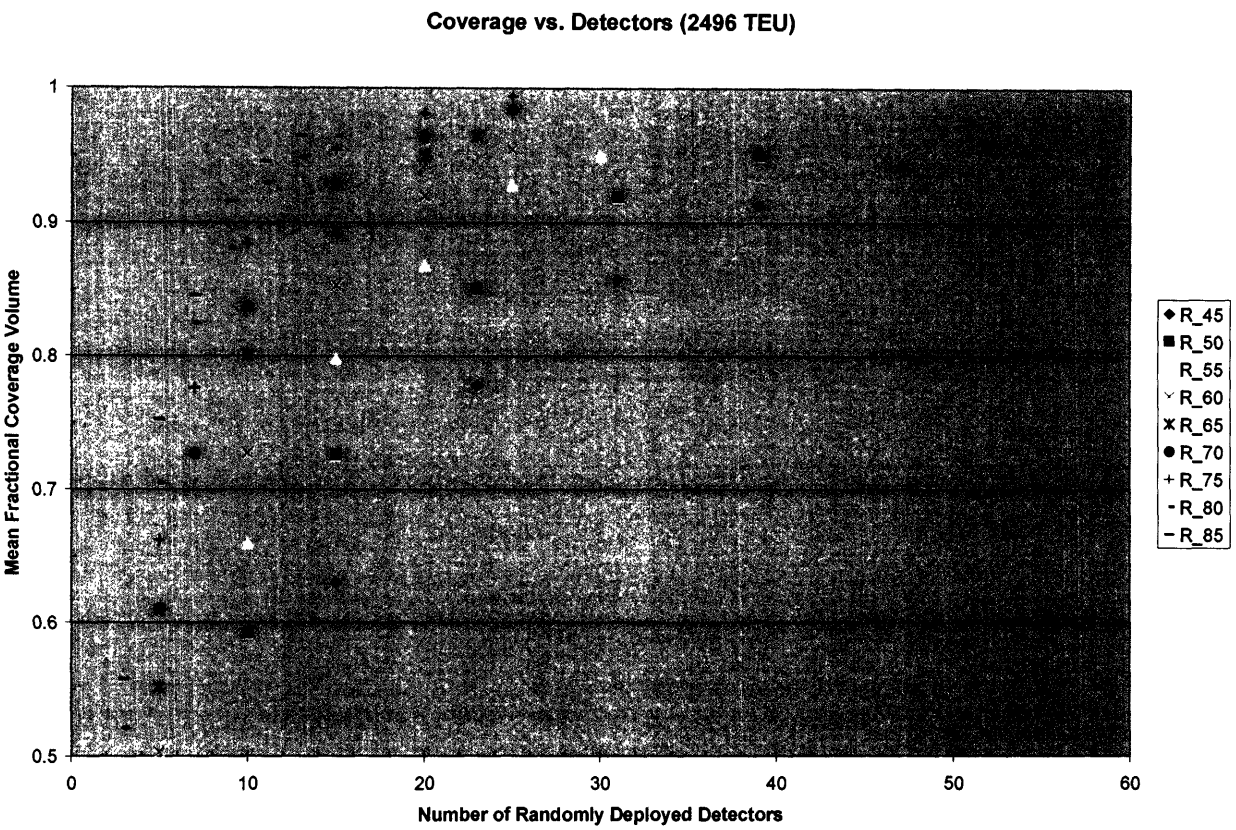

Figure 5-4: Coverage vs. Detectors plot for the 2496 TEU array [Random]

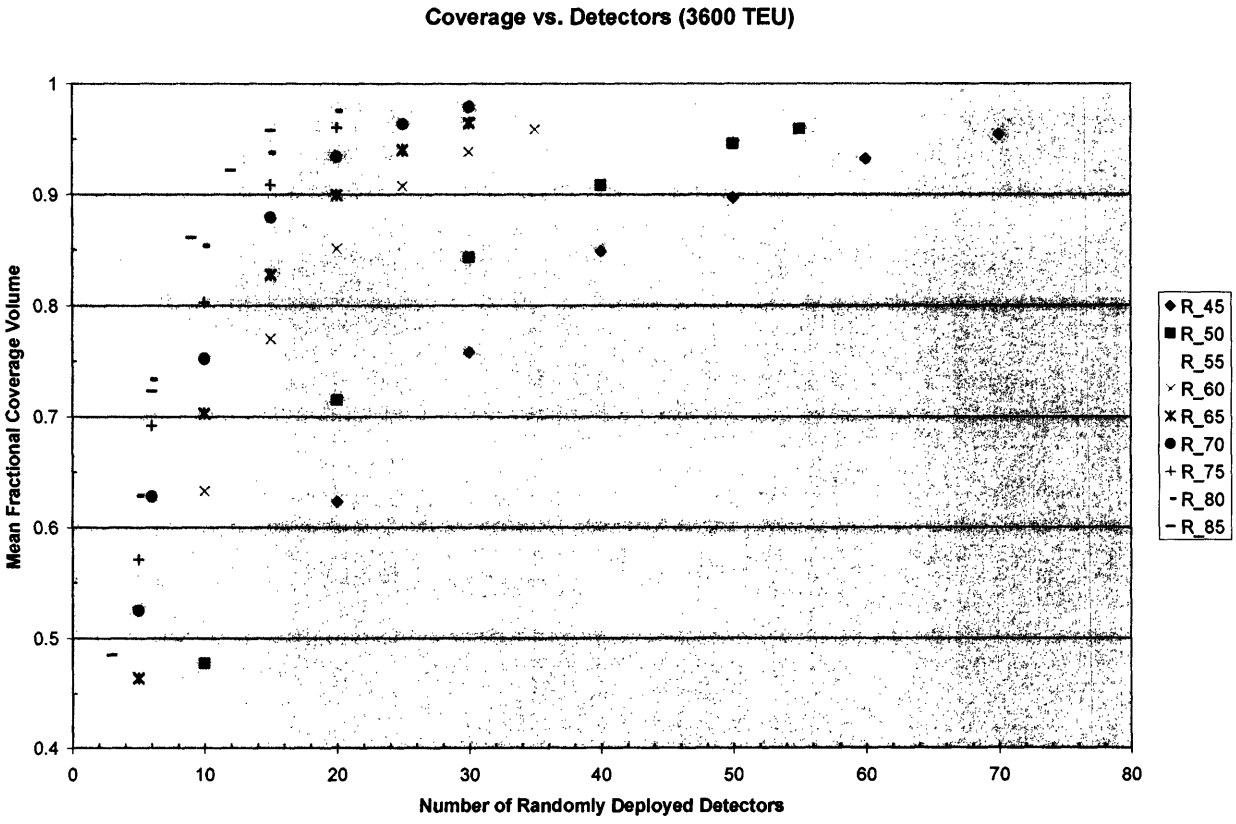

Figure 5-5: Coverage vs. Detectors plot for the 3600 TEU array [Random]

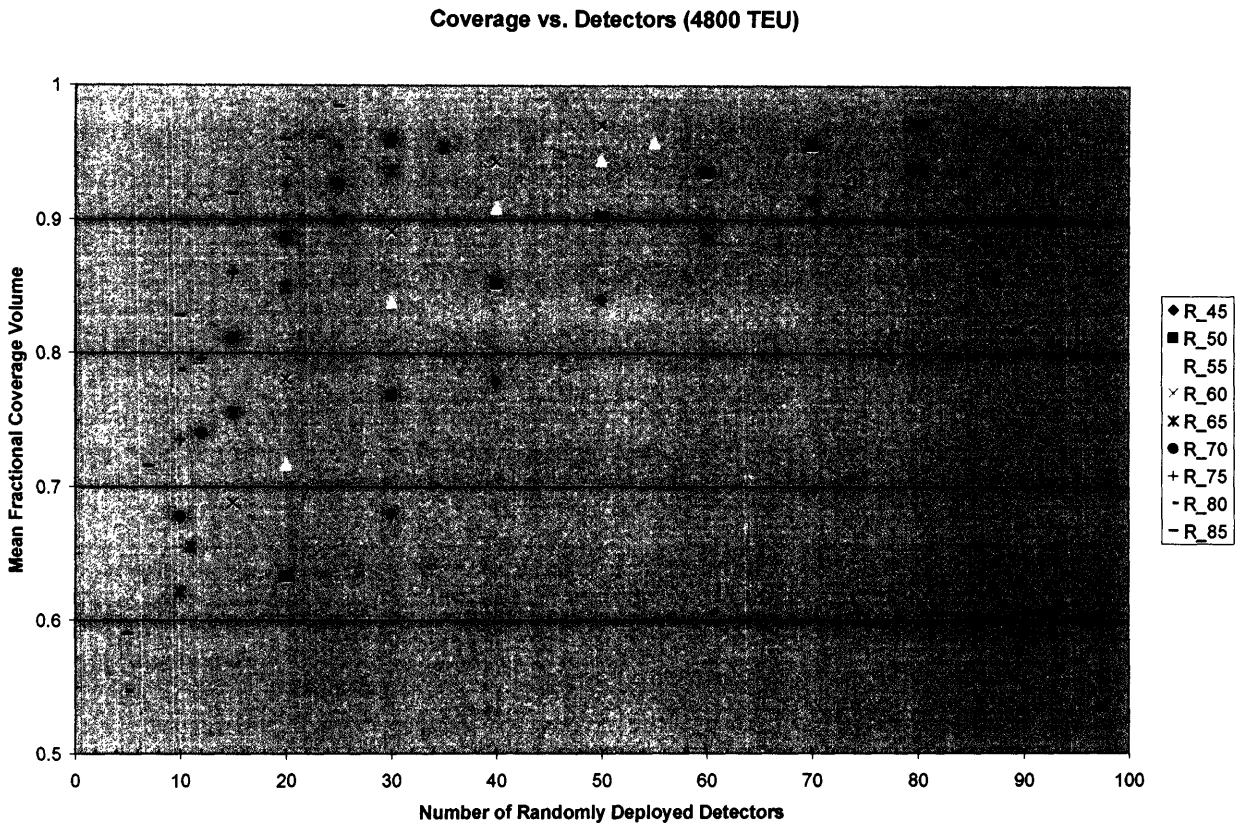

Figure 5-6: Coverage vs. Detectors plot for the 4800 TEU array [Random]

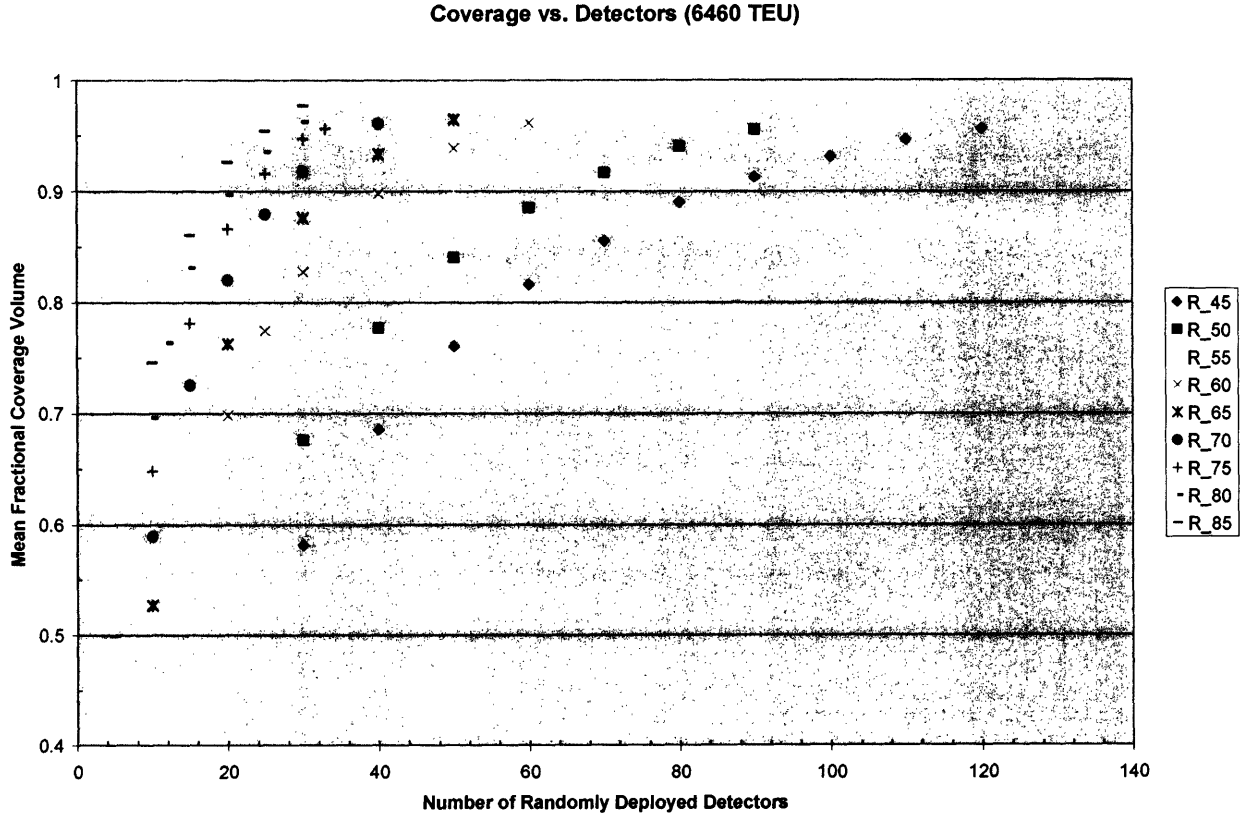

Figure 5-7: Coverage vs. Detectors plot for the 6460 TEU array [Random]

It is unclear what minimum acceptable level of detection coverage is appropriate, given the reality that it will not always be possible to provide 100% coverage of every containership and that attempting to do so will likely prove to be cost prohibitive. Acknowledging this uncertainty, all subsequent analysis will measure the system against three potential choices for minimum acceptable coverage. These three levels are 75%, 85%, and 95%.

To identify the number of detectors with a given range that are required to provide 75%, 85%, and 95% coverage for each of the 5 reference arrays, the mean fractional coverages for each simulated scenario were plotted and graphical techniques were employed. Figure 5-7 shows an example using the 1440 TEU reference array and detectors with a 65 ft. effective range (error bars represent $^{+}$/- 1 standard deviation).

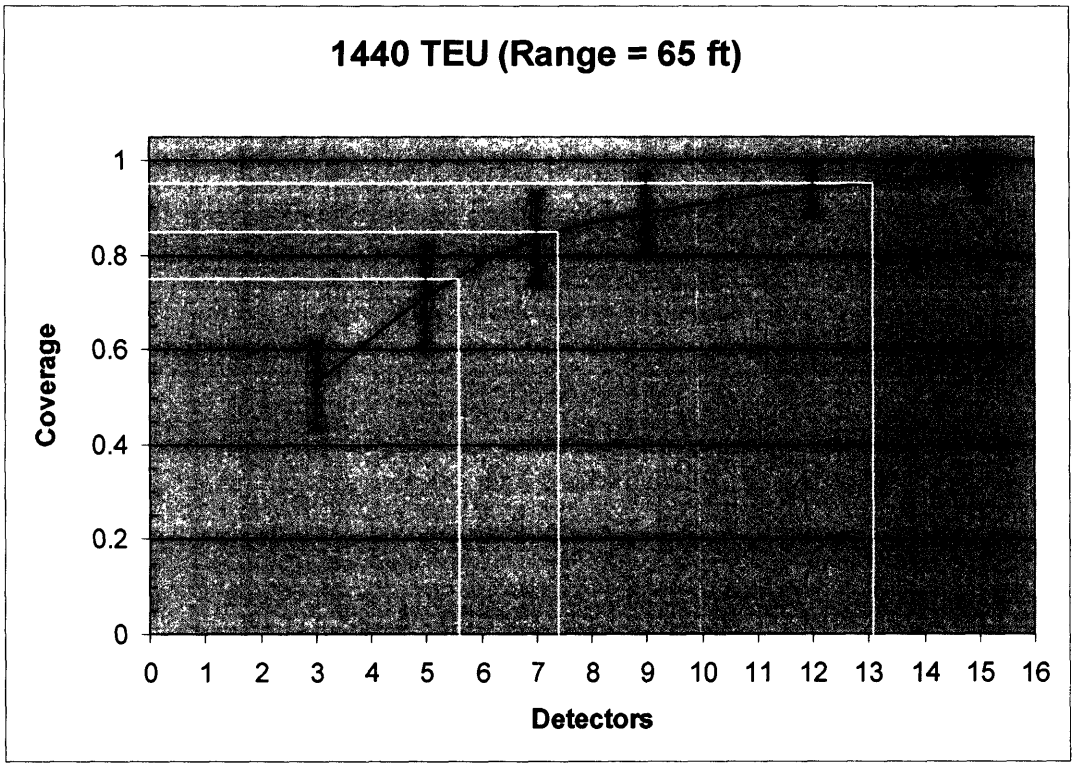

Figure 5-8: Graphical determination of detectors required for various coverage levels

For the example case illustrated in Figure 5-7, it was estimated that 75%, 85%, and 95% fractional detection coverage could be provided with 6, 8, and 14 detectors, respectively.

Results of these graphical analyses showing the estimated number of detectors needed to provide various levels of coverage for each scenario are listed in Table 5-6.

Table 5-6: Estimated number of detectors needed for various scenarios [Random]

Random Deployment		Reference Array Capacity (TEU)				
Range (ft)	Coverage	1440	2496	3600	4800	6460
45	0.75	13	21	30	37	59
	0.85	19	31	40	52	68
	0.95	32	50	69	88	117
50	0.75	11	17	22	29	37
	0.85	15	23	31	40	52
	0.95	25	39	53	69	88
55	0.75	9	13	18	23	30
	0.85	12	19	25	31	41
	0.95	19	30	41	53	70
60	0.75	7	11	15	18	24
	0.85	10	15	20	26	33
	0.95	15	25	34	43	55
65	0.75	6	9	12	15	20
	0.85	8	12	17	20	27
	0.95	14	21	27	34	45
70	0.75	5	8	10	13	16
	0.85	7	11	14	18	22
	0.95	11	18	23	29	38
75	0.75	5	7	9	11	14
	0.85	6	9	12	15	18
	0.95	10	15	19	24	31
80	0.75	4	6	8	9	12
	0.85	6	8	10	13	17
	0.95	9	14	17	21	29
85	0.75	4	5	7	8	10
	0.85	5	8	9	11	15
	0.95	8	12	15	19	25

One clear trend observed in the Figures above (particularly 5-2 through 5-6) are the diminishing returns in coverage afforded by the deployment of each additional detector, especially in the high coverage region (i.e. above around 0.80). It takes the addition of considerably more detectors to get from 85% to 95% coverage than it took to get from 75% to 85%. Using the scenario where detectors with a 65 ft. range were deployed in the 6460 TEU reference array as an example, it took 7 additional detectors to go from 75% to 85% coverage and 18 additional detectors to go from 85% to 95%.

The primary cause of this phenomenon is the fact that random deployment does not promise uniform distribution of detectors throughout a container array. As a result, randomized placement will unavoidably give rise to some well-covered regions with significant coverage overlap and some sparsely covered regions with little to no detection coverage. Detectors cannot be preferentially deployed to uncovered or inadequately covered areas. Therefore, to enhance the fractional coverage area with additional detectors, one must rely on the capricious nature of random placement to fortuitously deploy added units to sparsely covered regions. Inefficiencies associated with this process lead to the diminishing marginal returns observed in the simulation results. The extent to which random deployment is less efficient than optimal centerline deployment will be discussed in a later section.

Although the mechanism discussed above is the primary determinant, there is another factor at work in the deployment simulation that artificially magnifies the diminishing returns effect. Given that the simulation used for this analysis assumed that the center point of detectors could be placed at any point in space within the container array, there is a non-negligible probability, given by Eq. (9), that 2 detectors could be randomly assigned to the space that corresponds to a single container. The probability of this "double assignment" increases as the number of deployed detectors increases. Since double assignment is an inefficient distribution of detectors, it could make a small contribution to the diminishing returns effect. Table 5-7 shows the probability that any 2 detectors will be randomly assigned to the same 20' and 40' container volumes for a sampling of simulated scenarios.

Table 5-7: Double assignment probabilities for 20' and 40' containers [Random]

Capacity (TEU)	Detectors	Double Assign. Probability (20')	Double Assign. Probability (40')	Capacity (TEU)	Detectors	Double Assign. Probability (20')	Double Assign. Probability (40')
1440	3	0.002	0.004	3600	60	0.390	0.630
1440	5	0.007	0.014	3600	70	0.491	0.743
1440	10	0.031	0.061	4800	5	0.002	0.004
1440	15	0.071	0.137	4800	10	0.009	0.019
1440	20	0.124	0.234	4800	20	0.039	0.076
1440	25	0.189	0.344	4800	30	0.087	0.166
1440	30	0.262	0.458	4800	40	0.150	0.279
1440	35	0.341	0.568	4800	50	0.226	0.402
2496	3	0.001	0.002	4800	60	0.310	0.525
2496	5	0.004	0.008	4800	70	0.397	0.638
2496	10	0.018	0.036	4800	80	0.484	0.736
2496	15	0.041	0.081	4800	90	0.568	0.816
2496	20	0.074	0.142	6460	5	0.002	0.003
2496	25	0.114	0.215	6460	10	0.007	0.014
2496	30	0.161	0.296	6460	20	0.029	0.057
2496	39	0.258	0.451	6460	30	0.065	0.126
2496	47	0.353	0.584	6460	40	0.114	0.215
2496	52	0.414	0.660	6460	50	0.173	0.317
3600	3	0.001	0.002	6460	60	0.240	0.424
3600	5	0.003	0.006	6460	70	0.313	0.529
3600	10	0.012	0.025	6460	80	0.388	0.627
3600	20	0.052	0.101	6460	90	0.464	0.714
3600	30	0.114	0.216	6460	100	0.537	0.787
3600	40	0.195	0.354	6460	110	0.607	0.847
3600	50	0.290	0.497	6460	120	0.671	0.893

Table 5-7 shows the probability that any two detectors will be assigned to a single container becomes quite large as the number of deployed detectors gets large and in some extreme cases, double assignment is almost assured. Since this inefficient double assignment is non-physical, the fractional detection coverage output by the simulation will be marginally underestimated and the diminishing returns effect will be slightly exaggerated.

Another notable feature of the results captured in Table 5-6 is the strong relation between the number of detectors needed to provide a given fractional coverage level and the effective detection range of the deployed units. This dependence is illustrated in Figures 5-8 through 5-12 where the estimated number of detectors required for 75%, 85%, and 95% coverage are plotted against detection range for each of the 5 reference arrays.

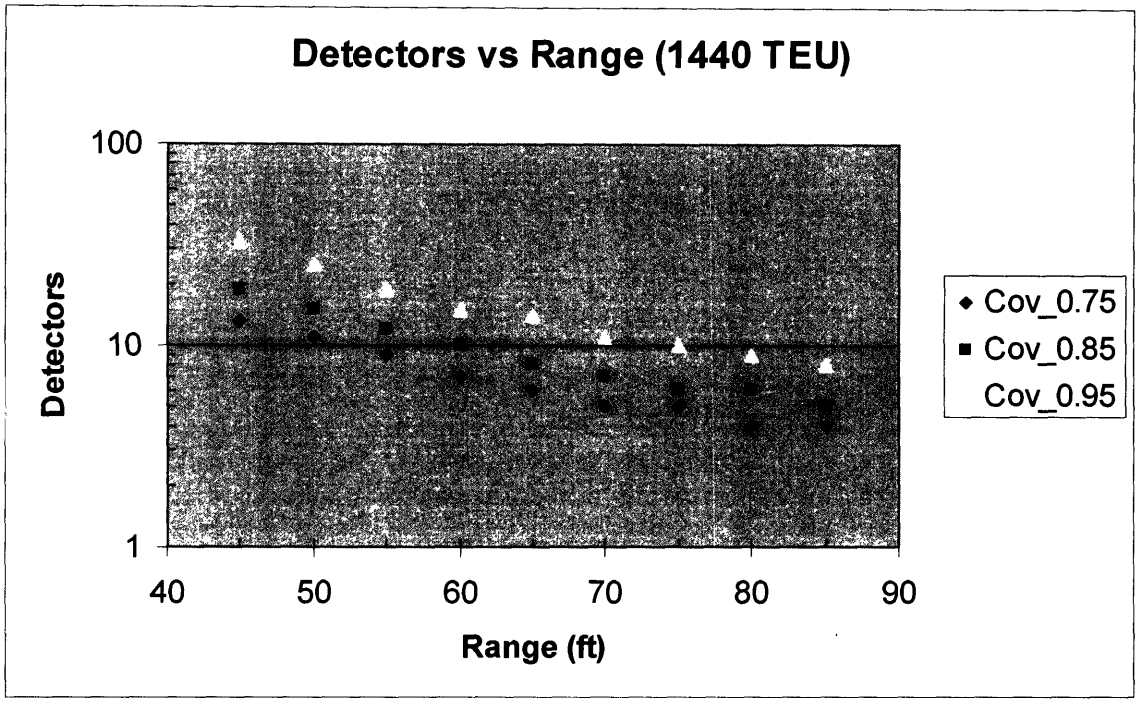

Figure 5-9: Required Detectors vs. Range for the 1440 TEU array [Random]

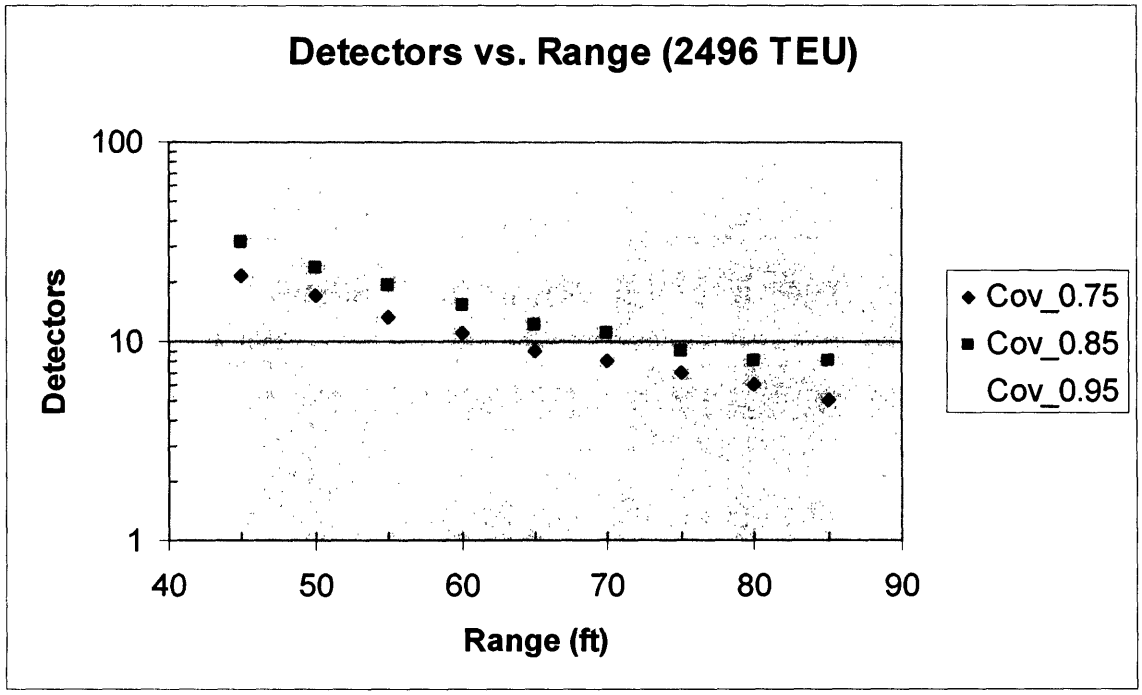

Figure 5-10: Required Detectors vs. Range for the 2496 TEU array [Random]

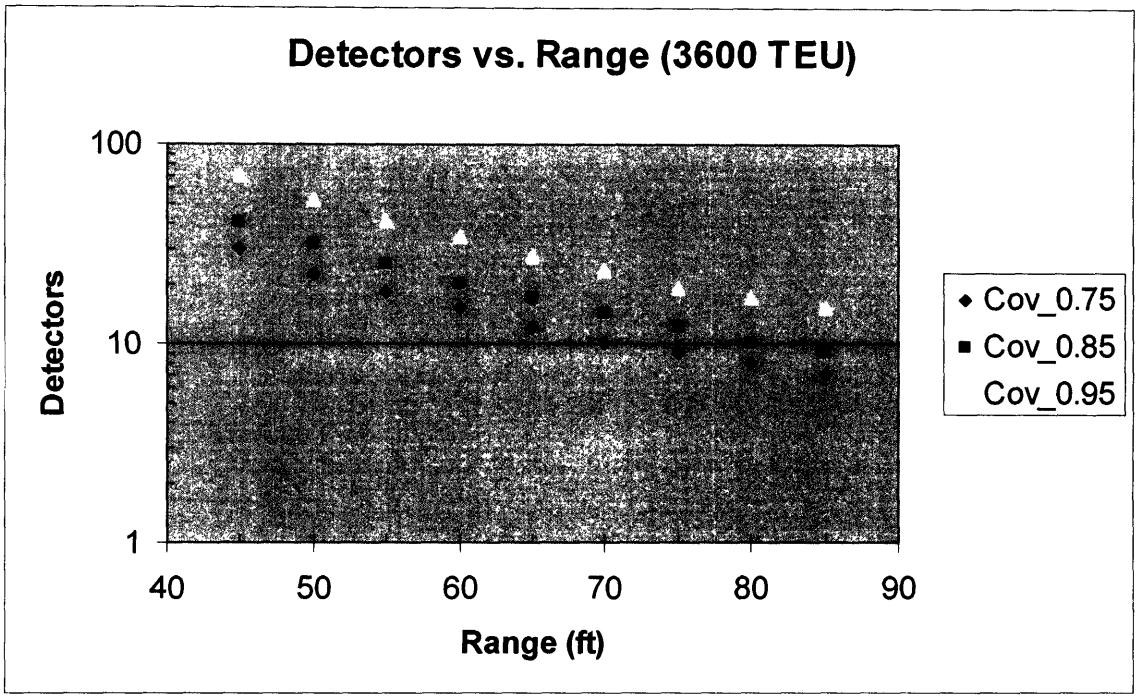

Figure 5-11: Required Detectors vs. Range for the 3600 TEU array [Random]

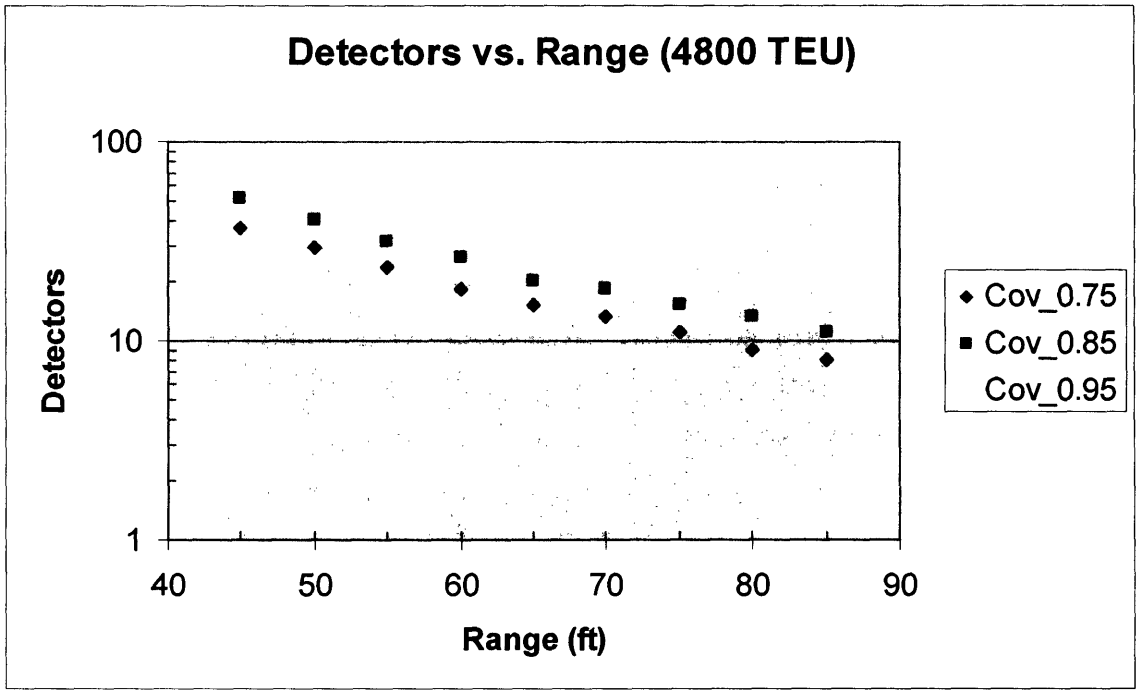

Figure 5-12: Required Detectors vs. Range for the 4800 TEU array [Random]

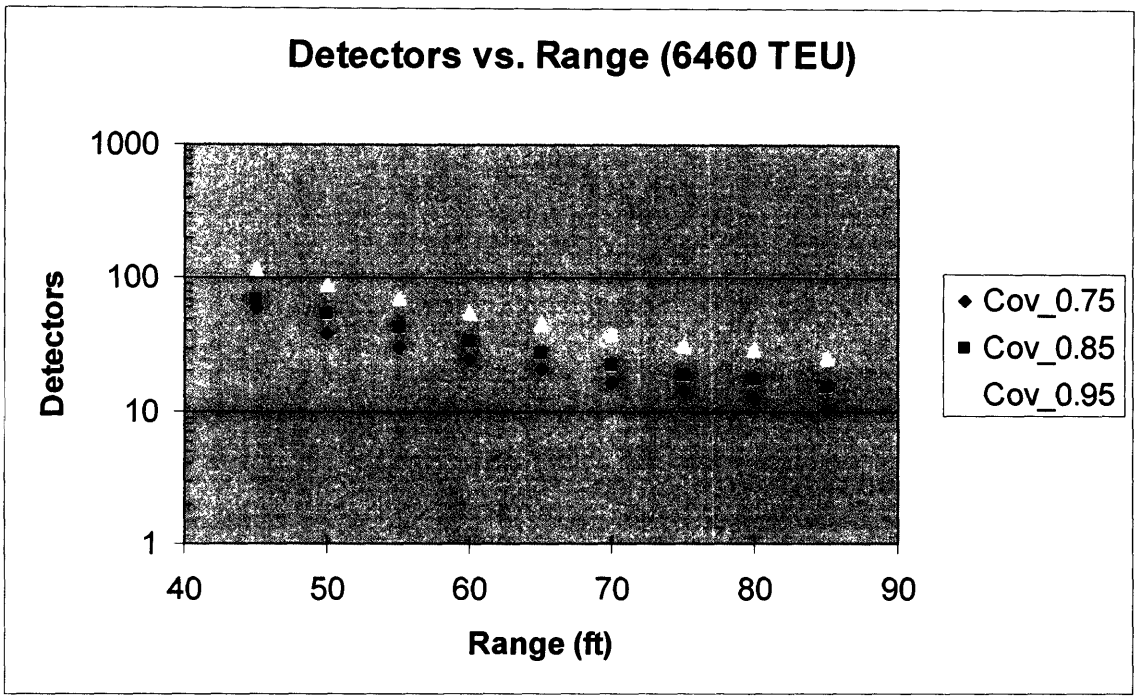

Figure 5-13: Required Detectors vs. Range for the 6460 TEU array [Random]

The pronounced "range effect" illustrated in Figures 5-8 through 5-12 can be explained by the relation between the effective detection range and the volume of coverage provided by a detection unit. Equation (12) shows that the volume of the idealized detection sphere increases as the cube of the effective detection radius. Therefore, the volume of a detection sphere created by a detector with an 85 ft. radius is 6.74 times greater than that of a detector with a 45 ft. radius. By covering a significantly larger detection volume per unit, fewer long-range detectors are needed, on average, to provide a given fractional coverage.

Finally, although the 6460 TEU reference array represents a larger container capacity than the 95th percentile vessel in the current fleet, it is likely that the trend to build and deploy larger and larger containerships will continue in the coming years until capacities exceed 10000 TEU [Ircha, 2002]. Figures 5-13 through 5-17 plot the number of detectors needed for given coverage levels versus vessel capacity for a representative sampling of ranges.

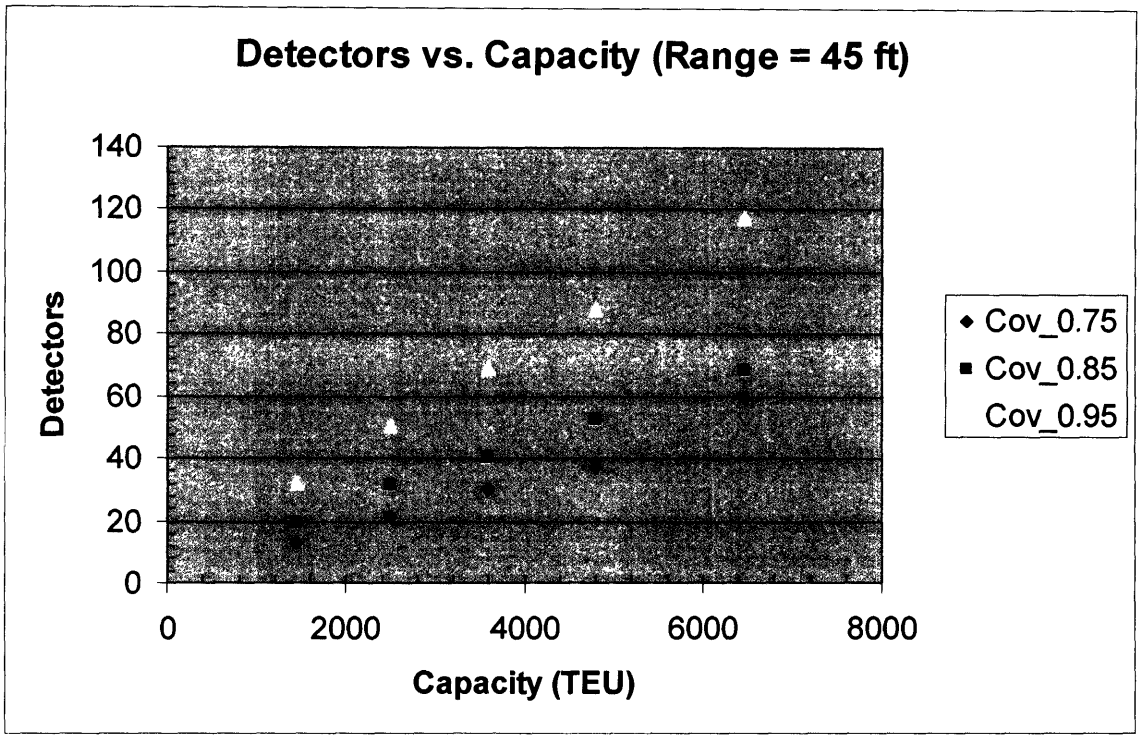

Figure 5-14: Required Detectors (with 45 ft. range) vs. Array Capacity [Random]

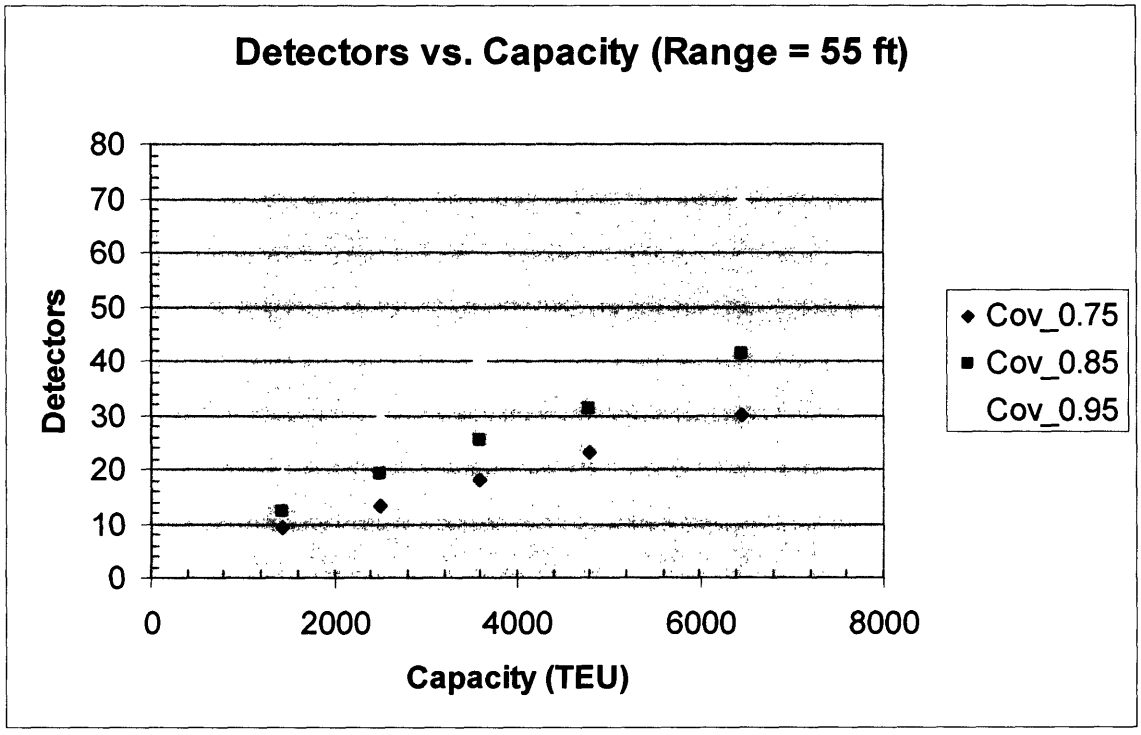

Figure 5-15: Required Detectors (with 55 ft. range) vs. Array Capacity [Random]

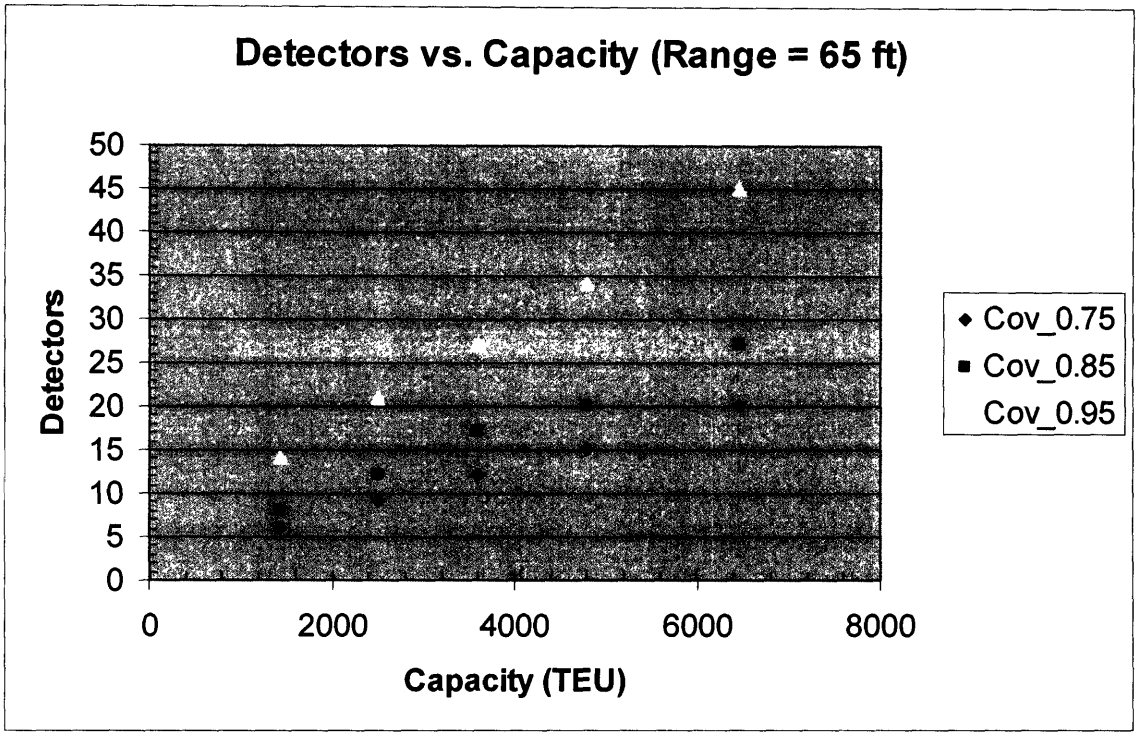

Figure 5-16: Required Detectors (with 65 ft. range) vs. Array Capacity [Random]

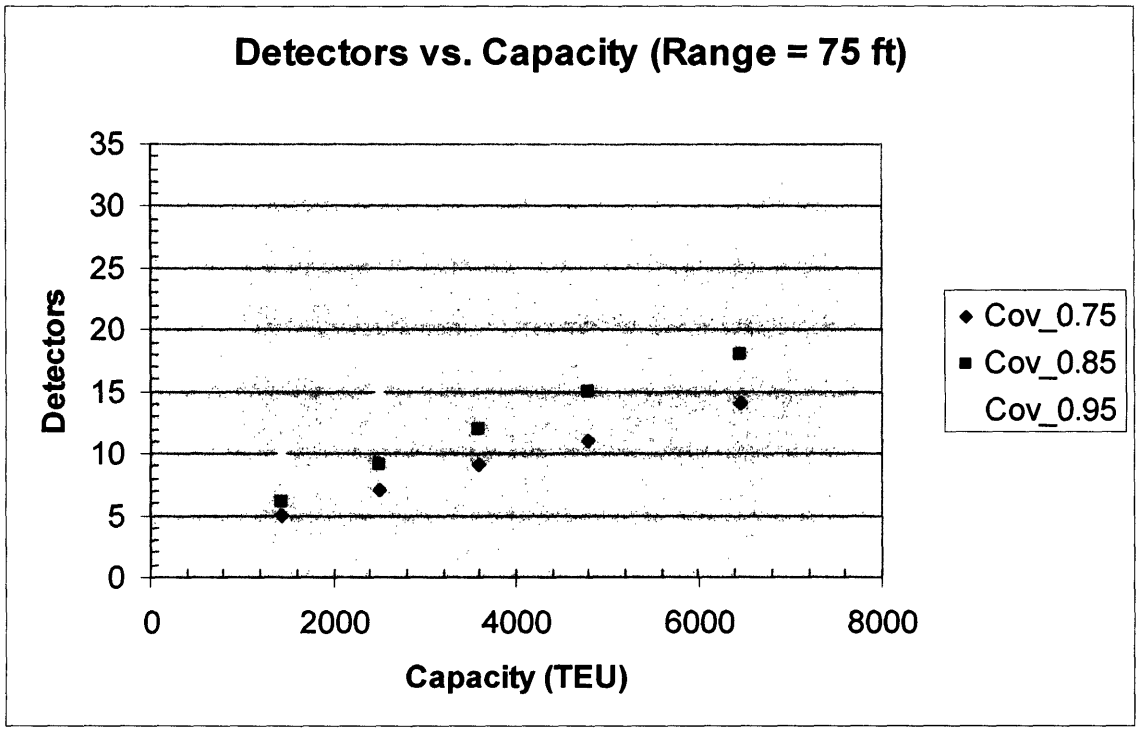

Figure 5-17: Required Detectors (with 75 ft. range) vs. Array Capacity [Random]

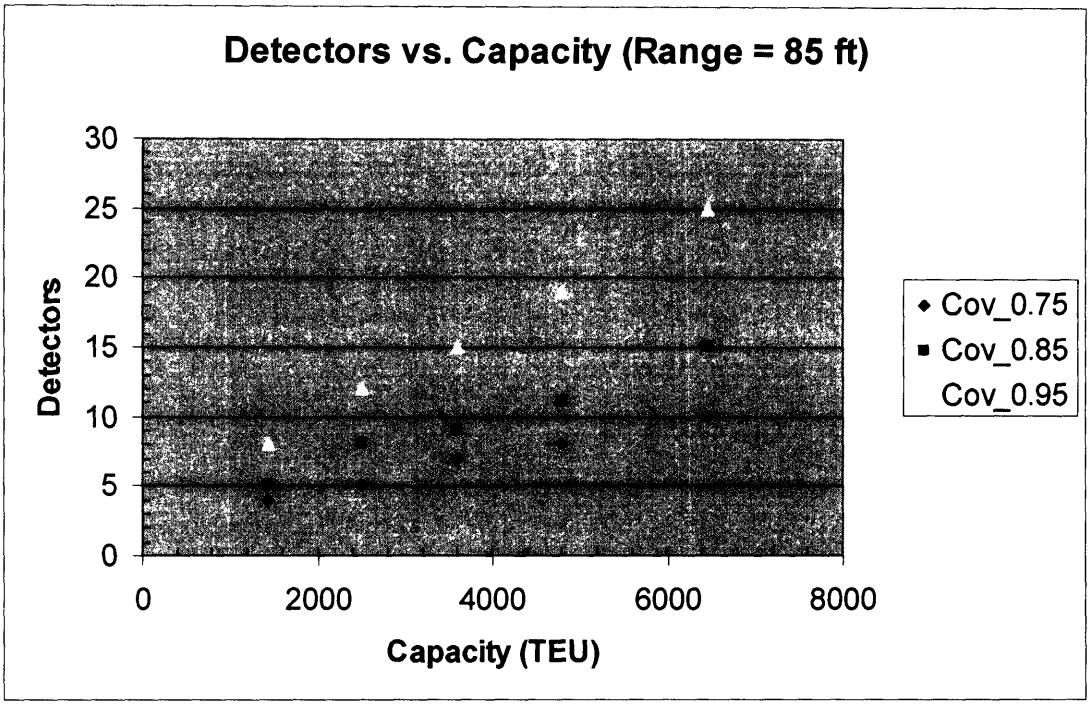

Figure 5-18: Required Detectors (with 85 ft. range) vs. Array Capacity [Random]

Figures 5-13 through 5-17 show relationships between the number of required detectors and vessel container capacities that are linear to a very good approximation. This linearity could be used in the future to estimate the number of detectors needed to provide coverage of proposed vessels with capacities exceeding those of containerships in the fleet today.

5.4 Constrained Deployment

Deviation from random deployment could challenge and potentially comprise the desired surreptitious nature of the ship-based approach and invite serious logistical difficulties. However, given the coverage inefficiencies that are an unavoidable consequence of completely random deployment, the constrained deployment strategy was investigated to determine the efficiency gains that could be reaped by imposing minimum loading constraints. In an effort to limit the undesirable and inefficient situation in which detectors are placed close to the edge or surface of the container array, the constrained

deployment simulation explicitly barred the assignment of detectors to space that corresponded to the first or last (TEU) container in any row, column, or span of the array. It is unclear whether even this limited constraint would be possible to impose in practice.

Constrained deployment simulation was carried out in the same manner as described above for random deployment. The only modification to the simulation schedule was the exclusion of scenarios with detectors having 45 ft. and 85 ft. effective ranges. Limited computing resources necessitated the tailoring of the simulation schedule and the excised scenarios were the most computationally intensive[11]. Table 5-8 shows the output statistics for constrained simulations.

[11] 45 ft. range scenarios were intensive due to the large number of detectors that had to be deployed to achieve desired fractional coverages. 85 ft. range scenarios were intensive because of the large number of computations required to construct their detection spheres.

Table 5-8: Constrained deployment simulation results

Capacity (TEU)	Specific Geometry width (cont)	height (cont)	length (cont)	Range (ft)	Detection Units	Coverage Statistics Mean	Median	Std. Dev.	Min	Max	Runs
1440	9	8	20	50	5	0.5894	0.5893	0.0707	0.4263	0.8495	200
1440	9	8	20	50	8	0.7295	0.7349	0.0922	0.2961	0.9292	200
1440	9	8	20	50	11	0.8309	0.8431	0.0726	0.4976	0.9554	200
1440	9	8	20	50	14	0.885	0.8929	0.0572	0.6397	0.9827	200
1440	9	8	20	50	17	0.9167	0.9308	0.0531	0.6639	0.9883	200
1440	9	8	20	50	21	0.9519	0.9617	0.0332	0.8216	0.9963	200
1440	9	8	20	50	24	0.9619	0.9715	0.0319	0.7597	0.995	200
1440	9	8	20	55	5	0.6446	0.6435	0.0921	0.404	0.8587	200
1440	9	8	20	55	8	0.7974	0.8024	0.091	0.5096	0.9709	200
1440	9	8	20	55	11	0.8786	0.8853	0.0699	0.5955	0.9798	200
1440	9	8	20	55	14	0.9219	0.9418	0.0599	0.7143	0.9969	200
1440	9	8	20	55	17	0.9479	0.9623	0.0474	0.7405	0.9986	200
1440	9	8	20	55	20	0.9633	0.9774	0.0433	0.7319	0.9996	200
1440	9	8	20	60	5	0.7096	0.7194	0.1036	0.3249	0.9107	200
1440	9	8	20	60	8	0.8574	0.8838	0.0851	0.5651	0.99	200
1440	9	8	20	60	11	0.9151	0.936	0.0709	0.6208	0.9947	200
1440	9	8	20	60	14	0.947	0.966	0.0537	0.6923	0.9994	200
1440	9	8	20	60	17	0.9666	0.9817	0.0402	0.7232	0.9999	200
1440	9	8	20	65	4	0.6941	0.7041	0.107	0.3183	0.9225	200
1440	9	8	20	65	5	0.7521	0.7568	0.1207	0.3912	0.9852	200
1440	9	8	20	65	8	0.8931	0.914	0.0926	0.5764	0.9988	200
1440	9	8	20	65	11	0.9504	0.9744	0.0572	0.7274	0.9998	200
1440	9	8	20	65	14	0.9641	0.9853	0.0499	0.7591	1	200
1440	9	8	20	70	3	0.631	0.6421	0.1198	0.3177	0.8896	200
1440	9	8	20	70	5	0.7844	0.7948	0.1073	0.4709	0.9884	200
1440	9	8	20	70	7	0.8807	0.9008	0.1031	0.494	0.9998	200
1440	9	8	20	70	9	0.9302	0.9602	0.0792	0.5846	1	200
1440	9	8	20	70	11	0.9545	0.9844	0.0653	0.6535	1	200
1440	9	8	20	75	3	0.6607	0.6702	0.1251	0.2978	0.9542	200
1440	9	8	20	75	5	0.8351	0.8505	0.1158	0.3682	0.9999	200
1440	9	8	20	75	7	0.9053	0.9335	0.0896	0.512	1	200
1440	9	8	20	75	9	0.9496	0.9788	0.0693	0.6389	1	200
1440	9	8	20	75	11	0.9609	0.9929	0.0597	0.6951	1	200

1440	9	8	20	80	3	0.7195	0.7206	0.1365	0.408	0.9714	200
1440	9	8	20	80	5	0.844	0.8619	0.1141	0.4884	0.9997	200
1440	9	8	20	80	7	0.9229	0.9522	0.0866	0.5527	1	200
1440	9	8	20	80	9	0.9542	0.9845	0.0617	0.6645	1	200
1440	9	8	20	80	11	0.9762	0.999	0.05	0.6821	1	200
2496	12	8	26	50	10	0.6353	0.6399	0.0671	0.4337	0.7705	200
2496	12	8	26	50	15	0.7713	0.7783	0.0559	0.581	0.8819	200
2496	12	8	26	50	20	0.8464	0.856	0.0506	0.667	0.9349	200
2496	12	8	26	50	25	0.8983	0.9054	0.0391	0.7529	0.9667	200
2496	12	8	26	50	30	0.929	0.9362	0.0314	0.8241	0.9842	200
2496	12	8	26	50	35	0.9448	0.9504	0.0288	0.8408	0.9904	200
2496	12	8	26	50	40	0.9585	0.9617	0.0227	0.8729	0.9953	200
2496	12	8	26	55	10	0.7088	0.7223	0.0792	0.4235	0.8565	200
2496	12	8	26	55	15	0.8356	0.8458	0.0613	0.6644	0.9662	200
2496	12	8	26	55	20	0.8977	0.9036	0.0437	0.7509	0.9779	200
2496	12	8	26	55	25	0.9392	0.948	0.0362	0.7393	0.9948	200
2496	12	8	26	55	30	0.9577	0.9639	0.0271	0.875	0.9951	200
2496	12	8	26	60	5	0.5377	0.5408	0.0787	0.3036	0.7045	200
2496	12	8	26	60	10	0.7852	0.7833	0.0761	0.5901	0.9519	200
2496	12	8	26	60	15	0.8856	0.8913	0.0543	0.6554	0.9851	200
2496	12	8	26	60	20	0.9368	0.9425	0.0379	0.8052	0.99	200
2496	12	8	26	60	25	0.9618	0.9731	0.0319	0.8403	0.9989	200
2496	12	8	26	65	5	0.5931	0.6009	0.0918	0.3189	0.8411	200
2496	12	8	26	65	10	0.8305	0.8392	0.0786	0.5694	0.9651	200
2496	12	8	26	65	15	0.9162	0.9296	0.0545	0.7165	0.9925	200
2496	12	8	26	65	20	0.9578	0.9681	0.0375	0.7825	0.999	200
2496	12	8	26	65	25	0.9769	0.9844	0.0248	0.8426	0.9999	200
2496	12	8	26	70	5	0.6471	0.6524	0.099	0.3393	0.8798	250
2496	12	8	26	70	10	0.8641	0.8843	0.0848	0.617	0.9876	200
2496	12	8	26	70	15	0.9426	0.9579	0.0497	0.7437	1	200
2496	12	8	26	70	20	0.9714	0.9835	0.0346	0.7802	1	200
2496	12	8	26	70	25	0.9859	0.9933	0.0196	0.8736	1	200
2496	12	8	26	75	5	0.6881	0.6903	0.106	0.3685	0.9176	200
2496	12	8	26	75	8	0.8409	0.8523	0.0903	0.4838	0.9852	200
2496	12	8	26	75	11	0.9089	0.9213	0.0706	0.6551	0.9988	200
2496	12	8	26	75	14	0.9539	0.9697	0.0462	0.7803	1	200
2496	12	8	26	80	5	0.7439	0.7529	0.1159	0.3937	0.9857	200

2496	12	8	26	80	8	0.8748	0.8905	0.0845	0.5871	0.9959	200
2496	12	8	26	80	11	0.9291	0.9564	0.074	0.5976	0.9999	200
2496	12	8	26	80	14	0.9611	0.9822	0.0498	0.741	1	200
3600	12	10	30	50	10	0.5282	0.531	0.0504	0.3553	0.6525	200
3600	12	10	30	50	20	0.7606	0.7664	0.0473	0.624	0.8773	200
3600	12	10	30	50	30	0.8657	0.8687	0.0356	0.7543	0.9515	200
3600	12	10	30	50	40	0.9209	0.9247	0.0266	0.8314	0.975	200
3600	12	10	30	50	50	0.9495	0.9532	0.0214	0.8662	0.9856	200
3600	12	10	30	50	55	0.9597	0.9631	0.0199	0.8763	0.9897	200
3600	12	10	30	55	10	0.6168	0.6208	0.0648	0.4349	0.7438	200
3600	12	10	30	55	20	0.8315	0.8353	0.0458	0.7121	0.9387	200
3600	12	10	30	55	30	0.9133	0.9142	0.0326	0.7648	0.9718	200
3600	12	10	30	55	40	0.9532	0.9599	0.0265	0.8352	0.9933	200
3600	12	10	30	55	50	0.9737	0.9785	0.0176	0.8576	0.9965	200
3600	12	10	30	60	10	0.6935	0.6977	0.0658	0.459	0.8387	200
3600	12	10	30	60	15	0.8175	0.8214	0.0558	0.6277	0.9489	200
3600	12	10	30	60	20	0.8792	0.8879	0.0494	0.7415	0.9668	200
3600	12	10	30	60	25	0.9276	0.9366	0.0363	0.785	0.9797	200
3600	12	10	30	60	30	0.9484	0.9565	0.0326	0.7803	0.9908	200
3600	12	10	30	60	35	0.9669	0.9718	0.0218	0.8742	0.9955	200
3600	12	10	30	65	10	0.7385	0.7541	0.0854	0.4998	0.9241	200
3600	12	10	30	65	15	0.8631	0.8727	0.0594	0.6878	0.9674	200
3600	12	10	30	65	20	0.9252	0.9318	0.0426	0.7305	0.993	200
3600	12	10	30	65	25	0.9525	0.963	0.0351	0.7809	0.9965	200
3600	12	10	30	70	5	0.5541	0.5599	0.0886	0.3103	0.7426	200
3600	12	10	30	70	7	0.6815	0.6907	0.0863	0.4187	0.8846	200
3600	12	10	30	70	10	0.8045	0.8169	0.0816	0.5283	0.9426	200
3600	12	10	30	70	15	0.9022	0.9162	0.0572	0.6775	0.9823	200
3600	12	10	30	70	20	0.9503	0.9578	0.038	0.7629	0.9972	200
3600	12	10	30	75	5	0.6253	0.6354	0.0962	0.3183	0.8485	200
3600	12	10	30	75	7	0.7333	0.7432	0.0966	0.4452	0.9415	200
3600	12	10	30	75	10	0.8376	0.8557	0.0956	0.4776	0.9826	200
3600	12	10	30	75	15	0.9224	0.9426	0.0604	0.7042	0.9979	200
3600	12	10	30	75	20	0.965	0.9802	0.037	0.7967	0.9996	200
3600	12	10	30	80	5	0.6674	0.6767	0.1057	0.2881	0.8927	200
3600	12	10	30	80	7	0.7827	0.7997	0.1012	0.428	0.9765	200
3600	12	10	30	80	10	0.8727	0.8902	0.0807	0.5687	0.985	200

3600	12	10	30	80	15	0.9532	0.9722	0.0482	0.7262	0.9993	200
3600	12	10	30	80	20	0.9708	0.9859	0.0409	0.6676	1	200
4800	15	10	32	50	20	0.6794	0.6822	0.0442	0.5536	0.7857	200
4800	15	10	32	50	30	0.808	0.8108	0.0351	0.7103	0.8958	200
4800	15	10	32	50	40	0.876	0.8783	0.0314	0.7861	0.941	200
4800	15	10	32	50	50	0.9162	0.9183	0.0234	0.8448	0.9614	200
4800	15	10	32	50	60	0.9418	0.9448	0.0218	0.86	0.9804	200
4800	15	10	32	50	65	0.9496	0.9528	0.0197	0.8841	0.9862	200
4800	15	10	32	50	70	0.9574	0.9606	0.0171	0.9049	0.9859	200
4800	15	10	32	55	15	0.6661	0.6711	0.0535	0.4997	0.7936	200
4800	15	10	32	55	20	0.7565	0.7588	0.047	0.5994	0.863	200
4800	15	10	32	55	30	0.8654	0.8703	0.0393	0.7212	0.9522	200
4800	15	10	32	55	40	0.9214	0.9255	0.0269	0.822	0.9652	200
4800	15	10	32	55	50	0.9507	0.955	0.0248	0.7755	0.9905	200
4800	15	10	32	60	15	0.7379	0.7411	0.0572	0.5806	0.8643	200
4800	15	10	32	60	20	0.8279	0.8349	0.0467	0.6626	0.9123	200
4800	15	10	32	60	30	0.9122	0.9167	0.0334	0.781	0.9771	200
4800	15	10	32	60	40	0.9518	0.9546	0.0225	0.8703	0.9901	200
4800	15	10	32	60	50	0.9719	0.9737	0.0162	0.863	0.9969	200
4800	15	10	32	65	10	0.6735	0.6844	0.0694	0.4289	0.8163	200
4800	15	10	32	65	15	0.7993	0.8001	0.0549	0.6308	0.9063	200
4800	15	10	32	65	20	0.8789	0.8834	0.0431	0.7329	0.9593	200
4800	15	10	32	65	25	0.9211	0.9269	0.0384	0.758	0.9872	200
4800	15	10	32	65	30	0.9434	0.9486	0.032	0.8038	0.9937	200
4800	15	10	32	65	35	0.961	0.9676	0.0258	0.8299	0.9975	200
4800	15	10	32	70	10	0.7268	0.7281	0.0777	0.4505	0.91	200
4800	15	10	32	70	15	0.8396	0.8475	0.0638	0.6156	0.9649	200
4800	15	10	32	70	20	0.9047	0.9124	0.0444	0.7838	0.9814	200
4800	15	10	32	70	25	0.9395	0.9499	0.0389	0.7419	0.9942	200
4800	15	10	32	70	30	0.9637	0.9713	0.0261	0.8593	0.9981	200
4800	15	10	32	75	5	0.5426	0.5491	0.0795	0.2932	0.7569	200
4800	15	10	32	75	10	0.7681	0.7735	0.0702	0.5733	0.9258	200
4800	15	10	32	75	15	0.8829	0.895	0.067	0.6283	0.9815	200
4800	15	10	32	75	20	0.9379	0.9459	0.0385	0.7916	0.995	200
4800	15	10	32	75	25	0.9625	0.971	0.0332	0.8197	0.9988	200
4800	15	10	32	80	5	0.5906	0.5966	0.0902	0.2934	0.7738	200
4800	15	10	32	80	10	0.8229	0.8296	0.0752	0.5624	0.9824	200

4800	15	10	32	80	15	0.9119	0.9275	0.0563	0.7379	0.9913	200
4800	15	10	32	80	20	0.9532	0.9671	0.0392	0.8112	0.9992	200
4800	15	10	32	80	25	0.9741	0.9833	0.0295	0.8222	1	200
6460	17	10	38	50	30	0.7231	0.7249	0.0372	0.6076	0.8117	200
6460	17	10	38	50	40	0.8075	0.8097	0.0294	0.7135	0.8645	200
6460	17	10	38	50	50	0.8606	0.8622	0.0283	0.7797	0.9257	200
6460	17	10	38	50	60	0.9004	0.9034	0.0253	0.8102	0.9592	200
6460	17	10	38	50	70	0.922	0.9258	0.0215	0.859	0.9962	200
6460	17	10	38	50	80	0.9437	0.9456	0.0168	0.8621	0.9794	200
6460	17	10	38	50	90	0.9561	0.9571	0.0139	0.9038	0.9846	200
6460	17	10	38	55	20	0.6692	0.6704	0.0452	0.5223	0.7702	200
6460	17	10	38	55	30	0.7985	0.7989	0.0343	0.6942	0.8808	200
6460	17	10	38	55	40	0.866	0.8687	0.0332	0.7598	0.9413	200
6460	17	10	38	55	50	0.9119	0.9139	0.0269	0.8182	0.9752	200
6460	17	10	38	55	60	0.9396	0.9426	0.0202	0.8822	0.9841	200
6460	17	10	38	55	70	0.9574	0.9565	0.0152	0.9076	0.9861	200
6460	17	10	38	60	20	0.7462	0.7421	0.0468	0.5936	0.8476	200
6460	17	10	38	60	30	0.8553	0.8583	0.0409	0.6984	0.9415	200
6460	17	10	38	60	40	0.9187	0.9205	0.0268	0.8246	0.9789	200
6460	17	10	38	60	50	0.9487	0.9525	0.0205	0.8892	0.9867	200
6460	17	10	38	60	60	0.9661	0.9702	0.0179	0.9049	0.995	200
6460	17	10	38	65	10	0.573	0.5738	0.0589	0.3929	0.71	200
6460	17	10	38	65	20	0.795	0.7983	0.0555	0.5836	0.899	200
6460	17	10	38	65	30	0.9014	0.9043	0.0371	0.7821	0.9793	200
6460	17	10	38	65	40	0.9447	0.9513	0.0272	0.8438	0.9898	200
6460	17	10	38	65	50	0.9688	0.9727	0.0186	0.899	0.9953	200
6460	17	10	38	70	10	0.6352	0.6409	0.0652	0.4363	0.7643	200
6460	17	10	38	70	20	0.8452	0.8507	0.0519	0.6727	0.9515	200
6460	17	10	38	70	30	0.9276	0.933	0.0324	0.8283	0.991	200
6460	17	10	38	70	40	0.9666	0.9717	0.0221	0.874	0.9976	200
6460	17	10	38	75	10	0.6904	0.6881	0.0625	0.427	0.8258	200
6460	17	10	38	75	15	0.8105	0.8167	0.0622	0.6069	0.9205	200
6460	17	10	38	75	20	0.8853	0.8912	0.045	0.701	0.9681	200
6460	17	10	38	75	25	0.9249	0.9272	0.0394	0.7635	0.9932	200
6460	17	10	38	75	30	0.949	0.9574	0.0339	0.7827	0.9971	200
6460	17	10	38	75	35	0.9695	0.9772	0.0245	0.836	0.9985	200
6460	17	10	38	80	10	0.7348	0.7387	0.0761	0.4949	0.8916	200

6460	17	10	38	80	15	0.8512	0.8591	0.0614	0.6062	0.949	200
6460	17	10	38	80	20	0.9126	0.9216	0.0474	0.7372	0.9911	200
6460	17	10	38	80	25	0.9484	0.9547	0.032	0.8316	0.9971	200
6460	17	10	38	80	30	0.9656	0.9714	0.0248	0.8879	0.9995	200

For ease of inspection, the mean fractional coverage volumes for each scenario and reference array are plotted in Figures 5-18 through 5-22.

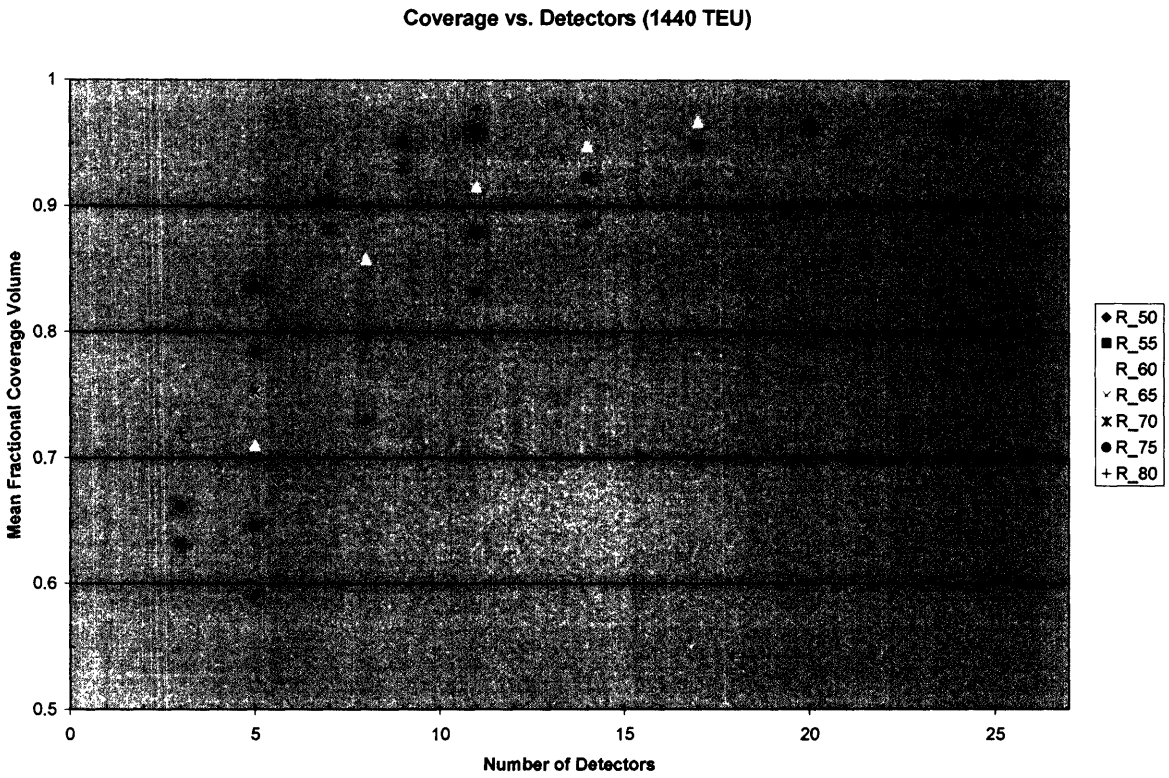

Figure 5-19: Coverage vs. Detectors plot for the 1440 TEU array [Constrained]

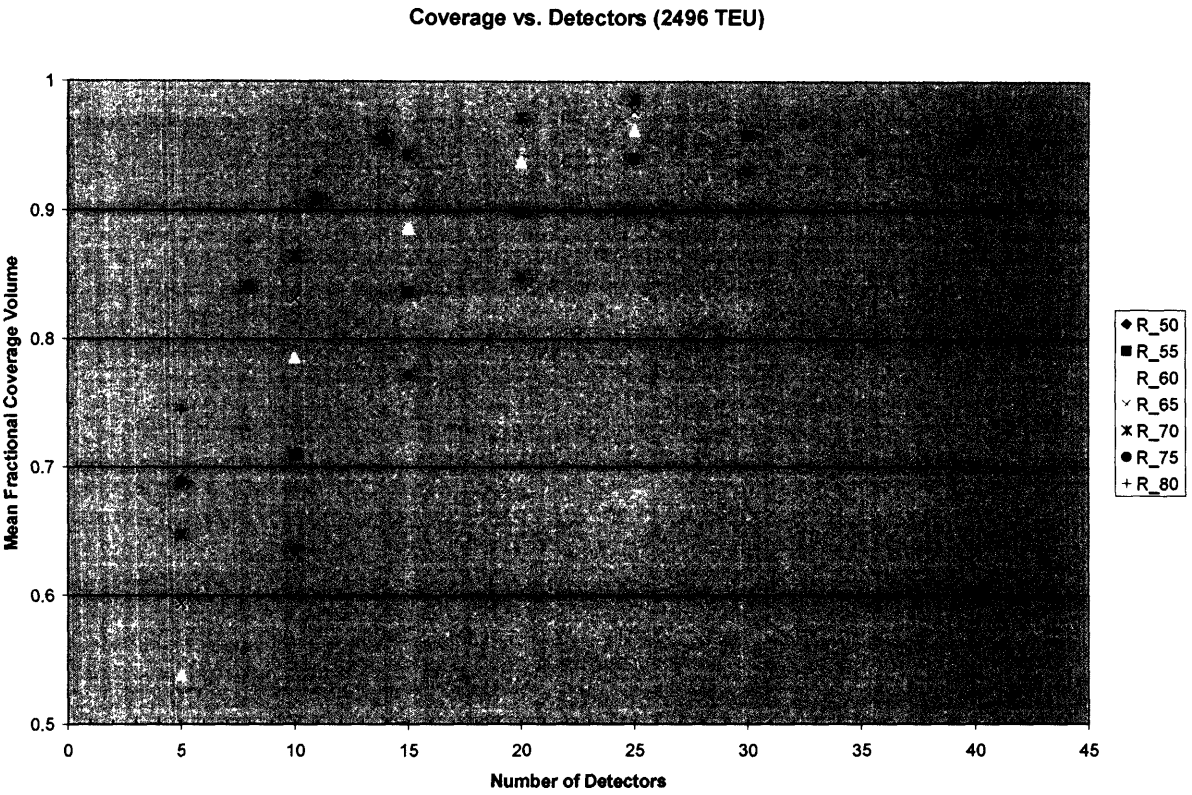

Figure 5-20: Coverage vs. Detectors plot for the 2496 TEU array [Constrained]

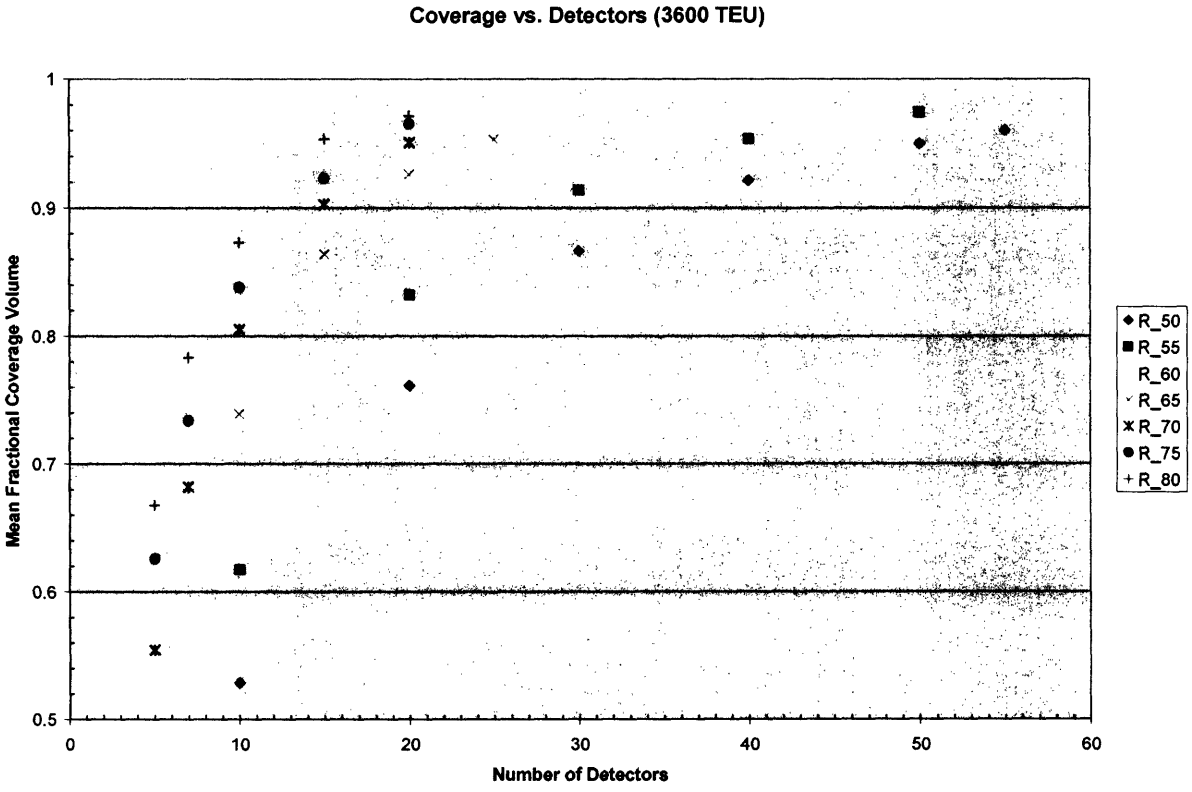

Figure 5-21: Coverage vs. Detectors plot for the 3600 TEU array [Constrained]

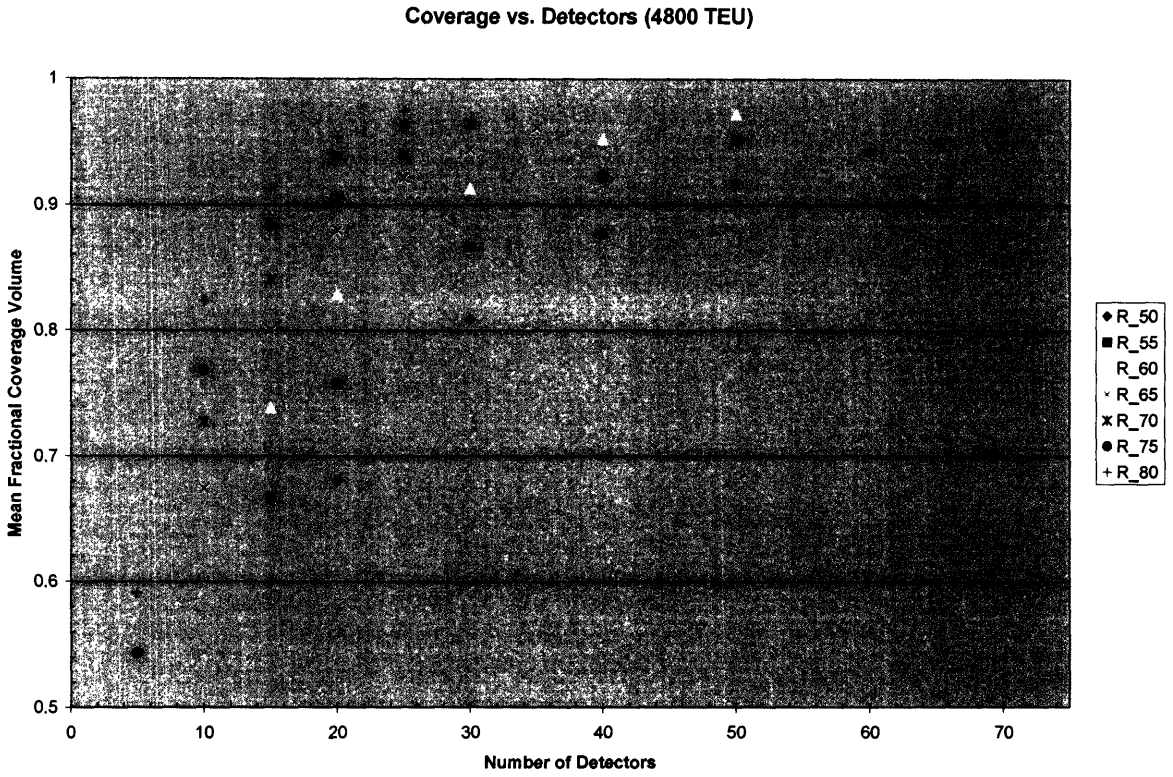

Figure 5-22: Coverage vs. Detectors plot for the 4800 TEU array [Constrained]

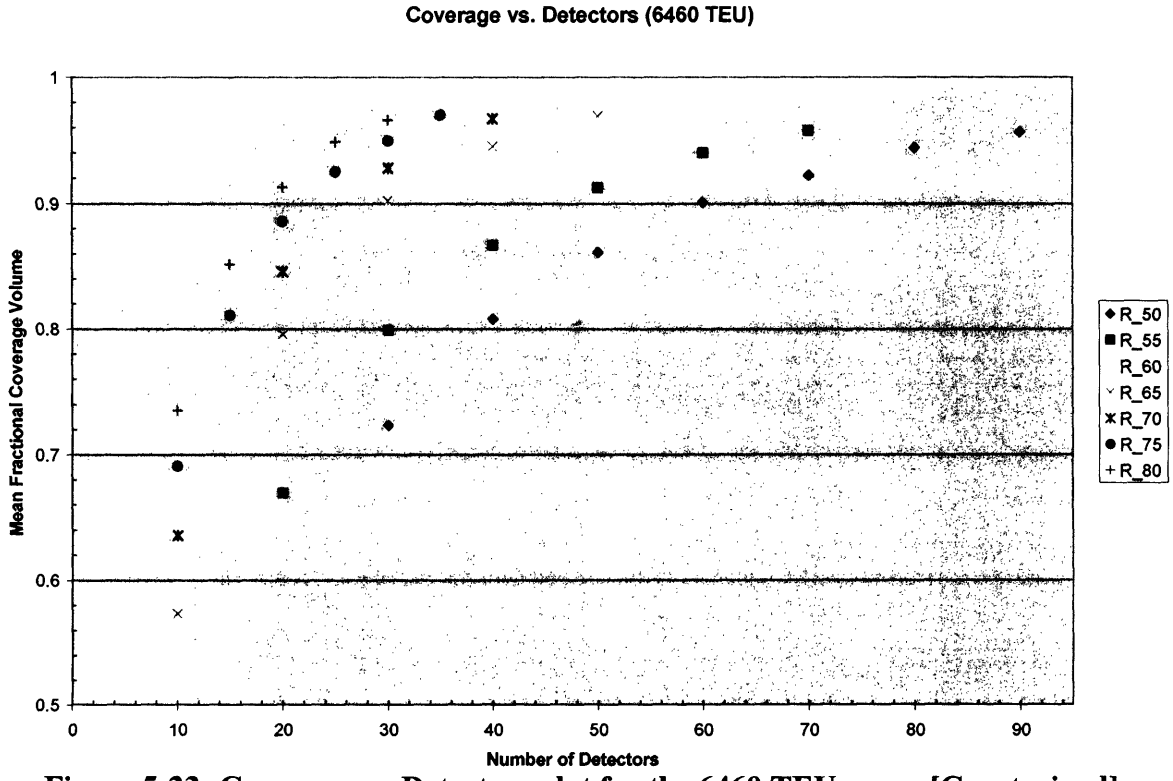

Figure 5-23: Coverage vs. Detectors plot for the 6460 TEU array [Constrained]

The number of detectors needed to provide 75%, 85%, and 95% coverage for each scenario were estimated in the same manner as described in the previous section and results are shown in Table 5-9.

Table 5-9: Estimated number of detectors needed for various scenarios [Constrained]

Constrained Deployment		Capacity (TEU)				
Range (ft)	Coverage	1440	2496	3600	4800	6460
50	0.75	9	14	20	25	33
	0.85	12	20	28	35	48
	0.95	21	38	51	65	86
55	0.75	7	12	16	20	26
	0.85	10	16	21	28	37
	0.95	18	28	39	50	65
60	0.75	6	9	12	15	21
	0.85	8	13	18	23	29
	0.95	15	23	31	40	51
65	0.75	5	8	11	13	18
	0.85	7	11	15	18	24
	0.95	11	19	25	32	43
70	0.75	5	8	9	11	15
	0.85	7	10	12	16	20
	0.95	11	16	20	28	36
75	0.75	4	7	8	10	15
	0.85	6	9	11	13	20
	0.95	9	14	18	23	35
80	0.75	4	6	7	9	11
	0.85	5	8	10	11	15
	0.95	9	13	15	20	26

When the numbers tabulated above for constrained deployment are compared to the random deployment results shown in Table 5-7, the differences are not particularly striking. Surprisingly, very little is gained in terms of coverage efficiency by constraining placement in containers along the surface of the array. It appears, that by excluding placement in such a large volume fraction of the total container array, that inefficient overlapping was promoted in the center. This seems to have offset efficiency gains that were realized by limiting coverage volume "losses" at the surface of the array. Double assignment effects also played a larger role in the constrained simulation because the (*xyz*) term in Eq. (9) was smaller due to the imposed placement constraint.

5.5 Centerline Deployment

Centerline deployment, where detectors are optimally distributed along the length of the middle row and column of the container array, is the least secure of the examined deployment strategies, in terms of concealing the location of detection units. It is also dubious as to whether this approach would be logistically feasible in practice. However, the completely constrained nature of this strategy does afford extremely efficient utilization of detector coverage. As a result, this deployment approach is useful for establishing a lower bound for the number of detectors that would be needed to cover a vessel with a given capacity. This lower bound can also be used to quantify the coverage efficiency losses resulting from full randomization.

Since the imposed constraints dictate that detectors could only be placed along the centerline of the reference arrays, the geometry of each scenario was uniquely specified so only one calculation (as opposed to multi-run Monte Carlo analysis) was needed to determine the coverage. For the purposes of these calculations, the centerline of each array was assumed to consist of 40' containers to more accurately model arrays encountered aboard actual containerships. It was further assumed that detectors were only placed in the center of these full-sized containers. The first scenario for each reference array would place a detector in each of the available full containers along the centerline. The next scenario would place detectors in every other container, then every third container, and so on. Sometimes using placement patterns of this fashion did not uniquely specify the arrangement of detectors. For example, if detectors are to be placed in every third full sized container and there are 15 containers along the length of the centerline, then the desired placement pattern can be realized with an equal number of detectors when the pattern is begun with a detector in the first, second, or third container in the line. Whenever there were degrees of freedom associated with which container to place the first detector in, the coverage for each available geometry was calculated and the arrangement with the highest coverage was used. The results of these calculations are shown in Table 5-10.

Table 5-10: Centerline deployment simulation results

Capacity (TEU)	Specific Geometry width (cont)	height (cont)	length (cont)	Range (ft)	40' Containers Along Length	Loading Pattern	Container w/ 1st Detector	Detection Units	Coverage
1440	9	8	20	45	10	Every	1st	10	0.9682
1440	9	8	20	45	10	Every 2nd	1st	5	0.7968
1440	9	8	20	45	10	Every 3rd	1st	4	0.6065
1440	9	8	20	45	10	Every 4th	1st	3	0.4720
1440	9	8	20	45	10	Every 5th	3rd	2	0.3398
1440	9	8	20	50	10	Every	1st	10	0.9961
1440	9	8	20	50	10	Every 2nd	1st	5	0.9008
1440	9	8	20	50	10	Every 3rd	1st	4	0.7100
1440	9	8	20	50	10	Every 4th	1st	3	0.5572
1440	9	8	20	50	10	Every 5th	3rd	2	0.4069
1440	9	8	20	55	10	Every	1st	10	1.0000
1440	9	8	20	55	10	Every 2nd	1st	5	0.9552
1440	9	8	20	55	10	Every 3rd	1st	4	0.8029
1440	9	8	20	55	10	Every 4th	1st	3	0.6345
1440	9	8	20	55	10	Every 5th	3rd	2	0.4686
1440	9	8	20	60	10	Every	1st	10	1.0000
1440	9	8	20	60	10	Every 2nd	1st	5	0.9794
1440	9	8	20	60	10	Every 3rd	1st	4	0.8906
1440	9	8	20	60	10	Every 4th	1st	3	0.7076
1440	9	8	20	60	10	Every 5th	3rd	2	0.5270
1440	9	8	20	65	10	Every	1st	10	1.0000
1440	9	8	20	65	10	Every 2nd	1st	5	0.9926
1440	9	8	20	65	10	Every 3rd	1st	4	0.9596
1440	9	8	20	65	10	Every 4th	1st	3	0.7764
1440	9	8	20	65	10	Every 5th	3rd	2	0.5839
1440	9	8	20	70	10	Every	1st	10	1.0000
1440	9	8	20	70	10	Every 2nd	1st	5	0.9985
1440	9	8	20	70	10	Every 3rd	1st	4	0.9926
1440	9	8	20	70	10	Every 4th	1st	3	0.8380
1440	9	8	20	70	10	Every 5th	3rd	2	0.6394
1440	9	8	20	75	10	Every	1st	10	1.0000
1440	9	8	20	75	10	Every 2nd	1st	5	0.9999
1440	9	8	20	75	10	Every 3rd	1st	4	0.9996

1440	9	8	20	75	10	Every 4th	1st	3	0.8939
1440	9	8	20	75	10	Every 5th	3rd	2	0.6940
1440	9	8	20	80	10	Every	1st	10	1.0000
1440	9	8	20	80	10	Every 2nd	1st	5	1.0000
1440	9	8	20	80	10	Every 3rd	1st	4	1.0000
1440	9	8	20	80	10	Every 4th	1st	3	0.9477
1440	9	8	20	80	10	Every 5th	3rd	2	0.7477
1440	9	8	20	85	10	Every	1st	10	1.0000
1440	9	8	20	85	10	Every 2nd	1st	5	1.0000
1440	9	8	20	85	10	Every 3rd	1st	4	1.0000
1440	9	8	20	85	10	Every 4th	1st	3	0.9870
1440	9	8	20	85	10	Every 5th	3rd	2	0.8011
2496	12	8	26	45	13	Every	1st	13	0.8099
2496	12	8	26	45	13	Every 2nd	1st	7	0.6803
2496	12	8	26	45	13	Every 3rd	1st	5	0.4829
2496	12	8	26	45	13	Every 4th	1st	4	0.3777
2496	12	8	26	45	13	Every 5th,	2nd	3	0.3154
2496	12	8	26	45	13	Every 7th	3rd	2	0.2103
2496	12	8	26	50	13	Every	1st	13	0.9055
2496	12	8	26	50	13	Every 2nd	1st	7	0.8131
2496	12	8	26	50	13	Every 3rd	1st	5	0.6019
2496	12	8	26	50	13	Every 4th	1st	4	0.4688
2496	12	8	26	50	13	Every 5th	2nd	3	0.3992
2496	12	8	26	50	13	Every 7th	3rd	2	0.2661
2496	12	8	26	55	13	Every	1st	13	0.9710
2496	12	8	26	55	13	Every 2nd	1st	7	0.9126
2496	12	8	26	55	13	Every 3rd	1st	5	0.7193
2496	12	8	26	55	13	Every 4th	1st	4	0.5581
2496	12	8	26	55	13	Every 5th	2nd	3	0.4835
2496	12	8	26	55	13	Every 7th	3rd	2	0.3223
2496	12	8	26	60	13	Every	1st	13	0.9957
2496	12	8	26	60	13	Every 2nd	1st	7	0.9699
2496	12	8	26	60	13	Every 3rd	1st	5	0.8255
2496	12	8	26	60	13	Every 4th	1st	4	0.6383
2496	12	8	26	60	13	Every 5th	2nd	3	0.5617
2496	12	8	26	60	13	Every 7th	3rd	2	0.3745
2496	12	8	26	65	13	Every	1st	13	1.0000

2496	12	8	26	65	13	Every 2nd	1st	7	0.9939
2496	12	8	26	65	13	Every 3rd	1st	5	0.9099
2496	12	8	26	65	13	Every 4th	1st	4	0.7110
2496	12	8	26	65	13	Every 5th	2nd	3	0.6310
2496	12	8	26	65	13	Every 7th	3rd	2	0.4227
2496	12	8	26	70	13	Every	1st	13	1.0000
2496	12	8	26	70	13	Every 2nd	1st	7	0.9995
2496	12	8	26	70	13	Every 3rd	1st	5	0.9624
2496	12	8	26	70	13	Every 4th	1st	4	0.7797
2496	12	8	26	70	13	Every 5th	2nd	3	0.6899
2496	12	8	26	70	13	Every 7th	3rd	2	0.4685
2496	12	8	26	75	13	Every	1st	13	1.0000
2496	12	8	26	75	13	Every 2nd	1st	7	1.0000
2496	12	8	26	75	13	Every 3rd	1st	5	0.9890
2496	12	8	26	75	13	Every 4th	1st	4	0.8461
2496	12	8	26	75	13	Every 5th	2nd	3	0.7408
2496	12	8	26	75	13	Every 7th,	3rd	2	0.5128
2496	12	8	26	80	13	Every	1st	13	1.0000
2496	12	8	26	80	13	Every 2nd	1st	7	1.0000
2496	12	8	26	80	13	Every 3rd	1st	5	0.9985
2496	12	8	26	80	13	Every 4th	1st	4	0.9108
2496	12	8	26	80	13	Every 5th	2nd	3	0.7863
2496	12	8	26	80	13	Every 7th	3rd	2	0.5559
2496	12	8	26	85	13	Every	1st	13	1.0000
2496	12	8	26	85	13	Every 2nd	1st	7	1.0000
2496	12	8	26	85	13	Every 3rd	1st	5	1.0000
2496	12	8	26	85	13	Every 4th	1st	4	0.9624
2496	12	8	26	85	13	Every 5th	2nd	3	0.8292
2496	12	8	26	85	13	Every 7th	3rd	2	0.5985
3600	12	10	30	45	15	Every	1st	15	0.7426
3600	12	10	30	45	15	Every 2nd	1st	8	0.6038
3600	12	10	30	45	15	Every 3rd	2nd	5	0.4034
3600	12	10	30	45	15	Every 4th	2nd	4	0.3227
3600	12	10	30	45	15	Every 5th	3rd	3	0.2420
3600	12	10	30	45	15	Every 8th	4th	2	0.1614
3600	12	10	30	50	15	Every	1st	15	0.8578
3600	12	10	30	50	15	Every 2nd	1st	8	0.7491

3600	12	10	30	50	15	Every 3rd	2nd	5	0.5260
3600	12	10	30	50	15	Every 4th	2nd	4	0.4208
3600	12	10	30	50	15	Every 5th	3rd	3	0.3156
3600	12	10	30	50	15	Every 8th	4th	2	0.2104
3600	12	10	30	55	15	Every	1st	15	0.9408
3600	12	10	30	55	15	Every 2nd	1st	8	0.8679
3600	12	10	30	55	15	Every 3rd	2nd	5	0.6518
3600	12	10	30	55	15	Every 4th	2nd	4	0.5214
3600	12	10	30	55	15	Every 5th	3rd	3	0.3911
3600	12	10	30	55	15	Every 8th	4th	2	0.2607
3600	12	10	30	60	15	Every	1st	15	0.9825
3600	12	10	30	60	15	Every 2nd	1st	8	0.9448
3600	12	10	30	60	15	Every 3rd	2nd	5	0.7713
3600	12	10	30	60	15	Every 4th	2nd	4	0.6170
3600	12	10	30	60	15	Every 5th	3rd	3	0.4628
3600	12	10	30	60	15	Every 8th	4th	2	0.3085
3600	12	10	30	65	15	Every	1st	15	0.9974
3600	12	10	30	65	15	Every 2nd	1st	8	0.9837
3600	12	10	30	65	15	Every 3rd	2nd	5	0.8717
3600	12	10	30	65	15	Every 4th	2nd	4	0.7038
3600	12	10	30	65	15	Every 5th	3rd	3	0.5295
3600	12	10	30	65	15	Every 8th	4th	2	0.3530
3600	12	10	30	70	15	Every	1st	15	1.0000
3600	12	10	30	70	15	Every 2nd	1st	8	0.9971
3600	12	10	30	70	15	Every 3rd	2nd	5	0.9408
3600	12	10	30	70	15	Every 4th	2nd	4	0.7799
3600	12	10	30	70	15	Every 5th	3rd	3	0.5918
3600	12	10	30	70	15	Every 8th	4th	2	0.3945
3600	12	10	30	75	15	Every	1st	15	1.0000
3600	12	10	30	75	15	Every 2nd	1st	8	0.9998
3600	12	10	30	75	15	Every 3rd	2nd	5	0.9794
3600	12	10	30	75	15	Every 4th	2nd	4	0.8471
3600	12	10	30	75	15	Every 5th	3rd	3	0.6512
3600	12	10	30	75	15	Every 8th	4th	2	0.4341
3600	12	10	30	80	15	Every	1st	15	1.0000
3600	12	10	30	80	15	Every 2nd	1st	8	1.0000
3600	12	10	30	80	15	Every 3rd	2nd	5	0.9954

3600	12	10	30	80	15	Every 4th	2nd	4	0.9077
3600	12	10	30	80	15	Every 5th	3rd	3	0.7086
3600	12	10	30	80	15	Every 8th	4th	2	0.4724
3600	12	10	30	85	15	Every	1st	15	1.0000
3600	12	10	30	85	15	Every 2nd	1st	8	1.0000
3600	12	10	30	85	15	Every 3rd	2nd	5	0.9995
3600	12	10	30	85	15	Every 4th	2nd	4	0.9565
3600	12	10	30	85	15	Every 5th	3rd	3	0.7651
3600	12	10	30	85	15	Every 8th	4th	2	0.5101
4800	15	10	32	45	16	Every	1st	16	0.5905
4800	15	10	32	45	16	Every 2nd	1st	8	0.4619
4800	15	10	32	45	16	Every 3rd	1st	6	0.3380
4800	15	10	32	45	16	Every 4th	2nd	4	0.2409
4800	15	10	32	45	16	Every 5th	1st	4	0.2176
4800	15	10	32	45	16	Every 6th	2nd	3	0.1807
4800	15	10	32	50	16	Every	1st	16	0.6996
4800	15	10	32	50	16	Every 2nd	1st	8	0.5850
4800	15	10	32	50	16	Every 3rd	1st	6	0.4417
4800	15	10	32	50	16	Every 4th	2nd	4	0.3184
4800	15	10	32	50	16	Every 5th	1st	4	0.2825
4800	15	10	32	50	16	Every 6th	2nd	3	0.2388
4800	15	10	32	55	16	Every	1st	16	0.7995
4800	15	10	32	55	16	Every 2nd	1st	8	0.7019
4800	15	10	32	55	16	Every 3rd	1st	6	0.5553
4800	15	10	32	55	16	Every 4th	2nd	4	0.4042
4800	15	10	32	55	16	Every 5th	1st	4	0.3531
4800	15	10	32	55	16	Every 6th	2nd	3	0.3032
4800	15	10	32	60	16	Every	1st	16	0.8951
4800	15	10	32	60	16	Every 2nd	1st	8	0.8117
4800	15	10	32	60	16	Every 3rd	1st	6	0.6787
4800	15	10	32	60	16	Every 4th	2nd	4	0.4982
4800	15	10	32	60	16	Every 5th	1st	4	0.4296
4800	15	10	32	60	16	Every 6th	2nd	3	0.3736
4800	15	10	32	65	16	Every	1st	16	0.9630
4800	15	10	32	65	16	Every 2nd	1st	8	0.9026
4800	15	10	32	65	16	Every 3rd	1st	6	0.7946
4800	15	10	32	65	16	Every 4th	2nd	4	0.5930

4800	15	10	32	65	16	Every 5th	1st	4	0.5057
4800	15	10	32	65	16	Every 6th	2nd	3	0.4445
4800	15	10	32	70	16	Every	1st	16	0.9922
4800	15	10	32	70	16	Every 2nd	1st	8	0.9612
4800	15	10	32	70	16	Every 3rd	1st	6	0.8827
4800	15	10	32	70	16	Every 4th	2nd	4	0.6801
4800	15	10	32	70	16	Every 5th	1st	4	0.5749
4800	15	10	32	70	16	Every 6th	2nd	3	0.5091
4800	15	10	32	75	16	Every	1st	16	0.9998
4800	15	10	32	75	16	Every 2nd	1st	8	0.9883
4800	15	10	32	75	16	Every 3rd	1st	6	0.9415
4800	15	10	32	75	16	Every 4th	2nd	4	0.7581
4800	15	10	32	75	16	Every 5th	1st	4	0.6374
4800	15	10	32	75	16	Every 6th	2nd	3	0.5665
4800	15	10	32	80	16	Every	1st	16	1.0000
4800	15	10	32	80	16	Every 2nd	1st	8	0.9970
4800	15	10	32	80	16	Every 3rd	1st	6	0.9767
4800	15	10	32	80	16	Every 4th	2nd	4	0.8291
4800	15	10	32	80	16	Every 5th	1st	4	0.6953
4800	15	10	32	80	16	Every 6th	2nd	3	0.6182
4800	15	10	32	85	16	Every	1st	16	1.0000
4800	15	10	32	85	16	Every 2nd	1st	8	0.9994
4800	15	10	32	85	16	Every 3rd	1st	6	0.9943
4800	15	10	32	85	16	Every 4th	2nd	4	0.8896
4800	15	10	32	85	16	Every 5th	1st	4	0.7513
4800	15	10	32	85	16	Every 6th	2nd	3	0.6664
6460	17	10	38	45	19	Every	1st	19	0.5210
6460	17	10	38	45	19	Every 2nd	1st	10	0.4227
6460	17	10	38	45	19	Every 3rd	1st	7	0.2959
6460	17	10	38	45	19	Every 4th	2nd	5	0.2238
6460	17	10	38	45	19	Every 5th	2nd	4	0.1790
6460	17	10	38	45	19	Every 6th	1st	4	0.1617
6460	17	10	38	50	19	Every	1st	19	0.6173
6460	17	10	38	50	19	Every 2nd	1st	10	0.5329
6460	17	10	38	50	19	Every 3rd	1st	7	0.3873
6460	17	10	38	50	19	Every 4th	2nd	5	0.2957
6460	17	10	38	50	19	Every 5th	2nd	4	0.2366

6460	17	10	38	50	19	Every 6th	1st	4	0.2099
6460	17	10	38	55	19	Every	1st	19	0.7055
6460	17	10	38	55	19	Every 2nd	1st	10	0.6361
6460	17	10	38	55	19	Every 3rd	1st	7	0.4877
6460	17	10	38	55	19	Every 4th	2nd	5	0.3754
6460	17	10	38	55	19	Every 5th	2nd	4	0.3004
6460	17	10	38	55	19	Every 6th	1st	4	0.2624
6460	17	10	38	60	19	Every	1st	19	0.7898
6460	17	10	38	60	19	Every 2nd	1st	10	0.7314
6460	17	10	38	60	19	Every 3rd	1st	7	0.5968
6460	17	10	38	60	19	Every 4th	2nd	5	0.4627
6460	17	10	38	60	19	Every 5th	2nd	4	0.3702
6460	17	10	38	60	19	Every 6th	1st	4	0.3192
6460	17	10	38	65	19	Every	1st	19	0.8718
6460	17	10	38	65	19	Every 2nd	1st	10	0.8206
6460	17	10	38	65	19	Every 3rd	1st	7	0.7079
6460	17	10	38	65	19	Every 4th	2nd	5	0.5565
6460	17	10	38	65	19	Every 5th	2nd	4	0.4455
6460	17	10	38	65	19	Every 6th	1st	4	0.3805
6460	17	10	38	70	19	Every	1st	19	0.9484
6460	17	10	38	70	19	Every 2nd	1st	10	0.9043
6460	17	10	38	70	19	Every 3rd	1st	7	0.8108
6460	17	10	38	70	19	Every 4th	2nd	5	0.6544
6460	17	10	38	70	19	Every 5th	2nd	4	0.5248
6460	17	10	38	70	19	Every 6th	1st	4	0.4456
6460	17	10	38	75	19	Every	1st	19	0.9870
6460	17	10	38	75	19	Every 2nd	1st	10	0.9631
6460	17	10	38	75	19	Every 3rd	1st	7	0.8900
6460	17	10	38	75	19	Every 4th	2nd	5	0.7454
6460	17	10	38	75	19	Every 5th	2nd	4	0.5995
6460	17	10	38	75	19	Every 6th	1st	4	0.5063
6460	17	10	38	80	19	Every	1st	19	0.9990
6460	17	10	38	80	19	Every 2nd	1st	10	0.9915
6460	17	10	38	80	19	Every 3rd	1st	7	0.9437
6460	17	10	38	80	19	Every 4th	2nd	5	0.8261
6460	17	10	38	80	19	Every 5th	2nd	4	0.6667
6460	17	10	38	80	19	Every 6th	1st	4	0.5608

6460	17	10	38	85	19	Every	1st	19	1.0000
6460	17	10	38	85	19	Every 2nd	1st	10	0.9991
6460	17	10	38	85	19	Every 3rd	1st	7	0.9768
6460	17	10	38	85	19	Every 4th	2nd	5	0.8924
6460	17	10	38	85	19	Every 5th	2nd	4	0.7281
6460	17	10	38	85	19	Every 6th	1st	4	0.6111

For ease of inspection, the fractional coverage volumes provided by selected detector loading patterns[12] in each reference array are plotted in Figures 5-23 through 5-27.

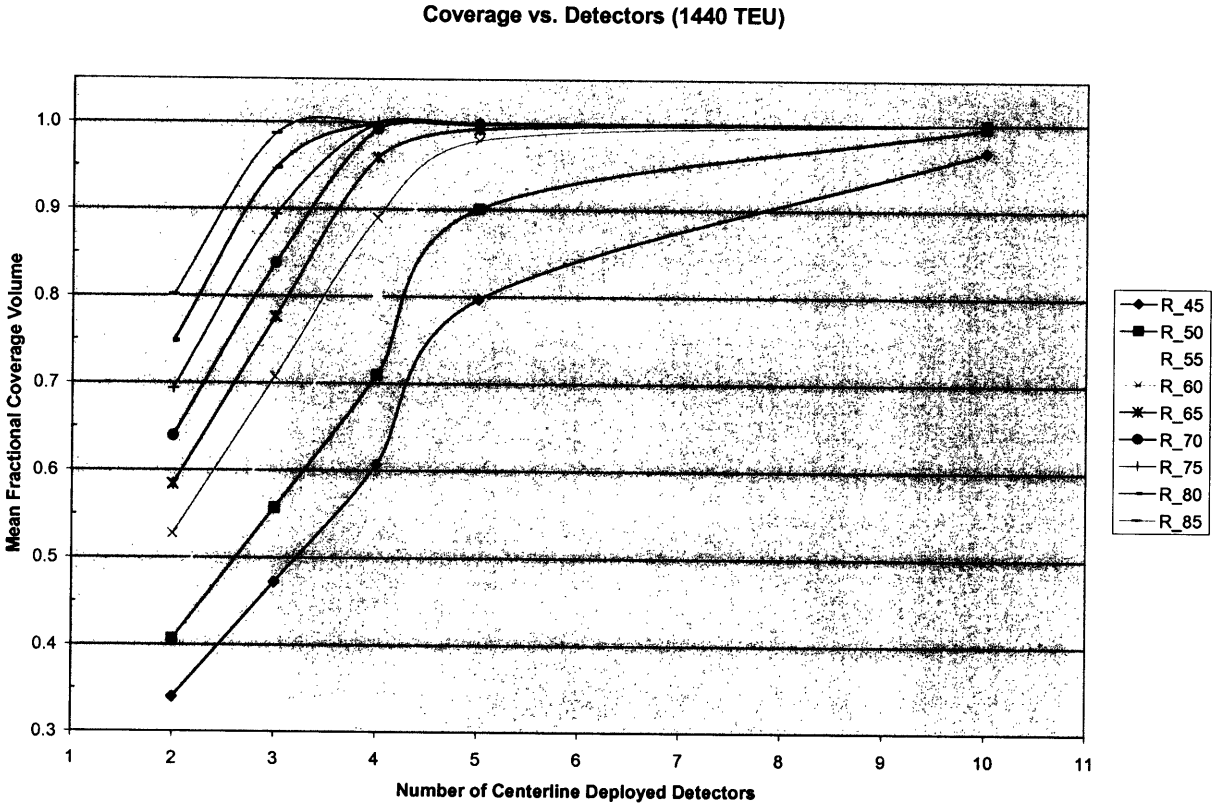

Figure 5-24: Coverage vs. Detectors plot for the 1440 TEU array [Centerline]

[12] When two or more loading patterns resulted in the same number of detectors being deployed, only the result from the pattern with the highest fractional coverage was plotted.

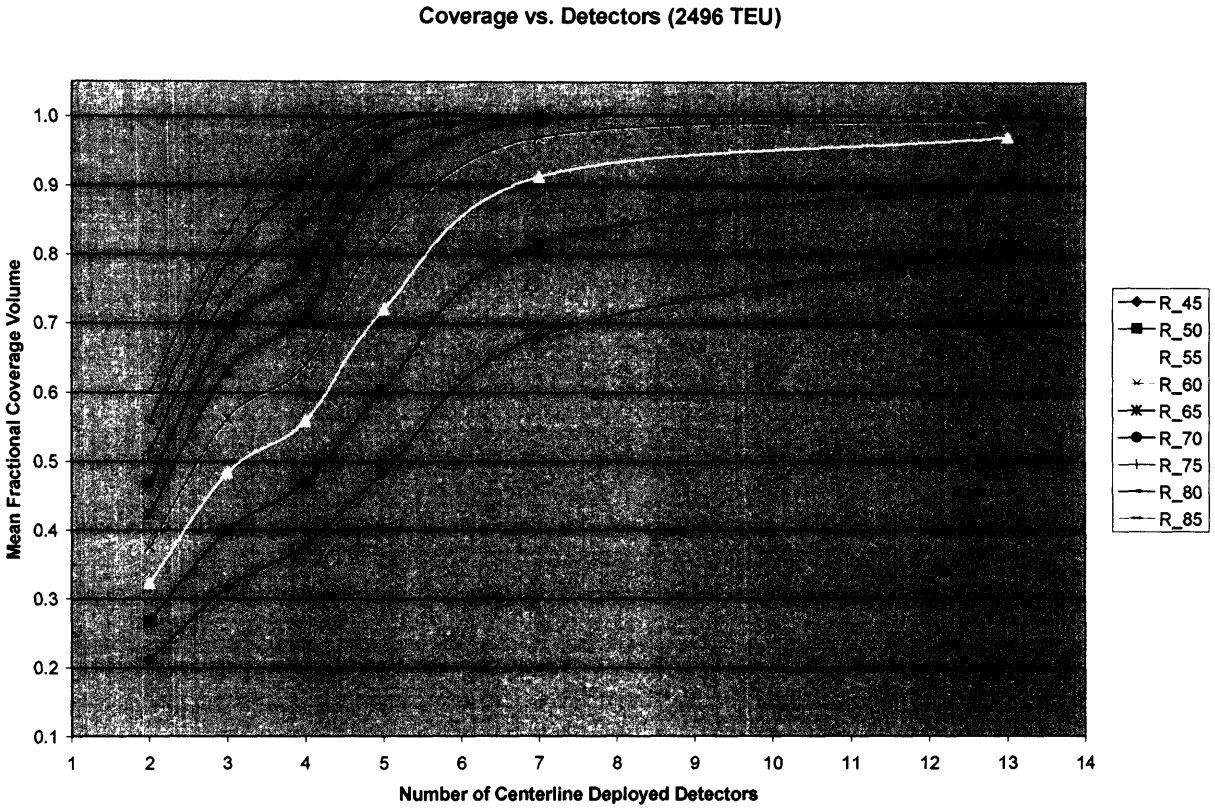

Figure 5-25: Coverage vs. Detectors plot for the 2496 TEU array [Centerline]

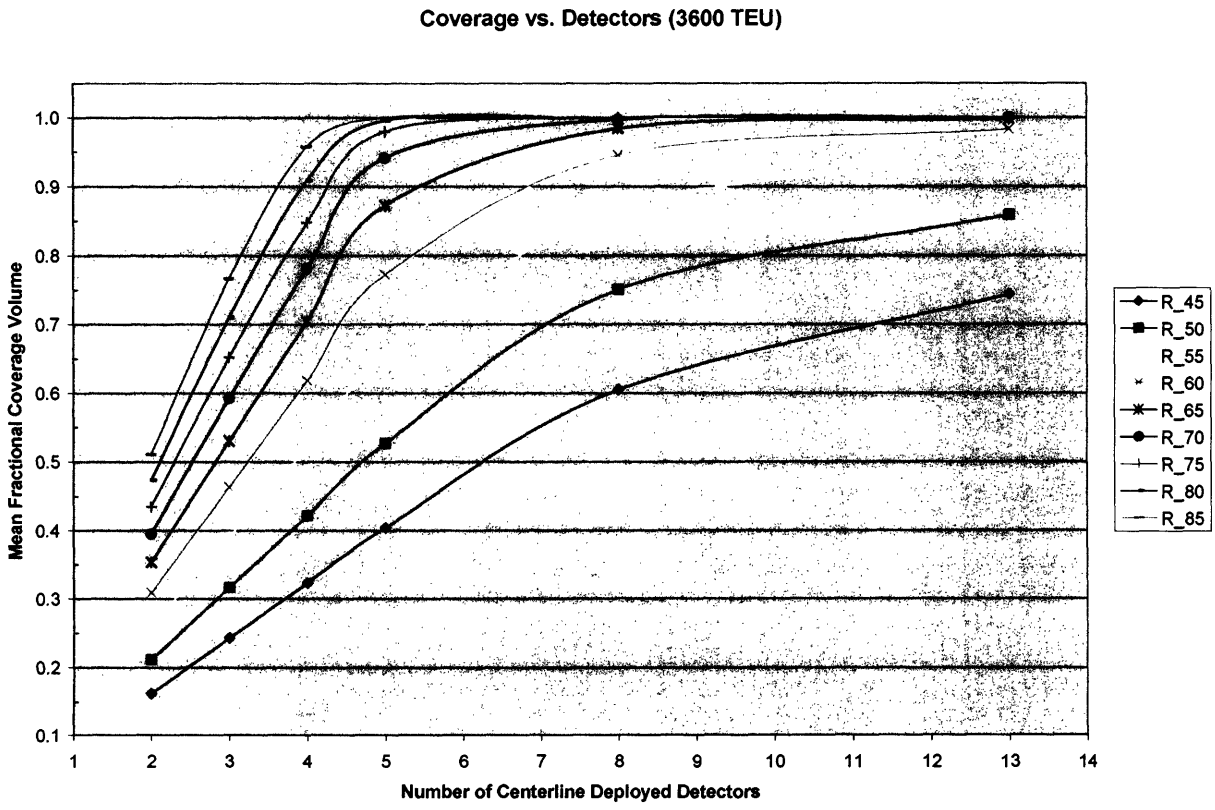

Figure 5-26: Coverage vs. Detectors plot for the 3600 TEU array [Centerline]

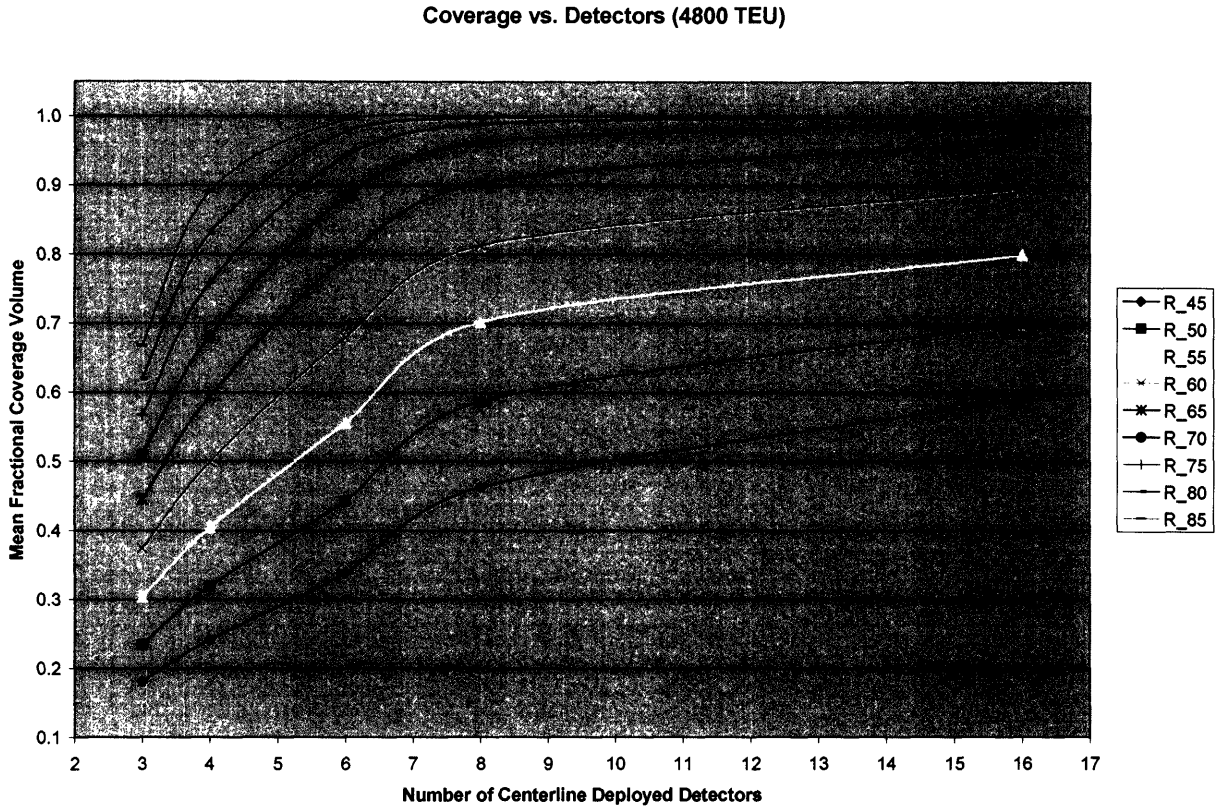

Figure 5-27: Coverage vs. Detectors plot for the 4800 TEU array [Centerline]

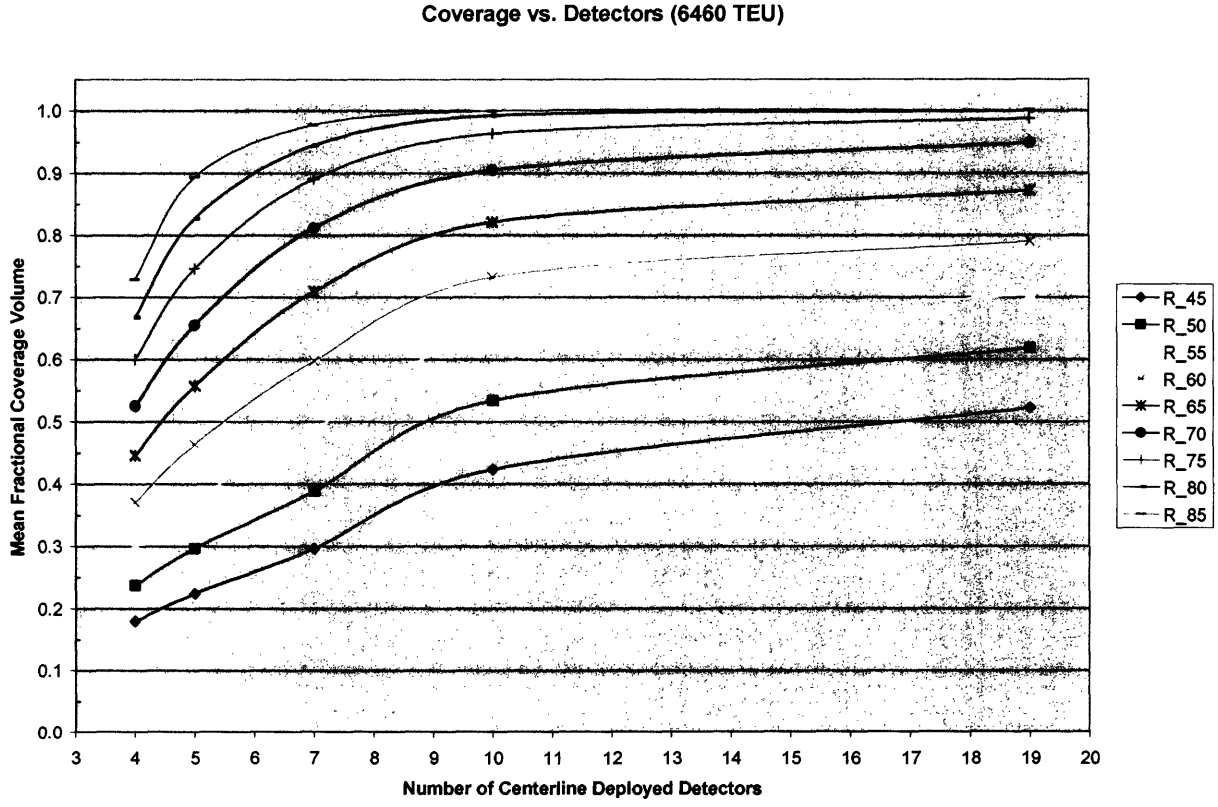

Figure 5-28: Coverage vs. Detectors plot for the 6460 TEU array [Centerline]

The number of centerline deployed detectors needed to provide 75%, 85%, and 95% coverage for each evaluated range and reference array are shown in Table 5-11.

Table 5-11: Estimated number of detectors needed for various scenarios [Centerline]

Centerline Deployment		Reference Array Capacity (TEU)				
Range (ft)	Coverage	1440	2496	3600	4800	6460
45	0.75	5	10	N/A	N/A	N/A
	0.85	7	N/A	N/A	N/A	N/A
	0.95	10	N/A	N/A	N/A	N/A
50	0.75	5	6	8	N/A	N/A
	0.85	5	9	13	N/A	N/A
	0.95	7	N/A	N/A	N/A	N/A
55	0.75	4	6	7	12	N/A
	0.85	5	6	8	N/A	N/A
	0.95	5	10	N/A	N/A	N/A
60	0.75	4	5	5	7	12
	0.85	4	6	6	12	N/A
	0.95	5	7	9	N/A	N/A
65	0.75	3	5	5	6	8
	0.85	4	5	5	7	15
	0.95	4	6	7	14	N/A
70	0.75	3	4	4	4	7
	0.85	4	5	5	6	8
	0.95	4	5	6	8	19
75	0.75	3	4	4	4	6
	0.85	3	5	4	5	7
	0.95	4	5	5	7	9
80	0.75	2	3	4	4	5
	0.85	3	4	4	5	6
	0.95	3	5	5	7	8
85	0.75	2	3	3	4	5
	0.85	3	4	4	4	5
	0.95	3	4	4	5	6

Depending on the effective range of the detection unit, there are some levels of coverage for certain reference arrays that cannot be achieved through the use of detectors deployed exclusively along the centerline (denoted in Table 5-11 as N/A). However, in cases where the range is sufficient to provide desirable coverage using only centerline deployment, the deployment efficiency resulting from the preferential placement attendant to this approach allows high levels of coverage to be achieved with a significant economy of detection units.

5.6 Deployment Comparison

The most germane comparison that can be drawn between the deployment strategies examined in the previous sections is to contrast the number of detectors required by each method to achieve given levels of fractional coverage when faced with identical range and array capacity scenarios. Since constrained deployment was not found to hold any significant efficiency advantages over random deployment (despite its stealth and logistical disadvantages), only random and centerline deployment will be considered in the following analysis.

Table 5-12 shows the number of detectors required for each scenario using both random and centerline deployment. It also tabulates the ratio of randomly deployed detectors to centerline deployed detectors for each case so that a measure of the efficiency cost of randomization can be obtained.

Table 5-12: Random vs. Centerline deployment comparison

Random vs. Centerline		Reference Array Capacity (TEU)														
		1440			2496			3600			4800			6460		
Range (ft)	Coverage	R	C	R/C	R	C	R/C	R	C	R/C	R	C	R/C	R	C	R/C
45	0.75	13	5	2.6	21	10	2.1	30			37			59		
	0.85	19	7	2.7	31			40			52			68		
	0.95	32	10	3.2	50			69			88			117		
50	0.75	11	5	2.2	17	6	2.8	22	8	2.8	29			37		
	0.85	15	5	3.0	23	9	2.6	31	13	2.4	40			52		
	0.95	25	7	3.6	39			53			69			88		
55	0.75	9	4	2.3	13	6	2.2	18	7	2.6	23	12	1.9	30		
	0.85	12	5	2.4	19	6	3.2	25	8	3.1	31			41		
	0.95	19	5	3.8	30	10	3.0	41			53			70		
60	0.75	7	4	1.8	11	5	2.2	15	5	3.0	18	7	2.6	24	12	2.0
	0.85	10	4	2.5	15	6	2.5	20	6	3.3	26	12	2.2	33		
	0.95	15	5	3.0	25	7	3.6	34	9	3.8	43			55		
65	0.75	6	3	2.0	9	5	1.8	12	5	2.4	15	6	2.5	20	8	2.5
	0.85	8	4	2.0	12	5	2.4	17	5	3.4	20	7	2.9	27	15	1.8
	0.95	14	4	3.5	21	6	3.5	27	7	3.9	34	14	2.4	45		
70	0.75	5	3	1.7	8	4	2.0	10	4	2.5	13	4	3.3	16	7	2.3
	0.85	7	4	1.8	11	5	2.2	14	5	2.8	18	6	3.0	22	8	2.8
	0.95	11	4	2.8	18	5	3.6	23	6	3.8	29	8	3.6	38	19	2.0
75	0.75	5	3	1.7	7	4	1.8	9	4	2.3	11	4	2.8	14	6	2.3
	0.85	6	3	2.0	9	5	1.8	12	4	3.0	15	5	3.0	18	7	2.6
	0.95	10	4	2.5	15	5	3.0	19	5	3.8	24	7	3.4	31	9	3.4
80	0.75	4	2	2.0	6	3	2.0	8	4	2.0	9	4	2.3	12	5	2.4
	0.85	6	3	2.0	8	4	2.0	10	4	2.5	13	5	2.6	17	6	2.8
	0.95	9	3	3.0	14	5	2.8	17	5	3.4	21	7	3.0	29	8	3.6
85	0.75	4	2	2.0	5	3	1.7	7	3	2.3	8	4	2.0	10	5	2.0
	0.85	5	3	1.7	8	4	2.0	9	4	2.3	11	4	2.8	15	5	3.0
	0.95	8	3	2.7	12	4	3.0	15	4	3.8	19	5	3.8	25	6	4.2

Comparisons between random and centerline deployment could be rendered moot if the centerline strategy is definitively judged to be logistically infeasible or if it is determined to be an unacceptable compromise of the stealth characteristics that are so important to the ship based approach. Additionally, centerline deployment, by itself, would presumably stop receiving serious consideration if the effective detection range is found to be too low to provide the minimum acceptable detection coverage for all vessels of interest. That said, Table 5-12 clearly illustrates the efficiency gains realized through centerline deployment. Table 5-13 shows the average random to centerline, R/C, values for the three analyzed fractional coverage volume targets.

Table 5-13: Average R/C values

	Fractional Coverage Volume		
	0.75	0.85	0.95
R/C	2.249	2.531	3.306

As Table 5-13 illustrates, the efficiency advantage enjoyed by centerline deploy increases as the desired level of coverage increases. This stems from the diminishing marginal returns phenomenon associated with random deployment. Unlike the random case, when additional detectors are deployed along the centerline to achieve a higher level of fractional detection coverage they will preferentially "fill in" uncovered or sparsely covered areas of the container array. Therefore, marginal returns are greater when employing the centerline approach and as a greater number of detectors are added to provide higher levels of coverage this amplifies the efficiency advantages over random deployment.

5.7 Total Detector Estimates

To estimate the total number of detectors required to field a comprehensive system (i.e. to cover every inbound commercial containership) the data compiled in the previous sections must be combined with information from the shipping industry and U.S. ports. If all classes of containerships called on U.S. ports with uniform frequency then the capacity distribution derived in Chapter 4 could be used directly to determine the total number of detectors. Some types of container vessels, however, make more port calls than others, so these vessels should receive a higher importance weighting in the analysis. Table 5-14 shows the relative frequency of calls at U.S. ports broken down by vessel size (i.e. container capacity) [MARAD, 2000] and the number of calls that these vessel classes would make out of the CY 2003 call total of 17287 [MARAD(1), 2004].

Table 5-14: U.S. port calls by vessel capacity

	Vessel Capacity (TEU)					
	<2000	2001-3000	3001-4000	4001-5000	>5000	Total
Relative Freq.	0.3491	0.2853	0.2129	0.1147	0.038	1
Calls	6035	4932	3680	1983	657	17287

Since one of the reference arrays described in the previous analysis fits approximately in the middle of each of the capacity bins shown in Table 5-14, the number of detectors found to be required to cover a given reference array can be considered roughly representative of the entire binned vessel class. Estimates for the total number of detectors needed for comprehensive deployment can now be made using the following expression,

$$Det_{Total} = \frac{1}{Avg_{c/v}} \sum_i C_i Det_i \qquad (13)$$

where $Avg_{c/v}$ is the average number of calls made per vessel, C_i is the number of calls for a given vessel class, and Det_i is the number of detectors required for a given vessel class. In 2003, the average number of calls made by containerships was 17 [MARAD(1), 2004].

Since the detection units have no inland destination and are intended solely for deployment aboard containerships, once they are discharged from a given vessel they can be redeployed with minimal downtime. Downtime that could be required for maintenance and calibration is not considered. For the purposes of this analysis, it is assumed that turn-around can occur immediately, so the discharged detection unit can be shipped out (i.e. transported back to a foreign port where it can be deployed for its intended purpose) without delay. It should be noted that the export leg of the detection unit's voyage could be used to perform performance reliability tests and to monitor for the unlikely event that a fissile or radiological source was being smuggled out of the United States, for use abroad. Stops between foreign ports on the export leg could also be used to monitor for radioactive material movement abroad, which could discourage or thwart international smuggling attempts and augment the ability of other nations to defend against nuclear or radiological attack.

Eq. (13) was applied to the results from the random and centerline deployment simulations and estimates for the total number of detectors that would be necessary using either deployment strategy are shown in Table 5-15.

Table 5-15: Total detector estimates

Total Detector Estimates		Deployment Strategy	
Range (ft)	Coverage	Random	Centerline
45	0.75	23798	
	0.85	33091	
	0.95	55589	
50	0.75	18412	
	0.85	25384	
	0.95	43112	
55	0.75	14705	
	0.85	20385	
	0.95	33211	
60	0.75	11951	5233
	0.85	16539	
	0.95	27079	
65	0.75	9861	4607
	0.85	13378	5349
	0.95	22612	
70	0.75	8395	3828
	0.85	11657	4962
	0.95	18957	5837
75	0.75	7578	3790
	0.85	9784	4235
	0.95	16012	5117
80	0.75	6406	3106
	0.85	8789	3906
	0.95	14507	4724
85	0.75	5706	2890
	0.85	7907	3751
	0.95	12751	3906

Table 5-15 shows that if only purely random or purely centerline deployment strategies are being considered, the option space is limited if the effective detection range of the containerized units is less than 70 ft. An additional advantage to units with effective ranges equal to or greater than 70 ft is the significant reduction in the number of detectors required to provide any of the evaluated fractional coverage volumes. Table 5-15 also demonstrates the reduction in detection units required for full deployment if the fractional coverage volume is chosen to be less than 95%.

Chapter 6: Summary, Conclusions, and Recommended Future Work

6.1 Summary

The rise of highly mobile, religiously motivated transnational terrorist organizations that are not restrained by conventional means of deterrence has changed the dynamics of the threat that nuclear weapons pose to the United States. The international commercial container trade that delivers over 19,000 cargo containers to U.S. ports every day is one possible avenue that could be exploited by a terrorist organization to mount an unconventional nuclear attack. Due to the unique power and range of nuclear weapons, defensive measures that have been envisioned or deployed that would not detect threats until they come ashore at U.S. ports do not provide adequate protection against attacks that are planned and executed by rational, determined adversaries.

We propose a new ship-based approach to fissile material detection where large effective area, commercial off the shelf, radiation detectors, enhanced with imaging capabilities, are enclosed in standard, non-descript cargo containers and shipped alongside commercial containers. When deployed in limited numbers aboard commercial vessels the detection units would passively measure any nuclear signature emitted by nearby containers with count times limited only by the duration of the voyage. By outfitting the dedicated detection units with communication hardware, identification and notification of a potential threat could be made while the danger was still safely removed from U.S. shores.

To better characterize the feasibility of the proposed ship-based approach, "external" uncertainties associated with the deployment environment and potential modes of deployment were investigated. Characteristics of the deployment environment that were evaluated included the count times that would be available on container import voyages terminating at U.S. ports, the container capacities of the vessel fleet that ply the international container trade, and the average densities of cargo being imported to the U.S. Table 6-1 summarizes the salient results of these analyses.

Table 6-1: Results summary for deployment environment analyses

	Vessel Capacity (TEU)	Avg. Density* (g/cm^3)	Count Time (days) To NY	To LA
Mean	3047	0.1977	19.2	13.3
Median	2722	0.1708	19.1	13.3
25th	1666	0.1664	21.7	15.1
75th	4173	0.2208	17.2	11.9
95th	6204	0.2620	15.9	11
99th	6782	0.2998	15.6	10.8

* 0.1977 g/cm^3 corresponds to 15.23 metric tons / 40'container

To study different potential modes of deployment, a Matlab-based simulator was developed. The simulator was used to evaluate and compare detection coverage efficiencies for fully random detector deployment, partially constrained deployment where containerized detection units could not be placed along the surface of container array, and fully constrained deployment where detectors could only be placed along the centerline of the array. Partially constrained deployment was not found to have any particularly desirable attributes. The number of detection units required to provide various degrees of coverage for random and centerline deployment are summarized in Tables 6-2 and 6-3 respectively. Coverage is defined as the fractional volume of a vessel's container array that is within the effective detection range of one of the deployed containerized detection units. The effective detection range is the expected maximum distance at which a source can be confidently and reliably detected in a given count time, under realistic conditions.

Table 6-2: Random deployment results summary

Random Deployment		Reference Array Capacity (TEU)					
Range (ft)	Coverage	1440	2496	3600	4800	6460	Total Detectors
45	0.75	13	21	30	37	59	23798
	0.85	19	31	40	52	68	33091
	0.95	32	50	69	88	117	55589
50	0.75	11	17	22	29	37	18412
	0.85	15	23	31	40	52	25384
	0.95	25	39	53	69	88	43112
55	0.75	9	13	18	23	30	14705
	0.85	12	19	25	31	41	20385
	0.95	19	30	41	53	70	33211
60	0.75	7	11	15	18	24	11951
	0.85	10	15	20	26	33	16539
	0.95	15	25	34	43	55	27079
65	0.75	6	9	12	15	20	9861
	0.85	8	12	17	20	27	13378
	0.95	14	21	27	34	45	22612
70	0.75	5	8	10	13	16	8395
	0.85	7	11	14	18	22	11657
	0.95	11	18	23	29	38	18957
75	0.75	5	7	9	11	14	7578
	0.85	6	9	12	15	18	9784
	0.95	10	15	19	24	31	16012
80	0.75	4	6	8	9	12	6406
	0.85	6	8	10	13	17	8789
	0.95	9	14	17	21	29	14507
85	0.75	4	5	7	8	10	5706
	0.85	5	8	9	11	15	7907
	0.95	8	12	15	19	25	12751

Table 6-3: Centerline deployment results summary

Centerline Deployment		Reference Array Capacity (TEU)					
Range (ft)	Coverage	1440	2496	3600	4800	6460	Total Detectors
45	0.75	5	10	N/A	N/A	N/A	
	0.85	7	N/A	N/A	N/A	N/A	
	0.95	10	N/A	N/A	N/A	N/A	
50	0.75	5	6	8	N/A	N/A	
	0.85	5	9	13	N/A	N/A	
	0.95	7	N/A	N/A	N/A	N/A	
55	0.75	4	6	7	12	N/A	
	0.85	5	6	8	N/A	N/A	
	0.95	5	10	N/A	N/A	N/A	
60	0.75	4	5	5	7	12	5233
	0.85	4	6	6	12	N/A	
	0.95	5	7	9	N/A	N/A	
65	0.75	3	5	5	6	8	4607
	0.85	4	5	5	7	15	5349
	0.95	4	6	7	14	N/A	
70	0.75	3	4	4	4	7	3828
	0.85	4	5	5	6	8	4962
	0.95	4	5	6	8	19	5837
75	0.75	3	4	4	4	6	3790
	0.85	3	5	4	5	7	4235
	0.95	4	5	5	7	9	5117
80	0.75	2	3	4	4	5	3106
	0.85	3	4	4	5	6	3906
	0.95	3	5	5	7	8	4724
85	0.75	2	3	3	4	5	2890
	0.85	3	4	4	4	5	3751
	0.95	3	4	4	5	6	3906

Tables 6-2 and 6-3 show that the geometrically optimal centerline deployment provides significantly more efficient detection coverage than the stealthier and more logistically appealing random deployment. The efficiency advantage of centerline deployment is evidenced by the finding that an average of 2.249, 2.531, and 3.306 times more randomly deployed detection units are required to provide 75%, 85%, and 95% fractional coverages, respectively, for vessels with a given container array. The preceding tables also demonstrate the considerable benefit to developing detection units with an effective detection range equal to, or greater than, 70 ft. Units with ranges at or exceeding 70 ft. will yield maximum flexibility in terms of deployment options and will significantly reduce the number of units required to cover a given vessel and to field a comprehensive ship-based detector network.

6.2 Conclusions

Since this work was performed as one element of an integrated effort, not all of the calculations and evaluations documented in this thesis may carry significant relevance and meaning when viewed alone. These results will be combined with, and serve as input to, ongoing work being conducted by Gallagher at MIT on system design and performance modeling. The end product of this continuing effort will yield crucial information regarding the expected performance of the detection units and the overall efficacy of the ship-based approach. Despite the essentially unfinished nature of system development, there are a number of notable conclusions that can be drawn strictly from the analysis presented and discussed in this document.

- First, and perhaps most importantly, none of the results obtained in the preceding analyses serve to discredit the overall feasibility of the ship-based approach. A primary objective of this thesis was to assess the practical viability of this new detection methodology and nothing was discovered that suggested the ship-based approach could not be viable and effective if prudent design and deployment decisions are made.

- Mean count time estimates for the representative East Coast and West Coast ports were particularly encouraging. With an average of 19.2 days and 13.3 days of available count time for voyages to New York and Los Angeles respectively, the ship-based detection units will have a lengthy window of opportunity to passively detect incoming fissile material and communicate warning to responders while the threat is still safely at sea.

- The results of deployment simulation highlighted the effective detection range of containerized units as being especially important to promoting and ensuring the viability of the ship-based approach. Special consideration should be paid to maximizing this parameter during upcoming design and optimization activities. Design decisions that increase the expected detection range at the expense of unit costs should be vigorously examined in light of the dramatic reductions in per vessel and total detectors required as effective range was increased. The observed relationship between the required number of detectors and the effective range suggests that while unit costs may increase as range enhancing features are incorporated, the total system costs could fall as less detectors are required on the whole.

- Simulation also helped to quantify the efficiency costs associated with random deployment. While a purely random deployment strategy is very desirable from both stealth and logistical standpoints, the use of this approach necessitates the deployment of 2.2 to 3.3 times more detectors (depending on the fractional coverage target) than the less covert strategy of deploying detection units only along the ship's centerline. This inefficiency could become quite costly. Therefore, some combination of random and centerline deployment may prove to be the most attractive strategy. In such a "hybrid" deployment scenario, if even a small number of detectors could be deployed along or near the array's centerline with the remaining detectors randomly distributed, an important degree of stealth would be preserved by the random component and a helpful boost in efficiency will be afforded by the centerline component.

6.3 Recommendations for Future Work

The deployment strategies described and modeled in this thesis were selected to represent archetypal cases useful in studying the fundamental trade-off between deployment stealth and coverage efficiency. Random deployment is at one end of the spectrum, being the stealthiest approach, but having less than optimal efficiency. Centerline deployment (i.e. fully constrained placement of detectors along the ship's centerline) resides at the opposite end of the spectrum, affording optimal efficiency, but being among the least covert of any potential strategies. Simulations documented in Chapter 5 provide some quantitative insights into the trade-offs involved when going from one end of the deployment spectrum to the other. This analysis, however, was somewhat divorced from important practical considerations that arise from the common practices and capabilities of the international shipping trade. For instance, it is unclear whether centerline deployment would be logistically feasible in practice. Therefore, a clear priority for any future deployment analysis should be to conduct more in-depth consultations with individuals possessing intimate knowledge of the shipping trade (particularly the loading and discharging of containerships) to better understand what types of placement constraints are and are not practicable. This practical knowledge is essential to understanding the true performance capabilities of a ship-based system and to developing an effective deployment strategy that can be reliably implemented in the real world.

Future deployment modeling conducted either to refine the results of this analysis or to study alternative deployment strategies could employ an enhanced version of the Monte Carlo simulation codes used to produce the results presented in this thesis. Simulation codes used in this analysis (and documented in Appendix B) assumed that detectors could be placed anywhere within a container being used as a dedicated detection unit. This assumption saved considerable computation time but also created the opportunity for unphysical situations (e.g. multiple detectors in a single container) to arise that underestimated the actual performance of the ensemble of deployed detectors.

Reality would be more accurately modeled if the locations where detectors could be randomly placed were limited to the centerpoints of simulated containers. Output distortions caused by double-assignment situations would be eliminated with this modification. Additionally, by imposing a minimum separation distance between detectors (i.e. the distance separating the centers of adjacent containers) better overall distribution should be observed. Therefore, the enhanced simulation would be expected to show better and more realistic coverage efficiencies than the results shown above.

Another assumption used in deployment modeling that warrants further attention is the geometry of the coverage volume provided by deployed detectors. In the preceding analysis, this volume was represented by a perfect sphere centered at a detector and having a radius equal to the effective detection range of the unit. A focus of future efforts should be to investigate factors that morph or distort this idealized sphere. This includes better characterization of important radiation transport phenomena, such as the effects of potential radiation streaming through tiny openings, or "pinholes", in commercial cargo packed in containers. More thorough understanding of these mechanisms can lead to more realistic and appropriate coverage patterns that can be incorporated in future performance and deployment models.

Another useful extension of the work presented above would be to model a number of different hybrid deployment scenarios where some detectors were placed along the ship's centerline (assuming this mode of deployment is found to be practicable) and the balance were randomly distributed. By performing parameter studies, an optimal ratio or mix of centerline to random detectors may be identified. The results from this optimized hybrid deployment could then be compared to the results of pure random and pure centerline deployment.

Some of the results presented and discussed in this thesis have direct and important implications for the on going design and performance assessment activities being conducted by Gallagher at MIT. One outcome with direct bearing on the continuing design process is the pronounced benefit of detectors that can achieve

effective detection ranges equal to, or greater than, 70 feet. Results of the parameter study undertaken as part of the deployment simulation demonstrated that significant gains in coverage efficiency and deployment flexibility were realized when detection units had effective ranges of 70 ft or higher. These findings strongly suggest that any available means to augment the detection range of the containerized detection suite should be investigated and seriously considered. Even design features that enhance range while increasing unit costs should be considered since the eventual reduction in the number of longer-range detectors required to provide a given degree of coverage may ultimately offset the unit cost increases.

Finally, while computer simulations are very instructive in guiding the design process and estimating the performance of the proposed ship-based containerized detection units, there is a limit to what can be confidently demonstrated on the strength of computer modeling alone. Therefore, at the earliest practical juncture, a full-scale prototype of a containerized unit, complete with a full detection suite, should be built and vigorously tested in environments as close to those that would be realistically encountered as possible.

References

Albright, D., O'Neill K. (eds.), The Challenges of Fissile Material Control, Institute for Science and International Security Press, Washington D.C., 1999.

Baryshevsky, V.G., A.A. Khrutchinsky, V.I. Moroz, M.D. Dezhurko, "Gamma-ray Spectroscopic System for Remote Detection and Monitoring of Fissile Materials," *IEEE Trans. on Nucl. Sci.*, Vol. 41, August 1994.

Bunn, M., A. Weir, J. Holdren, "Controlling Nuclear Warheads and Materials: A Report Card and Action Plan," Nuclear Threat Initiative, March 2003.

Bunn, M., J. Holdren, "Managing Military Uranium and Plutonium in the United States and the Former Soviet Union," *Annu. Rev. Energy Environ.*, Vol. 22, November 1997.

Carter, A., J. Deutch, P. Zelikow, "Catastrophic Terrorism," *Foreign Affairs*, Vol. 77, December 1998.

DOE (Department of Energy), "Additional Information Concerning Underground Weapon Test of Reactor-Grade Plutonium," *DOE Openness Press Conference Fact Sheets*, Washington, D.C., June 27, 1994.

Emsley, J., The Elements 3rd Ed., Oxford University Press, New York, 1999.

Evans, R., The Atomic Nucleus, McGraw Hill, New York, 1955.

Fetter(1), S., V. Frolov, M. Miller, R. Mozely, O.Prilutskii, S. Rodionov, R. Sagdeev, "Detecting Nuclear Warheads," *Science and Global Security*, Vol. 1, No. 3-4, 1990.

Fetter(2), S., V. Frolov, O. Prilutskii, R. Sagdeev, "Appendix A: Fissile Material and Weapons Design," *Science and Global Security*, Vol. 1, No. 3-4, 1990.

Fetter(3), S., T. Cochran, L. Grodzins, H. Lynch, M. Zucker, "Gamma-Ray Measurements of a Soviet Cruise-Missile Warhead," *Science*, Vol. 248, May 1990.

Fetter(4), S., R. Mozely, "Appendix B: Emission and Absorption of Radiation," *Science and Global Security*, Vol. 1, No. 3-4, 1990.

Frank, M., S. Prussin, P. Peterson, M. Tobin, "A Monte Carlo Model of Sea-Level Neutron Background: Directionality, Spectra, and Intensity," *Journal of Radioanalytical and Nuclear Chemistry*, Vol. 249, December 2000.

Gopalakrishnan, A., "Evolution of the Indian Nuclear Power Program," *Annu. Rev. Energy Environ.*, Vol. 27, November 2002.

Gosnell, T., "Detecting Fissile Material: Limitations of Current Technology," presentation for the Alternative Signatures for Detecting Fissile Materials Workshop, Livermore, CA, March 29, 2000.

Hammond, World Map, International Collector's Series Wall Map, Hammond Publishing, 1999

Hoffman, B., "Holy Terror: Implications of Terrorism Motivated by a Religious Imperative," *Studies in Conflict and Terrorism*, Vol. 18, December 1995.

IAEA (International Atomic Energy Agency) "IAEA Safeguards Glossary, 2001 Edition," *International Nuclear Verification Series No. 3*, 2001.

Ircha, M., "Handling Tomorrow's Mega-Size Container Ships," *Association of European Civil Engineering Facilities Newsletter*, January 2002.

Kang, J., F. Von Hippel, "U-232 and the Proliferation-Resistance of U-233 in Spent Fuel," *Science and Global Security*, Vol. 9, 2001.

Knorr, Klaus, "Controlling Nuclear War," *International Security*, Vol. 9, No. 4, Spring 1985.

Krane, K, Introductory Nuclear Physics, John Wiley & Sons, New York, 1988.

Laqueur, W., "Terror's New Face," *Harvard International Review*, Vol. 20, Fall 1998.

Lee, R., Nuclear Smuggling: Patterns and Responses, *Parameters*, Vol. 33, Spring 2003.

Lok, C. "Cargo Security," *Technology Review*, Vol. 107, June 2004.

MacGregor, "Now Samsung Steps Up to 8100 TEU Series," *MacGregor News*, Autumn 2003.

MARAD(1), "Vessel Calls at U.S. Ports: 2003," U.S. Department of Transportation Maritime Administration, July 2004.

MARAD(2), "Top 30 U.S. Container Ports by Direction CY 2003," U.S. Department of Transportation Maritime Administration, available online at http://www.marad.dot.gov/Marad_Statistics/Container-03.htm, March 2004.

MARAD(3), "Top 25 Container Trading Partners CY 2003," U.S. Department of Transportation Maritime Administration, available online at http://www.marad.dot.gov/Marad_Statistics/PIERS TRADING PARTNERS 2003.pdf, April 2004.

MARAD, "Top 15 U.S. Containership Ports by Port Calls and Vessel Size (CY 1999)," U.S. Department of Transportation Maritime Administration, May 2000.

MARAD, "Top 25 U.S. Ports by Direction (CY 2001)," U.S. Department of Transportation Maritime Administration, available at http://www.marad.dot.gov/Marad_Statistics/C-Port-Dir.html, October 2002.

Mark, C., "Reactor-grade Plutonium's Explosive Properties," Nuclear Control Institute, available online at www.nci.org/NEW/NT/rgpu-mark-90.pdf, August 1990.

Mark, C., T. Taylor, E. Eyster, W. Maraman, J. Wechsler, "Can Terrorists Build Nuclear Weapons?" Nuclear Control Institute, 1987.

Morgan, M., "The Origins of the New Terrorism," *Parameters*, Vol 34, Spring 2004.

NCT (National Commission on Terrorism), "Countering the Changing Threat of International Terrorism: Report of the National Commission on Terrorism," Government Printing Office, 2000.

NERAC (Nuclear Energy Research Advisory Committee), "Annex: Attributes of Proliferation Resistance for Civilian Nuclear Power Systems," issued by the U.S. Department of Energy, October 2000.

NIMA (National Imagery and Mapping Agency), "Publication 151 – Distance Between Ports," issued by the U.S. Department of Defense, 2001.

NTI (Nuclear Threat Initiative) "Technical Background: A Tutorial on Nuclear Weapons and Nuclear-Explosive Materials," NTI Research Library, available online at http://www.nti.org/e_research/cnwm/overview/technical2.asp, accessed April 2003.

O'Brien, K., H. Sandmeier, G. Hansen, J. Campbell, "Cosmic Ray Induced Neutron Background Sources and Fluxes for Geometries of Air Over Water, Ground, Iron, and Aluminum," *Journal of Geophysical Research*, Vol. 83, January 1978.

Oetting, F., "Average Beta Energy of ^{241}Pu by Calorimetry," *Phys. Rev.*, Vol. 168, April 1968.

Peurrung, A. "Predicting ^{232}U Content in Uranium," PNNL-12075, issued by Pacific Northwest National Laboratory, December 1998.

Sampson, E.A., J.L. Parker, "Application of Gamma-ray Spectrometry in the Quantitative Non-Destructive Assay of Special Nuclear Materials," *Nucl. Instr. and Meth.*, Vol 299A, December 1990.

Stone, R., "Radiological Terrorism: New Effort Aims to Thwart Dirty Bombers," *Science*, Vol. 296, June 2002.

Tozer, D., "Ultra-Large Container Ships: the Green Ships of the Future?" *Shipping World & Shipbuilder*, October 2003.

Turekian, K., Oceans, Prentice Hall Scientific, 1976.

Wijnolst, N., M. Scholtens, F. Waals, Malacca-max: The Ultimate Container Carrier, Delft University Press, 1999.

WNA (World Nuclear Association), "Information and Issue Briefs: Thorium," World Nuclear Association, available online at http://world-nuclear.org/info/inf62.htm, November 2003.

WSC (World Shipping Council), "In-Transit Container Security Enhancement," World Shipping Council, available at http://www.worldshipping.org/security_white_paper.pdf, September 2003.

Appendix A

Vessel name	Capacity (TEU)	Speed (knots)	Vessel name	Capacity (TEU)	Speed (knots)
A.P. Moller	6600	24.6	Yun Long		12.0
Agnete Maersk	1100	18.0	Yu Quan Shan	83	
Albert Maersk	1100	18.0	Yu Xi Quan	345	12.6
Alva Maersk	1100	18.0	Zeus II	2728	20.5
Amersham	658	14.8	Zhao Gang No.1	72	
Axel Maersk	6600	24.6	Zhao Qing He		16.5
Caroline Maersk	6600	24.6	Zhen He	3801	22.5
Carsten Maersk	6600	24.6	Zhen Wu	108	
Cecilie Maersk	1750	19.0	Zhi Shan 1	36	
Charlotte Maersk	6600	24.6	Zhong Hang 608	36	
Chastine Maersk	6600	24.6	Zhong Hang 901	80	
Chesham	658	14.8	Zhong Hang 903	80	
Christian Maersk	1550	18.9	Zhong Hang 905	80	
Claes Maersk	1750	19.0	Zhong Hang 909	60	
Clara Maersk	1550	18.9	Zhong Hang 912	104	
Clementine Maersk	6600	24.6	Zhong Hang 913	104	
Clifford Maersk	6600	24.6	Zhong Hang 915	120	
Columbine Maersk	6600	24.6	Zhong Hang 916	96	
Cornelia Maersk	6600	24.6	Zhong Hang 917	118	
Cornelius Maersk	6600	24.6	Zhong Hang 919	118	
Denham	658	14.8	Zhong Hang 920	118	
Dirch Maersk	4300	24.2	Zhong He	4215	22.0
Glasgow Maersk	4300	24.2	Zhuang He	1668	15.5
Gosport Maersk	4300	24.2	Zhu Chuan 992	42	
Grasmere Maersk	4300	24.2	Zhu Hai 203	72	
Greenwich Maersk	4300	24.2	ZIM Adriatic	2810	19.0
Jens Maersk	2840	22.4	ZIM America	3029	21.0
Jeppesen Maersk	2840	22.5	ZIM Asia	3429	21.7
Johannes Maersk	2840	22.5	ZIM Atlantic	3429	21.7
Josephine Maersk	2840	23.0	ZIM Barcelona	4992	24.0
Karen Maersk	6000	24.6	ZIM Buenos Aires		19.5
Kate Maersk	6000	24.6	ZIM California	4992	24.0
Katrine Maersk	6000	24.6	ZIM Canada	3029	21.0
Kirsten Maersk	6000	24.6	ZIM China	3429	21.7
Knud Maersk	6000	24.6	ZIM Dalian	2998	21.0
Laura Maersk	3700	24.7	ZIM Eilat I	2606	21.0
Laust Maersk	3700	27.7	ZIM Europa	3429	21.7
Leda Maersk	3700	24.7	ZIM Florida	3005	20.0
Lexa Maersk	3700	24.7	ZIM Haifa I	2810	19.0
Lica Maersk	3700	25.0	ZIM Hong Kong	3029	21.0
Luna Maersk	3700	25.0	ZIM Iberia	3429	21.7
Madison Maersk	4300	23.5	ZIM Israel	3029	21.0
Maersk Aberdeen	1100	18.0	ZIM Italia	3029	21.0
Maersk Ahram	1100	18.0	ZIM Jamaica	3429	21.7
Maersk Antwerp	1100	18.0	ZIM Japan	3029	21.0
Maersk Arun	1100	18.0	ZIM Keelung	2810	19.0
Maersk Atlantic	1100	18.0	ZIM Korea	3029	21.0
Maersk Avon	1100	18.0	ZIM Mediterranean		24.0
Maersk Carolina	4300	24,20	ZIM New York	4992	24.0
Maersk Gairloch	4300	24.2	ZIM Pacific	3429	21.0

Maersk Gateshead	4300	24.0	ZIM Panama	4992	24.0
Maersk Georgia	4300	24.2	ZIM Piraeus	5000	
Maersk Gironde	4300	24.2	ZIM Ravenna I	2998	21.0
Maersk Missouri	4300	24.3	ZIM Shanghai	4992	24.0
Maersk Virginia	4300	24.0	ZIM Shenzhen	2633	21.0
Magleby Maersk	4300	23.5	ZIM Singapore I	2474	21.0
Majestic Maersk	4300	23.5	ZIM USA	3429	21.7
Marchen Maersk	4300	23.0	ZIM Venezia II	2682	21.0
Maren Maersk	4300	23.0	ZIM Virginia	4992	24.0
Margrethe Maersk	4300	23.0	Zi Ya He	764	19.2
Marie Maersk	4300	23.5	Hyundai Republic	6479	26.4
Marit Maersk	4300	23.0	Hyundai Kingdom	6479	26.4
Marstal Maersk	4000	24.5	Hyundai National	6479	26.4
Mathilde Maersk	4300	23.0	Hyundai Dominion	6479	26.4
Mayview Maersk	4300	23.5	Hyundai Patriot	6479	26.4
Mc-Kinney Maersk	4300	23.5	Hyundai Independence	5551	25.6
Mette Maersk	4300	23.0	Hyundai Liberty	5551	25.6
Munkebo Mærsk	4000	24.5	Hyundai Discovery	5551	25.6
Nele Maersk	2200	21,80	Hyundai Freedom	5551	25.6
Nexoe Maersk	2200	21,80	Hyundai Fortune	5551	25.6
Nicolai Maersk	2200	21,80	Hyundai General	5551	25.6
Nikoline Maersk	2200	21,80	Hyundai Highness	5551	25.6
Nora Maersk	2200	21,80	Hyundai Admiral	4411	25.1
Nysted Maersk	2026	21.8	Hyundai Baron	4411	25.1
Regina Maersk	6000	24.6	Hyundai Commandore	4411	25.1
Sea-Land Champion	3733	24.0	Hyundai Duke	4411	25.1
Sea-Land Charger	3733	24.0	Hyundai Emporer	4411	25.1
Sea-Land Comet	3733	24.0	Hyundai Federal	4411	25.1
Sea-Land Eagle	3733	24.0	Hyundai Explorer	3014	21.7
Sea-Land Freedom	2344	20.3	Hyundai Poineer	3014	21.7
Sea-Land Intrepid	3733	24.0	Hyundai Frontier	3014	21.7
Sea-Land Lightning	3733	24.0	Hyundai Commander	3014	21.7
Sea-Land Mariner	2344	20.3	Hyundai Vladivostok	2174	21.5
Sea-Land Mercury	3733	24.0	Hyundai Future	2174	21.5
Sea-Land Meteor	3733	24.0	Hyundai Stride	2174	21.5
Sea-Land Pride	3918	21.0	Hyundai Advance	2174	21.5
Sea-Land Racer	3733	24.0	Hyundai Sprinter	2174	21.5
Sea-Land Value	3612	21.0	Hyundai Progress	2174	21.5
Sally Maersk	6600	24.6	Hyundai Highway	2174	21.5
Sine Maersk	6600	24.6	Hyundai Bridge	2174	21.5
Skagen Maersk	6600	24.6	Hyundai Primorskiy	628	15.8
Sofie Maersk	6600	24.6	Hyundai Infinity	2241	23.0
Soroe Maersk	6600	24.6	Hyundai Nobility	2241	23.0
Sovereign Maersk	6600	24.6	Suzuran	1177	18.1
Susan Maersk	6600	24.6	Asian Zephyr	1032	18.5
Svend Maersk	6600	24.6	Cape Canet	834	18.0
Svendborg Maersk	6600	24.6	Doris Waluff	1203	19.5
Taasinge Maersk	1750	19.0	Saturn	1129	18.5
Thies Maersk	1350	18.6	Star Eagle		15.0
Thomas Maersk	1500	18.9	Star Evanger		15.0
Thuroe Maersk	1350	18.6	Star Evviva		15.0
Tinglev Maersk	1500	18.9	Star Florida		15.0

Tobias Maersk	1300	18.0
Torben Maerks	1300	18.0
Tove Maersk	1350	18.6
Trein Maersk	1300	18.0
Troense Maersk	1350	18.6
Achim		15.5
ACX Dahlia	1430	19.5
ACX Hibiscus	1430	19.5
ACX Lily	1250	19.0
ACX Magnolia	181	19.5
ACX Marguerite	1480	19.0
ACX Marigold	1467	19.0
ACX Primrose	820	19.5
ACX Rafflesia	1430	19.5
Agios Dimitrios I	3428	18.5
Akashi Bridge	3456	23.0
Akinada Bridge	5600	25.0
Alexandria	400	17.5
Al Mariyah	2199	
Alva Star	3209	21.0
Al Wajba	2199	
Ambassador Bridge		21.5
America Senator	2661	
Anan Bhum	993	16.5
An Rong 1	116	
Aotea	1842	
Apollon I	1566	21.0
Arafura	2432	
Aramac	2732	
Aris I	1810	
Asian Glory	357	14.3
Asian Gyro	1032	18.5
Astoria Bridge	2258	20.0
Atlantic Cartier	3100	18.0
Atlantic Companion	3100	18.0
Atlantic Compass	3100	18.0
Atlantic Concert	3100	18.0
Atlantic Conveyor	3110	18.0
Australia Bridge	2400	
Bai Yun He	1674	20.0
Baltrum Trader	2470	21.0
Banga Bijoy	456	
Banga Biraj	669	
Banga Birol	606	
Banga Bodor	510	
Banga Bonik	500	
Banga Borak	510	
Banga Borat	846	
Banga Lanka	538	
Bao Zhong 23	66	
Bao Zhong 68	140	
Barcelona Bridge	3965	23.1
Star Fraser		15.0
Star Fuji		15.0
Star Geiranger		15.0
Star Gran		15.0
Star Grindanger		15.0
Star Grip		15.0
Star Hidra		16.0
Star Hoyanger		16.0
Star Ikebana		17.0
Star Inventana		17.0
Star Isoldana		17.0
Star Istind		17.0
Star Isfjord		17.0
Star Ismene		17.0
Adeline Delmas	937	13.5
Africa	1935	18.0
Alpana	1664	20.0
Astrid	574	13.5
Blandine Delmas	937	13.5
Bougainville	1730	
Caroline Delmas	937	13.5
Delmas Acacia	676	18.5
Delmas Aloe	676	18.5
Delmas Blosseville	1202	19.0
Delmas Cartier	1728	20.0
Delmas Casablanca	518	15.5
Delmas Charcot	1706	19.6
Delmas Forbin	1740	21.0
Delmas Fjacaranda	676	18.5
Delmas Kenya	1158	17.0
Delmas Kerguelen	1740	20.5
Delmas Mascareignes	1466	18.5
Delmas Sycamore	789	18.0
Delmas Tourville	1730	20.0
Delphine Delmas	937	13.5
Eax Sanctity	940	
Elisa Delmas	1614	20.3
Flora Delmas	1614	20.3
Gaby Delmas	1614	20.3
Giorgia	1935	18.0
Heide	582	15.5
Kaduna	511	15.3
Kamina	1113	16.5
Kwanza	4355	19.0
La Bourdonnais	1600	
Laura Delmas	4473	19.0
Lauren	2150	23.0
Lucie Delmas	4473	19.0
Madagascar	1346	
Marie Delmas	2207	22.6
Mirella	2152	19.0
Mol Horizon	1113	16.5

Bay Bridge	2257	20.0
Beauty River	1932	17.5
Berlin Senator	3007	21.0
Bimba 1	74	
Bin Cheng	724	15.5
Bin Dong Shan	78	9.0
Bing He	1696	14.5
Blue Moon	614	16.0
Bonn Express	2803	22.8
Bonvoy 88	279	11.5
Bo Shi Ji 386	45	
Bosporus Bridge	3210	24.0
BPW 2031	350	
Bremen Bridge	5576	
Bremen Senator	1730	
Bunga Mas Empat	135	
Bu Yi He	3400	21.0
Cai Yun He	1432	19.0
California Luna	2916	22.0
California Senator	2850	
Camilla Rickmers	1728	20.0
Cap Colville	1510	
Cap Delgado	2442	21.5
Cape Campbell	834	18.5
Cape Canaveral	356	16.0
Cape Canet	590	18.5
Cape Coldbek	834	18.5
Cape Cook	834	18.5
Caraka JN3-9		10.0
Caraka JN319	128	10.0
Carinthia	2824	24.0
Caroline Schulte	2532	21.0
CEC Mayflower	650	20.2
CEC Morning	650	20.2
Centre Point 28	80	
Chang An 104	104	
Chang Jiang Bridge	3456	24.0
Chang Sheng 301	74	
Chang Xing 108	48	
Chang Xing 208	48	
Chao He	1322	17.2
Chao Shan He	836	17.0
Cherokee Bridge	4226	24.5
Chesapeak Bridge	4226	24.5
Chesapeak Bay Bridge	3400	21.0
Chicago Bridge	5576	25.0
Chiswick Bridge	5600	25.0
Chuan He	5446	22.5
Chun He	1322	16.0
Concord	1452	
Concord Bridge	3482	23.0
Conti Arabian	1466	18.5
Mol Karina	770	
Nicolas Delmas	2207	22.6
Paraguay	1935	18.0
Parana	2129	17.5
Patricia Delmas	1113	16.5
Ponl Mahe	1104	
Rejane Delmas	1684	18.0
Reunion	1364	
Rokia Delmas	5278	16.0
Roland Delmas	3308	17.0
Romain Delmas	3308	17.0
Rosa Delmas	2578	16.0
Roxanne Delmas	3590	15.5
Saint Roch	3308	17.0
Santa Barbara I	1742	19.2
Santa Margherita	1895	20.0
Sassandra	4355	19.0
St Pauli	411	14.0
Trave Trader	1608	21.0
CSAV Shanghai	2214	
Copiapo	2074	
Ikoma	1613	
CSAV Callao	2524	
CSAV Shenzhen	2450	
Buxfavourite	2456	
IGA	1613	
Sea Puma	2205	
IZU	1613	
Alice Rickmers	1900	
Donna Schulte	2256	
CSAV Livorno	1878	
CCNI Ancud	1816	
CSAV Barcelona	1878	
CSAV Genova	1829	
Alianca Bahia	2460	
Alianca Brasil	2045	
Alianca Europa	2045	
Alianca Hong Kong	2468	
Alianca Ipanema	2233	
Alianca Macarena	2233	
Alianca Sao Paulo	2524	
Alianca Shanghai	2442	
Alianca Singapore	2456	
Alianca Urca	1151	
Ankara	1388	
Arnis	1208	
Berulan	907	
Cabo Creus	2524	
Cap Aguilar	1740	
Cap Blanco	2154	
Cap Bonavista	2442	
Cap Carmel	2542	

Conti Cartagena	2432	20.0
Conti Jork	1597	18.0
Conti Valencia	2305	21.0
Cosco Antwerp	5446	24.5
Cosco Atlantic	2054	21.4
Cosco Cape Town		22.2
Cosco Felixstowe	5446	24.5
Cosco Hamburg	5446	24.5
Cosco Hong Kong	5446	24.5
Cosco Kiku	542	18.0
Cosco New York	2728	17.5
Cosco Norfolk	3330	22.0
Cosco Qingdao	5446	24.5
Cosco Ran	542	18.0
Cosco Redsea	1164	18.7
Cosco Rotterdam	5446	24.5
Cosco Sakura	542	18.0
Cosco Sao Paulo		22.2
Cosco Shanghai	5446	24.5
Cosco Singapore	5446	24.5
Cosco Tianjin	5752	26.3
CRC No. 1	96	
Da He	3801	24.0
Dainty River	1932	18.5
Da Qing He	764	19.2
Daxin	588	15.6
Delaware Bridge	4452	
Diman II	1822	19.0
Donau Bridge	4038	
Dong He	2761	18.5
Dong Rong	58	
Dong Xu	83	9.5
Dong Yun 009	36	
Dong Yun 030	24	
Dong Yun 556	96	
Dubai	2199	
Duburg	1464	
Eagle Express	1704	21.0
Eagle Strength	725	17.0
E Cheng	680	18.3
Elbe Bridge		24.5
Elisabeth Schulte	2532	21.9
Empress Dragon	3494	21.0
Empress Heaven	3494	21.0
Empress Phoenix	3494	21.0
Empress Sea	3494	21.0
En Hui	88	
En Yuan	88	
Ever Able	1164	20.5
Ever Ally	1164	20.5
Ever Apex	1164	20.5
Ever Dainty	4211	25.0

Cap Castillo	2442
Cap Colorado	1510
Cap Colville	1510
Cap Cortes	1651
Cap Domingo	2100
Cap Ferrato	2478
Cap Finisterre	2023
Cap Frio	2456
Cap Lobos	1645
Cap Norte	2468
Cap Ortegal	2442
Cap Pasado	1550
Cap Pilar	1581
Cap Polonio	2023
Cap Reinga	1651
Cap Roca	2640
Cap San Antonio	3739
Cap San Augustin	3739
Cap San Lorenzo	3739
Cap San Marco	3739
Cap San Nicolas	3739
Cap San Raphael	3739
Cap Velas	1709
Cap Vilano	1742
Cap Vincent	1835
Castor	1129
City of Glasgow	956
City of Hamburg	2228
City of Istanbul	1232
City of Manchester	300
City of Tunis	1709
Columbian Express	752
Columbus Australia	2062
Columbus Canada	1215
Columbus China	2524
Columbus Florida	1651
Columbus Victoria	1229
Columbus Waikato	1837
Copacabana	1402
Courier	1452
Damaskus	1645
Flamengo	1254
Independente	1138
Intrepido	1138
Kairo	1709
Kapitan Kurov	1250
Karthago	1354
Leblon	1157
Mekhanik Kalyuzhniy	1167
Santa Felicita	2169
Santa Fiorenza	2169
Santa Francesca	2169

Ever Delight	4211	25.0
Ever Deluxe	4211	25.0
Ever Diadem	4211	25.0
Ever Diamond	4211	25.0
Ever Dynamic	4211	25.0
Ever Gaining	3428	21.7
Ever Gallant		22.1
Ever Garden	2728	21.7
Ever Gather	2728	20.5
Ever General	3428	20.7
Ever Genius	2868	21.3
Ever Gentle	2868	21.3
Ever Gentry	2868	21.3
Ever Gifted	2728	21.0
Ever Given	3428	22.2
Ever Glowing		21.9
Ever Golden	2868	21.3
Ever Goods	3428	22.2
Ever Govern	2868	21.3
Ever Growth	2728	22.5
Ever Guest	3428	22.2
Ever Guide	2390	22.0
Ever Uberty	5364	25.0
Ever Ultra	5625	
Ever Union	5364	
Ever Unique	5364	25.0
Ever Unison	5364	25.0
Ever United	5364	26.7
Ever Uranus	5652	
Ever Urban	5652	
Ever Useful	5652	25.0
Fair Wind 18	120	
Fair Wind 28	120	
Faith I	3428	18.5
Fang Gang 1001	54	8.0
Fang Gang 3	32	
Fang Gang 6	45	8.0
Fei He	3764	23.0
Fei Yun He	1702	20.2
Feng Da 328	16	7.0
Feng Guang 2	80	
Feng Shun 8	208	
Feng Yun He	1432	19.0
Fo Hang 906	60	
France	4158	23.1
Franconia	946	20.0
Franklin Strait	518	15.5
Fu Feng	132	
Fu Feng Shan	132	
Fu Gang 811	96	
Fu Gang 812	52	
Fu Gang 815	96	

Santa Isabella	2400	
Santos Express	2532	
Sea Tiger	2562	
Stoja	703	
Tausala Samoa	1116	
Uranus	1835	
Vernuda	703	
Westmed II	1181	
Global Rio		14.0
Bruarfoss	724	
Dettifoss	1457	
Godafoss	1457	
Manafoss	518	
Selfoss	724	
Skogafoss	416	
Heinrich S	2474	21.0
Agiasofia	1555	17.6
Angeln	657	17.5
Athena I	1894	21.0
Birk	657	17.0
Cala Paestum	1645	21.0
Caribbean Sea	3681	24.0
Conti Barcelona	1597	18.0
Dimitra II	1894	21.0
Ever Gleamy	2728	20.5
Ever Grade	2728	20.5
Ever Peace	1618	19.3
Ever Pearl	1618	19.3
Ever Racer	4229	23.0
Ever Reach	4229	23.0
Ever Refine	4229	23.2
Ever Renown	4229	23.2
Ever Repute	4229	23.2
Ever Result	4229	23.2
Ever Reward	4229	23.2
Ever Right	4229	23.0
Ever Round	4229	23.0
Ever Royal	4229	23.0
Ever Unific	5652	25.0
Ever Unity	5652	25.0
Green Modest	951	15.5
Green Moral	951	15.5
Hansa Africa	3424	23.5
Hansa India	3424	22.8
Hatsu Ethic	6332	24.5
LT Going	2728	20.5
Pelopensian Pride	3428	18.0
Poseidon VII	1894	21.0
Rhoneborg	1643	17.5
UNI Accord	1164	18.7
UNI Ahead	1164	18.7
UNI Ardent	1164	18.7

Fu Gang 816	96	
Fu Gang 818	96	
Fu Tai	63	10.0
Gallant Wave	1510	18.0
Ganta Bhum	1094	18.0
Gao Cheng	724	15.6
Gao He	2761	18.5
Gao Yao Gang No. 1	36	9.0
Genoa Bridge	5600	25.0
George Washington Bridge		21.5
Gigi	152	11.0
Gihock	504	14.0
Gijoo	152	11.0
Gikim	276	10.5
Gileong	597	14.0
Gi Lian	396	12.0
Gimeng	235	12.5
Ginter Star	278	15.0
Giseng	191	11.0
Gisiang	384	13.5
Gisoon	191	11.0
Giswee	202	11.0
Global 3	100	8.0
Glory D	946	18.0
Golden Cloud	618	
Golden Gate Bridge	5610	24.4
Golden Star	208	
Great Pride	538	14.2
Guang Da Lun	45	
Guang Liong Lun	45	
Guang Xing Lun	45	
Guan Hang 109	64	10.0
Guan Hang 238	60	
Guan Hang 278	60	9.0
Guan Hang 362	84	
Guan Hang 393	45	
Gulf Bridge	1984	19.0
Guo Dian 1001	106	
Haifenglianfa	358	13.5
Hai Feng Shan	283	11.5
Hakone	1864	
Han Bo 1 Hao	66	
Han Bo 2 Hao	66	
Han Da	51	10.0
Hang Feng	140	
Ha Ni He	3400	21.0
Han Jiang He	422	17.5
Hanjin Amsterdam	5618	26.3
Hanjin Athens	5618	26.3
Hanjin Barcelona	4024	24.0
Hanjin Basel	5753	26.3
Hanjin Beijing	5302	26.4
UNI Assent	1164	18.7
UNI Forever	978	16.5
UNI Fortune	953	16.5
UNI Oasis	1170	15.6
UNI Onward	1278	14.8
UNI Order	1170	15.6
UNI Orient	1182	14.8
UNI Phoenix	1618	18.7
Vlaherna	1555	17.6
Vladivostok	1748	18.5
Kapitan Afanasyev	1748	18.5
Fesco Voyager	1684	20.0
Amsteldiep	446	
Anna J	198	
APL Manaus	1016	
Argana	353	
Argonaut	1236	
Astor	1129	
Aynur Urkmez	580	
Baltimar Boreas	256	
Beliz Urkmez	580	
Cape Falcon	1200	
Castor	446	
Chesapeak Bay	2411	
City of Cape Town	3126	
City of Stuttgart	1900	
Colombo Bay	4224	
Columbus New Zealand	4112	
Delaware Bay	2411	
Endeavor	1928	
Endurance	1928	
Enterprise	1928	
Genua Express	2157	
Heemskerck	3230	
Heide J	202	
Ijsseldijk	301	
Jervis Bay	4224	
Karin B	350	
Luetjenburg	3510	
Marivia	2082	
Mercosul Palometa	1512	
Mercosul Pescada	1730	
Mercosul Uruguay	740	
Merkur Lake	1012	
Mount Ida	724	
Nedlloyd Africa	3604	
Nedlloyd America	3604	
Nedlloyd Asia	3604	
Nedlloyd Clarence	2515	
Nedlloyd Clement	2470	
Nedlloyd Europa	3604	
Nedlloyd Hong Kong	4169	

Hanjin Bremen	2692	22.0	Nedlloyd Honshu	4181
Hanjin Brussels	5618	26.3	Nedlloyd Oceania	3604
Hanjin Cairo	5447	25.9	Newport Bay	4224
Hanjin Chicago	5752	26.3	Olivia	1452
Hanjin Colombo	4024	24.0	Oriental Bay	4180
Hanjin Copenhagen	5618	26.3	P&O Nedlloyd Abidjan	2506
Hanjin Elisabeth	2846	21.0	P&O Nedlloyd Acapulco	2556
Hanjin Felixstowe	2692	21.0	P&O Nedlloyd Accra	2506
Hanjin Geneva	5752	26.3	P&O Nedlloyd Aconcagua	2556
Hanjin Gothenburg	5447	24.0	P&O Nedlloyd Adelaide	3005
Hanjin Hamburg	2692	21.0	P&O Nedlloyd Adriana	2556
Hanjin Helsinki	5447	24.2	P&O Nedlloyd Agulhas	2506
Hanjin Kaohsiung	2692	21.0	P&O Nedlloyd Algoa	2506
Hanjin Kelung	2668	22.0	P&O Nedlloyd Altiplano	2556
Hanjin Lisbon	5752	26.3	P&O Nedlloyd Andes	2556
Hanjin London	5306	26.4	P&O Nedlloyd Antisana	2556
Hanjin Los Angeles	4024	24.0	P&O Nedlloyd Apapa	2506
Hanjin Madrid	5752	26.3	P&O Nedlloyd Araucania	1102
Hanjin Malta	4024	24.0	P&O Nedlloyd Atacama	2556
Hanjin Marseilles	4024	24.0	P&O Nedlloyd Bantam	3430
Hanjin Nagoya	4024	24.0	P&O Nedlloyd Barentsz	5468
Hanjin New York	4038	22.0	P&O Nedlloyd Barossa Valley	2602
Hanjin Osaka	4024	24.0	P&O Nedlloyd Beirut	1717
Hanjin Oslo	5308	26.0	P&O Nedlloyd Botany	4112
Hanjin Ottawa	5618	26.3	P&O Nedlloyd Brisbane	2686
Hanjin Paris	5302	26.4	P&O Nedlloyd Brunel	2080
Hanjin Pennsylvania	4389	24.3	P&O Nedlloyd Buenos Aires	1779
Hanjin Philadelphia	4389	24.3	P&O Nedlloyd Cagliari	970
Hanjin Phoenix	4389	24.3	P&O Nedlloyd Calypso	1730
Hanjin Portland	4024	24.0	P&O Nedlloyd Caracas	4253
Hanjin Praha	4389	24.3	P&O Nedlloyd Caribbean	4253
Hanjin Pretoria	4389	24.3	P&O Nedlloyd Cesme	1022
Hanjin Rome	5308	26.4	P&O Nedlloyd Chania	1012
Hanjin San Francisco	4024	24.1	P&O Nedlloyd Christine	856
Hanjin Savannah	4038	22.0	P&O Nedlloyd Chusan	3430
Hanjin Shanghai	4024	24.0	P&O Nedlloyd Cobra	4038
Hanjin Singapore	2666	22.0	P&O Nedlloyd Cook	6802
Hanjin Taipei	5447	25.9	P&O Nedlloyd Curacao	1012
Hanjin Tokyo	4024	24.0	P&O Nedlloyd Damietta	3607
Hanjin Valencia	4024	24.0	P&O Nedlloyd Dejima	3430
Hanjin Vancouver	2692	21.0	P&O Nedlloyd Drake	5468
Hanjin Vienna	5752	26.3	P&O Nedlloyd Dubai	2732
Hanjin Washington	5302	26.4	P&O Nedlloyd Encounter	4112
Hanjin Wilmington	4024	24.0	P&O Nedlloyd Houston	1779
Han Long	52	10.0	P&O Nedlloyd Houtman	6802
Hansa Stavanger		20.0	P&O Nedlloyd Hudson	5468
Hanseduo	500	16.0	P&O Nedlloyd Hunter Valley	2478
Han Shui He	422	17.5	P&O Nedlloyd Inca	923
Han Tao He	422	17.5	P&O Nedlloyd Juliana	2556
Han Zhong He	422	17.5	P&O Nedlloyd Kobe	6690
Hao Sheng 101	96		P&O Nedlloyd Kowloon	6690
Happy Island	400	15.0	P&O Nedlloyd Los Angeles	1548

Hatsu Eagle	6332	24.5	P&O Nedlloyd Magellan	5642
Hatsu Elite	6332	24.5	P&O Nedlloyd Mahe	1104
Hatsu Envoy	6332	24.5	P&O Nedlloyd Mairangi	4112
Hatsu Excel	6332	24.5	P&O Nedlloyd Malindi	1116
Hatsu Pride	1618		P&O Nedlloyd Marita	2556
Hatsu Prima	1618	18.7	P&O nedlloyd Maxima	2556
Heidelberg Express	3468	22.0	P&O Nedlloyd Mercator	5468
Henry Hudson Bridge		21.5	P&O Nedlloyd Muisca	1102
Hera	2728	18.5	P&O Nedlloyd Nina	2014
Hermes III	1926		P&O Nedlloyd Obock	384
Hong Kong Senator	2850	21.3	P&O Nedlloyd Olinda	3430
Hong Yun He	1700	20.0	P&O Nedlloyd Palliser	4112
Honor River	1932	16.5	P&O Nedlloyd Panama	3014
Hope	3480	21.0	P&O Nedlloyd Pantanal	2474
Howrah Bridge	2257	20.0	P&O Nedlloyd Pinta	2394
Hsh Ubin	2097	17.0	P&O Nedlloyd Regina	2556
Hua Chang Hai 16	150		P&O Nedlloyd Remuera	4112
Hua Hang 229	36		P&O Nedlloyd Rotterdam	6690
Huai Ji He	424	16.9	P&O Nedlloyd Salsa	2061
Huai Lai He	724	17.3	P&O Nedlloyd Samba	1742
Hua Lun 1	100		P&O Nedlloyd San Francisco	1716
Hua Tai He	1216	24.8	P&O Nedlloyd Seattle	3450
Hua Yun He	1700	20.0	P&O Nedlloyd Shackleton	6802
Hui Long 7		154.0	P&O Nedlloyd Singapore	2169
Hui Xin Hang 508		60.0	P&O Nedlloyd Southampton	6690
Humber Bridge	3456	21.0	P&O Nedlloyd Stuyvesant	6802
Humen Bridge	3008	21.0	P&O Nedlloyd Surat	3430
Hunsa Bhum	1094	18.0	P&O Nedlloyd Susana	2556
Hu Tuo He	764	19.2	P&O Nedlloyd Taranaki	1270
Hyundai Challenger	3014	20.5	P&O Nedlloyd Tasman	5468
Hyundai Innovator	3014	20.5	P&O Nedlloyd Tema	1511
Ibn Sina	2850		P&O Nedlloyd Teslin	2556
Indonesian Star	1203	16.0	P&O Nedlloyd Thekwini	1055
Intra Bhum		14.5	P&O Nedlloyd Torres	5642
Jade Trader	1122	19.8	P&O Nedlloyd Trinidad	384
James River Bride	5610	25.0	P&O Nedlloyd Valentina	2556
Japan Senator	2661	19.5	P&O Nedlloyd Vera Cruz	1779
Jaru Bhum	640	14.5	P&O Nedlloyd Vespucci	5642
Ji Hai Xiang	96		P&O Nedlloyd Xiamen	2986
Jing Po He	3400	21.0	Peninsula Bay	4180
Jin Hai Feng	36	8.5	Providence Bay	4224
Jin Hai Yan	52	8.5	Repulse Bay	4224
Jin He	5446	23.0	San Lorezo I	1512
Jin Long Jiang	71	10.0	Santa Federica	2169
Jin Sheng	386	18.0	Shenzhen Bay	4224
Jing Yun He	1432	19.0	Singapore Bay	4224
Jun Chuan 9	120		Stadt Kiel	373
Jupiter Bridge	5551	25.9	Sydney Express	4112
Jurong Bauhinia	802	16.5	Tai Chuang	1034
Kaido	450	15.0	Ulsnis	1388
Kai Fa	90		Volkers	374
Kai Yue	113		Providence	1624

Kasuga 1	2450	
Khaled Ibn Al Waleed	2211	
Kota benar	764	17.0
Kota Bintang	476	15.0
Ksh Kusu	1674	17.5
Kuoyu	1169	18.0
Kwong Ta No. 8	132	
Lan Shi 10	64	
Lausanne	2826	24.0
Lian Fa 66	140	
Lian Fa 67	140	
Lian Feng		12.0
Liao He	1234	17.7
Lilium	387	15.0
Ling Chang He	377	12.5
Ling Quan He	672	16.1
Ling Yun He	1702	20.3
Lin Hai 103	54	
Lions Gate Bridge	5610	25.0
London Senator	2850	
Long Beach Bridge	5576	25.0
Long He	725	18.9
Long Lun 103	52	10.0
LT Garland	3428	21.0
LT Genova	2987	21.0
LT Giant	2728	17.5
LT Grand	2728	20.5
LT Greet	2728	17.5
LT Guard	2868	
LT Lloydiana	2511	20.0
LT Pearl	1618	19.3
LT Popular	1566	21.0
LT Power	1618	18.7
LT Trieste	2820	17.5
LT Ulysees	5652	25.0
LT Unica	4948	25.0
LT Unicorn	5652	25.0
LT Unity	5652	25.0
LT Universo	5346	25.0
LT Ursula	5652	
LT Usodimare	4948	25.0
LT Utile	5652	25.0
Lu He	5446	24.5
Lumoso Express	138	
Lunar River	494	19.5
Luo Ba He	3400	21.0
Luo He	1234	18.3
Lu Sheng	127	
Lykes Ambassador	3266	11.5
Lykes Deliverer	4051	
Lykes Discoverer	3026	18.8
Lykes Explorer	3026	18.8
Karukera	1624	
Anterpen Express	4890	24.0
Tokyo Express	4890	24.0
Bremen Express	4890	24.0
Rotterdam Express	4890	24.0
Kuala Lumpur Express	4890	24.0
New York Express	4890	24.0
Singapore Express	4890	24.0
Kobe Express	4612	24.0
Dusseldorf Express	4612	24.0
London Express	4612	24.0
Hannover Express	4639	23.0
Leverkusen Express	4639	23.0
Dresden Express	4639	23.0
Hoechst Express	4639	23.0
Ludwigshafen Express	4639	23.0
Essen Express	4639	23.0
Stuttgart Express	4639	23.0
Paris Express	4639	23.0
Busan Express	6732	25.6
San Francisco Express	6732	25.6
Bankok Express	6732	25.6
Los Angeles Express	6732	25.6
Berlin Express	7506	25.0
Hong Kong Express	7506	25.0
Hamburg Express	7506	25.0
Shanghai Express	7506	25.0
Santiago Express	2181	18.0
Humboldt Express	2181	18.0
Frankfurt Express	3430	23.0
Abu Dhabi	3800	
Al Abdali	3800	
Al Farahidi	3800	
Alnoof	3800	
Asir	3800	
Deira	3800	
Fowairet	3800	
AlMutanabbi	3800	
Najran	3800	
Al Sabahia	3800	
MSC Brasilia	3074	
MSC Carla	3022	
MSC Germany	2708	
MSC Levina	2900	
MSC Maria Laura	2557	
MSC Pretoria	2829	
Hammurabi	2199	
Hanjin Berlin	5302	
Al Ihsa'a	2199	
PONL Beirut	1665	
Port Said Senator	1718	
AL Manakh	2199	

Lykes Hero	3026	21.0
Lykes Innovator	2808	22.0
Lykes Liberator	3026	18.8
Lykes Motivator	2954	21.7
Lykes Navigator	3026	18.8
Lykes Pathfinder	2280	19.8
Mackinac Bridge	2875	21.5
Maersk Doha	4158	
Maersk Norfolk	2300	20.0
Man Fu	72	
Manhattan Bridge		22.4
Maple River	2157	18.0
Mare Balticum	1054	17.5
Mare Doricum	1054	17.5
Mare Lycium	3900	24.0
Mare Thracium		21.0
Margret Knueppel	532	16.0
Mathu Bhum	1080	17.0
Matsuko	564	20.7
Med Taipei	2550	21.0
Mentor	294	
Mercury Bridge	5551	25.9
Merkur Bay		23.0
Methi Bhum	928	17.0
Mild Lin	746	15.5
Mild Star	422	15.0
Mild Sun	422	15.0
Mild Union	443	14.0
Min Feng	308	
Ming America	3494	21.2
Ming Asia	3604	21.2
Ming Bamboo	5551	25.9
Ming Cheng	724	15.6
Ming Cosmos	5551	25.9
Ming Cypress		25.9
Ming East	3502	24.0
Ming Europe	3604	21.2
Ming Green	5551	25.9
Ming Longevity	1984	19.0
Ming North	3502	24.0
Ming Ocean	1984	19.0
Ming Orchid	5551	25.9
Ming Pine	5551	25.9
Ming Plum	5551	25.9
Ming South	3502	24.0
Ming West	3502	24.0
Ming Zenith	3052	24.0
Min He	2761	18.5
Min Su	144	
Min Tai No.2	106	
Min Tai No.4	140	
Min Tai No.5	80	
Canmar Bravery	1737	
Canmar Endurance	1952	
Canada Senator	2017	
Canmar Glory	1074	
Canmar Triumph	1061	
Canmar Valour	1061	
Canmar Victory	1053	
Al Mirqab	2199	
Qatari Ibn Al Fuja'a	2199	
Norasia Valparaiso	4100	
CMA-CGM Eiffel	3900	
Norasia Enterprise	4444	
CMA-CGM Vernet	3538	
CMA-CGM Vega	3900	
CMA-CGM Mercure	4369	
CMA-CGM Neptune	4365	
DAL Kalahari	3177	
DAL Madagascar	1730	
Karonga	1191	
OOCL Hamburg	8063	
OOCL Long Beach	8063	
OOCL Ningbo	8063	
OOCL Qingdao	8063	
OOCL Rotterdam	8063	
OOCL Shenzhen	8063	
OOCL Chicago	5714	
OOCL San Francisco	5714	
OOCL Netherlands	5390	
OOCL Singapore	5390	
OOCL America	5344	
OOCL Britain	5344	
OOCL California	5344	
OOCL China	5344	
OOCL Hong Kong	5344	
OOCL Friendship	3218	
OOCL Fair	3161	
OOCL Fidelity	3161	
OOCL Freedom	3161	
OOCL Envoy	2544	
OOCL Exporter	2544	
OOCL Montreal	4402	
OOCL Belgium	2808	
MV Helgafell	703	16.5
MV Arnafell	703	16.5
MV Skaftafell	364	15.5
MS Jokulfell	140	13.8
MV Regina J	395	15.0
MV Kurske	266	13.0
MV Adele J	202	12.5
MV Carina	202	12.5
MV Virtsu	266	14.0
MV Dirhami	266	14.0

Min Tai No.6	72	
Min Yun He	1432	19.0
Mol Glory	2400	20.6
Mol Triumph	2400	22.0
mol Wellington	1600	
Montreal Senator	1174	18.0
MSC New Plymouth	1550	
Na Xi He	3400	21.0
Nevelsk	270	12.5
New Blessing	706	16.5
Newpac Cirrus	650	20.2
Newpac Cumulus	650	20.2
Newport Bridge	3456	23.0
Nicolas Delamus	2207	21.8
Nithi Bhum	928	17.0
Noble River	969	15.0
Nordseas	1400	20.0
Nordstrand	2280	20.0
Nordsun	1158	17.0
Norfolk Express	3607	23.5
Normandie Bridge		23.0
Northern Fortune	1899	19.3
Northern Virtue	2987	22.0
NYK Prosperity		22.5
OOCL Atlantic	3607	23.5
OOCL Europe		23.8
OOCL Faith	3161	20.5
OOCL Fortune	2880	20.5
OOCL Harmony	2500	22.0
OOCL Japan	5344	23.0
OOCL Japan	2762	22.0
Oriental Bright	1001	17.0
Orient Brilliancy	545	15.0
OSG Argosy	279	
Oxford	821	
P&O Nedkowlown	6690	
P&O Nedlloyd Auckland	2890	21.5
P&O Nedlloyd Genoa	2890	21.5
P&O Nedlloyd Jakarta	2890	21.5
P&O Nedlloyd Marseille	2890	21.5
P&O Nedlloyd Newark	2720	22.0
P&O Nedlloyd Sydney	2890	21.5
Pac Bali	306	
Pac Banda	314	
Pac Bintan	306	
Pacific Envoy	728	16.3
Pacific Senator	2661	18.0
Palermo Senator	2661	18.0
Panagia Tinou		22.0
Pancaran Sinar	916	16.0
Pan He	725	16.8
Patmos Senator	2661	18.0
MV Kalana	266	14.0
MV Muuga	266	13.0
CMA-CGM Rodin	2602	21.5
Libra New York	2526	21.7
Ocean Trader	1608	21.0
Libra Buenos Aires	2470	22.0
MV Marienborg	1684	19.0
ACX Cherry	1048	
ACX Cosmos	1048	
ACX Hokuto	338	
ACX Lilac	1430	
ACX Sakura	1350	
ACX Swan	484	
Angela J	260	
California Jupiter	2841	
California Mercury	2990	
Cape Charles	2829	
Cape May	2826	
Commodore	2764	
Conti Malaga	2432	
Hansa Constitution	2760	
Hotaka Maru	1939	
Ipanema	1613	
Iris	2113	
Iwaki	1613	
Iwashiro	1613	
Kaedi	2020	
Kaga	3618	
Kamakura	3611	
Katsuragi	3609	
Kitano	3618	
NYK Andromeda	6141	
NYK Antares	6141	
NYK Aphrodite	6200	
NYK Apollo	6200	
NYK Aquarius	6238	
NYK Argus	6238	
NYK Artemis	6200	
NYK Athena	6200	
NYK Canopus	6135	
NYK Castor	6135	
NYK Fantasia	2532	
NYK Freesia	3468	
NYK Kai	3618	
NYK Leo	6200	
NYK Libra	6200	
NYK Lodestar	6200	
NYK Lynx	6200	
NYK Lyra	6200	
NYK Pegasus	6200	
NYK Phoenix	6238	
NYK Pride	2641	

Peking Senator	4545	23.7
Penang Senator	4545	23.7
Pira Bhum	628	15.5
Pohang Senator	4545	23.7
Ponl Nelson	1600	
Portland Senator	4545	23.7
Portugal Senator	4545	23.7
Potomac Bridge	3965	23.1
Precious River	969	15.0
Pretty Lake	420	
Pretty Ripple	420	14.0
Pretty River	1932	18.5
Pretty Sea	316	15.9
Pretty Wave	316	14.0
Progress 3	126	7.0
Pudong Senator	4545	23.7
Pugwash Senator	4545	23.7
Pu He	2716	18.0
Punjab Senator	4545	23.7
Pusan Senator	4545	23.7
Qian Jin 303	16	
Qian Jin 310	36	
Qian Yuan Shan	137	
Quin Yun He	1702	20.3
Qing Yun No.2	30	9.0
Qui He	1318	15.5
Qi Yun He	1432	19.1
Rainbow Bridge		21.5
Ratha Bhum	628	15.5
Ratstor	516	16.0
Reestborg	558	17.5
Resourceful	100	16.0
Rhein Bridge		23.0
Rialto Bridge	3681	23.0
Ri Feng	65	
River Aquamarine	542	18.0
River Crystal	2157	18.0
River Elegance	3802	25.2
River Wisdom	3802	22.5
Rong Feng	524	14.5
Rotterdam Bridge	5576	25.0
Rui Yun He	1702	21.0
Saipan Winner	428	14.5
San Pedro Bridge	3482	21.5
Santa Elena		21.5
Santa Giovanna	1664	17.5
Santiago	2000	19.0
Savannah	2868	21.0
Sea Breeze	261	12.5
Seabright	517	15.0
Sea Dragon	424	15.1
Seto Bridge	2310	23.0
NYK Procyon	4895	
NYK Sirius	6135	
NYK Springtide	2893	
NYK Starlight	2918	
Provider	1782	
Sagar	1005	
Sakura	4931	
Sandra Azul	4895	
Sandra Blanca	4895	
Santa Barbara	2893	
Santa Cruz	2918	
Santa Monica	2905	
Sanuki	1157	
Satsuki	1181	
Settsu	1152	
Shima	1152	
Shion	1122	
Soga	1091	
Sophia Britannia	3618	
Sumida	1100	
Sumire	1181	
Victory 1	3066	
America Feeder	584	17.5
Angelica Schulte	366	15.3
ANL Australia	2668	19.0
ANL Bass Trader	642	16.0
ANL Emblem	3300	22.5
ANL Explorer	2266	21.0
ANL Pacific	4250	23.3
ANL Progress	910	19.0
Anne Catharina	298	12.5
APL Cyprine	5016	22.5
Aron	333	13.5
Asturia	2202	20.0
Athlete F	369	15.0
Baltic Tern	357	13.5
Banjaard	550	14.5
Barrier	912	17.0
Burak Bayraktar	860	16.0
Cap Canaille	133	16.0
Cap Melville	2532	21.5
Carola	1107	18.5
Cervantes	538	15.5
Cimil	426	13.5
City of Lisbon	700	16.5
City of Oporto	700	16.5
CMA CGM Aegean	2811	22.0
CMA CGM Alabama	2758	21.5
CMA CGM Alger	678	17.0
CMA CGM Amazonia	405	15.0
CMA CGM Arno	1668	19.5
CMA CGM Balzac	6447	25.9

Sha He	1234	18.3
Shamrock	350	16.0
Shang Cheng	724	15.5
Shanghai Bridge	5576	25.0
Shanghai Senator	2661	18.0
San He	3801	22.0
Sheng He	725	18.0
Shi Gang 233	45	
Shi Gang 388	75	11.0
Shimanami	450	15.0
Shi Tai 3 Hao	90	
Shuang Feng Shan	140	
Sinar Bali	1060	18.0
Sinar Bangka	1054	18.0
Sinar Batam	1556	18.5
Sinar Bintan	1054	18.0
Sinar Bontang	1054	18.0
Sinar Java	1146	17.0
Sinar Lombok	816	18.0
Sinar Salju	197	16.0
Sinar Solo	1060	18.0
Sinar Sunda	1556	18.5
Sinar Surya	1556	18.5
Sing Ping	96	
Siri Bhum	550	14.5
Sky Light	746	16.5
Sky River	1960	23.0
Sky Success	617	14.0
Song Cheng	724	15.5
Song He	1688	15.5
Song Yun He	1432	19.0
Star River	494	19.2
Steamers Prudence	779	17.5
St Petersburg Mariner	3005	20.0
Su Da	288	14.0
Suez Canal Bridge	5608	25.0
Sui Da 3	36	
Sui Jian Hang JI 129	45	9.0
Sui Jian Hang JI 131	45	9.0
Sui Jian Hang 133	45	7.5
Sui Shun 101	100	
Sui Shun Hang 28	45	
Sui Shun Hang 32	45	
Sui Sun 77	48	
Sui Wu 501	24	
Sui Xing 3	36	9.0
Sui Yue 2 Hao	39	
Sun Hop Lee	124	
Synthesis No.28	96	
Tai Hang 302	42	10.0
Tai Heng 8	51	9.5
Takeko	564	20.7
CMA CGM Baudelaire	6447	25.9
CMA CGM Belem	1162	17.0
CMA CGM Bellini	5700	24.5
CMA CGM Berlioz	6627	25.9
CMA CGM Bizet	6627	25.9
CMA CGM Capella	3538	22.5
CMA CGM Caribbean	516	15.5
CMA CGM Chardin	3300	22.5
CMA CGM Chopin	5700	24.5
CMA CGM Claudel	2602	21.5
CMA CGM Colombie	2113	20.0
CMA CGM Condor	1354	19.5
CMA CGM Constellation	3359	22.5
CMA CGM Debussy	6627	25.9
CMA CGM Eygpt	2811	22.0
CMA CGM Elbe	2917	22.0
CMA CGM Emerald	2458	21.0
CMA CGM Energy	2438	20.5
CMA CGM Falcon	2432	21.0
CMA CGM Force	2438	20.5
CMA CGM Fort St Georges	2260	21.5
CMA CGM Fort St Louis	2260	21.5
CMA CGM Fort St Pierre	2260	21.5
CMA CGM St Marie	2260	21.5
CMA CGM Greece	2824	24.0
CMA CGM Hispaniola	1367	17.8
CMA CGM Hudson	1668	19.5
CMA CGM Hugo	8200	24.5
CMA CGM Impala	1726	19.6
CMA CGM Kalamata	2917	22.0
CMA CGM Kingston	4250	23.3
CMA CGM Kiwi	1730	20.0
CMA CGM Komodo	2917	22.0
CMA CGM La Bourdonnais	1684	18.0
CMA CGM Latour	2272	21.5
CMA CGM Lea	541	15.0
CMA CGM Licorne	1728	20.0
CMA CGM Maghreb	580	17.0
CMA CGM Makassar	2917	22.0
CMA CGM Manet	2272	21.5
CMA CGM Marmara	2811	22.0
CMA CGM Matisse	2262	20.5
CMA CGM Mozart	5700	24.5
CMA CGM Normandie	4688	24.0
CMA CGM Okapi	1708	19.8
CMA CGM Oran	352	13.0
CMA CGM Papagayo	1354	19.5
CMA CGM Pasteur	2023	19.0
CMA CGM Potomac	1645	19.5
CMA CGM Puccini	5700	24.5
CMA CGM Puget	4404	24.0
CMA CGM Puma	1716	21.8

Teng He	3764	22.0
Teng Yun He	1702	20.2
TMM Campeche	3032	20.5
TMM Yucatan	3200	21.6
Tong Jie	80	
Tong Wei	75	
Tower Bridge	2140	20.6
Trade Eternity	2480	19.0
Trade Freda	4038	24.0
Trade Hallie	4038	24.0
Trade Harvest	2227	20.0
Trade Selene	2480	19.0
Trade Tesia	4038	24.0
Trade Worlder	442	
Trisk	204	
Tsing Ma Bridge	5610	25.0
Twadika	267	12.5
Umeko	564	20.7
UNI Active		18.7
UNI Adroit		18.7
UNI Ample	1164	18.7
UNI Angel	1164	18.7
UNI Arise	1164	18.7
UNI Aspire	1164	18.7
UNI Assure	1164	18.7
UNI Chart	998	17.0
UNI Concert	998	17.0
UNI Concord	998	17.0
UNI Corona	998	17.0
UNI Crown	998	17.0
UNI Forward	956	16.5
UNI Pacific	1618	18.7
UNI Patriot	1618	18.7
UNI Perfect	1618	18.0
UNI Popular	1618	18.0
UNI Premier	1618	18.0
UNI Probity	1618	18.0
UNI Promote	1618	18.0
UNI Prosper	1618	18.0
UNI Prudent	1618	18.7
UNI Ahead		18.7
UNI Phoenix		18.7
Van Xuan	594	15.0
Vega Diamond	784	19.6
Venus Bridge	5551	25.9
Victoria Bridge	3482	23.0
Victoria Strait	1118	19.2
VN Sapphire	1020	17.0
Wadi Alrayan	2500	21.6
Wang Foong 18	228	
Wang Foong 9	130	
WanHai 215	500	
CMA CGM Rabat	976	17.5
CMA CGM Ravel	6712	25.8
CMA CGM Rio Para	511	15.3
CMA CGM Romania	2478	21.7
CMA CGM Rossini	5700	24.5
CMA CGM Santiago	370	15.3
CMA CGM Sapphire	2986	21.5
CMA CGM Seagull	2732	22.5
CMA CGM Seine	2917	22.0
CMA CGM Skikda	516	16.0
CMA CGM Springbok	1608	21.0
CMA CGM St Laurent	1162	17.0
CMA CGM St Martin	1162	17.0
CMA CGM Strauss	5700	24.5
CMA CGM Tage	1645	19.5
CMA CGM Tatiana	822	18.5
CMA CGM Tucano	2008	21.5
CMA CGM Turkey	2811	22.0
CMA CGM Ukraine	2824	24.0
CMA CGM Utrillo	2262	20.5
CMA CGM Verdi	5700	24.5
CMA CGM Verlaine	6456	25.8
CMA CGM Virginia	2811	22.0
CMA CGM Vivaldi	8200	24.5
CMA CGM Voltaire	6456	25.8
CMA CGM Wagner	5700	24.5
CMA CGM Wallaby	1684	20.0
CMA CGM Yantian	4250	23.3
Corona	372	15.5
Denizhan Bayraktar	470	15.0
Doerte	448	15.5
Dollart Trader	1608	21.0
Dutch Runner	221	12.5
Enforcer	750	18.0
Engiadina	2824	24.0
Er Caen	2556	21.5
Er Calais	2556	21.5
Er Camargue	2556	21.5
Er Cannes	2556	21.5
Er Sydney	3359	22.5
Euro Storm	686	17.6
Fas Damman	847	17.5
Fas Gulf	1102	20.0
Fas Provence	581	15.5
Fas Var	601	14.3
Gascogne	558	17.5
Holger	508	15.0
Iduna	325	14.5
Indamex Delaware	2890	21.8
Indamex Godavari	3607	23.5
Ingo J	202	11.5
Jan D	440	14.0

WanHai 262	1240	21.0
Wan Hai 266	2496	22.0
Wan Hai 301	2496	22.0
Wan Hai 302	2496	22.0
Wan Hai 303	2496	22.0
Wan Hai 305	2496	22.0
Wan Hai 307	2496	22.0
Wan He	5446	22.5
Washington Senator	2850	
Wehr Bille	2546	19.8
Wehr Havel	2526	22.0
Wei Xing	65	10.0
Welcome	437	14.0
Well Grace	132	
Well Union	124	
Westerhever	1572	20.0
Wide Tech 23	72	
Wide Tech 33	100	
Wing Hing NO.18	120	
Wing Lee No.1	120	
Wing On 838	120	
World D	934	
Xetha Bhum	1080	17.0
XHSJ 0288	64	
Xiang Da	200	12.0
Xiang Dan	200	12.0
Xiang He	1686	14.5
Xiang Kun	582	15.0
Xiang Lain	200	12.0
Xiang Peng	576	15.0
Xiang Qian	582	15.0
Xiang Tan Huo 0029	392	
Xiang Xing	316	14.0
Xiang Yun He	1702	20.3
Xi Bo He	3400	21.0
Xie Hang 1	36	
Xie Hang 12	36	
Xie Hang 198	120	
Xie Hang 2	60	
Xie Hang 28	45	10.0
Xie Hang 313	96	
Xie Hang 88	80	
Xie Hang 9	96	
Xing He	1328	17.6
Xin Hai Run	612	15.5
Xin Hui He	836	16.5
Xin Hui JI 12	10	8.0
Xin Hui JI 13	36	9.0
Xin Hui JI 15	48	9.0
Xin Hui JI 16	48	9.0
Xin Hui JI 19	16	9.0
Xin Hui JI 20	12	8.0
Janina	678	17.0
Kappel N	657	17.5
Karina	847	17.5
Madeleine Rickmers	1728	19.6
Margaretha	868	18.5
Maria Schulte	366	15.3
Neva	263	12.5
Nicola	847	17.5
Nordmed	2478	21.7
Northern Dignity	3607	23.8
Orient Aishwarya	1020	17.0
Pacheco	300	13.5
Priwall	2480	20.0
Promoter N	756	13.5
Rahana	1122	18.5
Renate Schulte	1354	19.5
Rigena	1810	17.0
Rybno	261	12.5
Sadan Bayraktar	596	15.0
Saipan Carrier	602	14.0
Saipan Harvester	576	14.0
Saipan Voyager	701	14.0
Sea Explorer	384	15.0
Sieltor	516	15.5
Stella J	520	16.0
Sunshine II	347	13.5
Sylvette	844	17.5
VD Mina Qaboos	132	12.0
Ville D'Antares	4030	23.7
Ville D'Aquarius	3961	23.7
Ville De Dubai	847	17.5
Ville De Mars	2954	21.5
Ville De Mijo	601	14.3
Ville De Mimosa	3961	23.7
Ville De Tanya	4031	23.8
Ville De Taurus	3961	23.7
Ville De Virgo	4030	23.7
Ville D'Orion	3961	23.7
Westerland	2764	22.0
Wotan	297	12.5
Xiang Ling	210	12.5
Andalusia	2262	21.5
Safmarine Cotonou	1737	19.5
Alicantia	2262	21.5
Safmarine Maluti	2063	21.5
Safmarine Cameroun	2096	21.0
Safmarine Concord	1799	17.5
Safmarine Asia	1972	17.5
Safmarine Europe	1972	17.5
Safmarine Lobito	428	14.5
Safmarine Soyo	428	15.0
Elise D	428	14.5

Xin Hui Jl 22	12	8.0	Safemarine Gabon	428	14.5
Xin Hui Jl 23	36		Theofano	640	13.0
Xin Hui Jl 3	16	8.0	Safmarine Bioko	925	15.0
Xin Hui Jl 5	16	8.0	Safmarine Onne	519	15.5
Xin Hui Jl 9	36	8.0	Safmarine Houston	525	15.5
Xin Tong 16	24		Safmarine Douala	925	14.0
Xiu Shan	66		Safmarine Evagelia	414	14.0
Yang Jiang He		16.5	Safmarine Meroula	414	14.0
Yang Xian 8	54		Safmarine Congo	414	14.0
Yan He	725	16.8	Elizabeth	448	15.5
Yantra Bhum	1080	17.0	Portlink Caravel	390	15.0
Yellow Sea	3681		Portlink Pacer	523	15.5
Yin He	1328	16.5	Sven Oltmann	510	16.5
YM Athens	5618	26.3	SA Winterberg	3101	20.5
YM Bremens	5576		Maersk Constantia	3101	20.5
YM Earth	1620	19.7	SA Sederberg	3101	20.5
YM Fountain	5551	25.9	SA Helderberg	3101	20.5
YM Genova II	1400		Safmarine Letaba	2080	21.0
YM Great	5576	25.0	Safmarine Mgeni	1730	20.0
YM March	5576	25.0	Safmarine Kei	2474	22.2
YM Milano	2800	22.0	Pongola	797	18.0
YM Napoli	3359	22.4	Safmarine Zambezi	2496	21.7
YM New york	4038	22.2	Safmarine Tugela	2063	21.5
YM Pearl River I	1464	18.0	Maersk Dakar	2106	21.0
YM People	1620	19.7	Safmarine Igoli	3152	22.0
YM Savannah	4038	22.2	Safmarine Ibhayi	2732	22.5
YM Sky	1620	19.7	Safmarine Ikapa	2732	22.5
YM Success	5551	25.9	LT Grace	2728	20.5
YM Tacoma	3456	24.0	LT Greet	2728	20.5
YM Wealth	5551	25.9	LT Garland	3428	20.7
YM Wilmington	4038	22.2	LT Glamor	3428	20.7
YM Yantian	3916	22.5	LT Usodimare	5652	25.0
Yokohama Senator	4545	23.7	LT Unica	5652	25.0
Yong Ding He	764	17.0	LT Universo	5652	25.0
Yong Feng	140		MV R.J. Pfeiffer	2229	23.0
Yong Hang 9	45		MV Mahimahi	2824	23.0
Yongyue No.6	631	12.0	MV Mokihana	2824	23.0
Young Liberty	1295	17.0	MV Manoa	2824	23.0
Yuan He	3764	24.0	MV Manukai	2600	22.5
Yu Chang 2	118		S.S. Maui	2600	22.5
Yue An Yun 05	72		S.S. Chief Gadao	1981	21.0
Yue Feng 902	60		S.S. Lurline	1379	21.5
Yue Feng 903	60		S.S. Kauai	1626	22.5
Yue Hai 1028	96		S.S. Lihue	1979	21.0
Yue He	5446	24.7	S.S. Ewa	2015	21.0
Yu Feng	65		S.S. Matsonia	1712	21.5
Yu Gu He	3400	20.0	Independent Trader	1208	17.5
Yu He	1686	14.5	Independent Venture	1468	18.5
Yun Bao	98		Independent Endeavor	1452	19.0
Yun He	5446	24.5	Independent Action	1388	17.5

Appendix B

```
%Random Deployment Simulation

function cov = cov_3d(X,Y,Z,r,num_det,N)     % X: Height of container array (in TEUs)
                                             % Y: Width of container array (in TEUs)
                                             % Z: Length of container array (in TEUs)
                                             % r: Effective detection range (in feet)
                                             % num_det: Number of detectors to be deployed
                                             % N: Number of runs

tic

x = 8 * X;  % Conversion from TEUs to feet
y = 8 * Y;  % Conversion from TEUs to feet
z = 20 * Z; % Conversion from TEUs to feet

for l = 1:N % Number of runs loop

    D0 = logical(zeros(x,y,z));      % Constructs initial geometry matrix
    count = 1;
    pos = rand(1,3);                 % Generates random number vector

    while count < (num_det + 1)      % Number of detectors loop

        D1 = logical(zeros(x,y,z)); % Constructs a new detector matrix
        pos = rand(1,3);
        dx = ceil(pos(1)*x);         % Fixes the x-coordinate of the detector
        dy = ceil(pos(2)*y);         % Fixes the y-coordinate of the detector
        dz = ceil(pos(3)*z);         % Fixes the z-coordinate of the detector
        D1(dx,dy,dz) = 1;            % Establishes the detector's center-point
                                     % in the detector matrix

            for i = dx-r:dx+r            % x-axis loop
                if ((i < 1) | (i > x))   % Ensures detector & geometry matrices
                                         % remain equi-dimensional
                    continue
                end

                for j = dy-r:dy+r            % y-axis loop
                    if ((j < 1) | (j > y))   % Dimension control
                        continue
                    end

                    for k = dz-r:dz+r            % z-axis loop
                        if ((k < 1) | (k > z))   % Dimension control
                            continue
                        end

                        if sqrt((i-dx)^2+(j-dy)^2+(k-dz)^2) <= r     % Checks whether
                                                                     % element is within
                                                                     % the detection
                                                                     % sphere
```

```
                        D1(i,j,k) = 1;  % Fills in the detector matrix
                    end
                end
            end
        end

        D0 = D0 | D1;    % Current geometry matrix and detector matrix are 'OR'ed together
        count = count + 1;

    end

    det_cov = sum(sum(sum(D0)));     % Sums the number of elements within detection spheres
    cov(1) = det_cov/(x*y*z);        % Calculates fractional coverage volume and writes it
                                     % to an output vector
end

cov = cov'                           %
mean_cov = mean(cov)                 %
median_cov = median(cov)             % Statistical analysis of full output vector
std_cov = std(cov)                   %
min_cov = min(cov)                   %
max_cov = max(cov)                   %

toc
```

```
% Constrained Deployment Simulator

function cov = new_3d(X,Y,Z,r,num_det,N)     % X: Height of container array (in TEUs)
                                             % Y: Width of container array (in TEUs)
                                             % Z: Length of container array (in TEUs)
                                             % r: Effective detection range (in feet)
                                             % num_det: Number of detectors to be deployed
                                             % N: Number of runs

tic

x = 8 * X;  % Conversion from TEUs to feet
y = 8 * Y;  % Conversion from TEUs to feet
z = 20 * Z; % Conversion from TEUs to feet

for l = 1:N

    D0 = logical(zeros(x,y,z));      % Constructs initial geometry matrix
    count = 1;
    pos = rand(1,20);                % Generates random number vector

    while count < (num_det + 1)      % Number of detectors loop

        D1 = logical(zeros(x,y,z)); % Constructs a new detector matrix

        pos = rand(1,20);
        rnd_cnt = 1;
        x_switch = 0;                %
        y_switch = 0;                % Initializes constraint test variables
        z_switch = 0;                %

        while x_switch < 1                              %
            dx_test = ceil(pos(rnd_cnt)*x);             %
            if ((dx_test > 8) & (dx_test < (x-7)))      %  Checks if x-coordinate
                dx = dx_test;                           %  satisfies constraints
                rnd_cnt = rnd_cnt +1;                   %
                x_switch = 1;                           %
            else
                rnd_cnt = rnd_cnt + 1;
            end
        end

        while y_switch < 1                              %
            dy_test = ceil(pos(rnd_cnt)*y);             %
            if ((dy_test > 8) & (dy_test < (y-7)))      %  Checks if y-coordinate
                dy = dy_test;                           %  satisfies constraints
                rnd_cnt = rnd_cnt + 1;                  %
                y_switch = 1;                           %
            else
                rnd_cnt = rnd_cnt + 1;
```

```
        end
    end

    while z_switch < 1                                  %
        dz_test = ceil(pos(rnd_cnt)*z);                 %
        if ((dz_test > 20) & (dz_test < (z-19)))        %  Checks if z-coordinate
            dz = dz_test;                               %  satisfies constraints
            rnd_cnt = rnd_cnt + 1;                      %
            z_switch = 1;                               %
        else
            rnd_cnt = rnd_cnt + 1;
        end
    end

D1(dx,dy,dz) = 1;                               % Establishs detector center-point
                                                % in the detector matrix

        for i = dx-r:dx+r                       % x-axis loop
            if ((i < 1) | (i > x))              % Dimension control
                continue
            end

            for j = dy-r:dy+r                   % y-axis loop
                if ((j < 1) | (j > y))          % Dimension control
                    continue
                end

                for k = dz-r:dz+r               % z-axis loop
                    if ((k < 1) | (k > z))      % Dimension control
                        continue
                    end

                    if sqrt((i-dx)^2+(j-dy)^2+(k-dz)^2) <= r    % Checks whether
                                                                % element is within
                                                                % the detection
                                                                % sphere

                        D1(i,j,k) = 1;              % Fills in the detector matrix
                    end

                end
            end
        end

    D0 = D0 | D1;    % Current geometry matrix and detector matrix are 'OR'ed together
    count = count + 1;
    rnd_cnt = 1;
```

```
    end

    det_cov = sum(sum(sum(D0)));     % Sums the number of elements within detection spheres
    cov(l) = det_cov/(x*y*z);        % Calculates fractional coverage volume and writes it
                                     % to an output vector
end

File = strcat(num2str(X),'_',num2str(Y),'_',num2str(Z),'_',num2str(r),'_',num2str(num_det ↙
),'_',num2str(N))

mean_cov = mean(cov)                 %
median_cov = median(cov)             %
std_cov = std(cov)                   % Statistical analysis of full output vector
min_cov = min(cov)                   %
max_cov = max(cov)                   %

toc
```

```
% Centerline Deployment Simulator

function cov = centerline(X,Y,Z,r,det_start,det_step,det_stop)

tic

x = 8 * X;  % Conversion from TEUs to feet
y = 8 * Y;  % Conversion from TEUs to feet
z = 20 * Z; % Conversion from TEUs to feet

    D0 = logical(zeros(x,y,z));     % Constructs initial geometry matrix

    for det = det_start : det_step : det_stop   % Detector placement loop

        D1 = logical (zeros(x,y,z));            % Constructs a new detector matrix
        dx = ?;                                 % 1440 TEU -> dx = 28
                                                % 2496 TEU -> dx = 36
                                                % 3600 TEU -> dx = 36
                                                % 4800 TEU -> dx = 36
                                                % 6460 TEU -> dx = 36
        dy = ?;                                 % 1440 TEU -> dy = 36
                                                % 2496 TEU -> dy = 44
                                                % 3600 TEU -> dy = 44
                                                % 4800 TEU -> dy = 60
                                                % 6460 TEU -> dy = 68

        dz = det                                % Places detectors along the length

        D1(dx,dy,dz) = 1;                       % Fixes center-point of detector in
                                                % the detector matrix

            for i = dx-r:dx+r                   % x-axis loop
                if ((i < 1) | (i > x))          % Dimension control
                    continue
                end

                for  j = dy-r:dy+r              % y-axis loop
                    if ((j < 1) | (j > y))      % Dimension control
                        continue
                    end

                    for k = dz-r:dz+r           % z-axis
                        if ((k < 1) | (k > z))  % Dimension control
                            continue
                        end

                        if sqrt((i-dx)^2+(j-dy)^2+(k-dz)^2) <= r    % Checks whether
                                                                    % element is within
                                                                    % the detection
                                                                    % sphere
```

```
                        D1(i,j,k) = 1;  % Fills in the detector matrix
                    end
                end
            end
        end

    D0 = D0 | D1;    % Current geometry matrix and detector matrix are 'OR'ed together

end

det_cov = sum(sum(sum(D0)));     % Sums the number of elements within detection spheres
cov = det_cov/(x*y*z);           % Calculates fractional coverage volume

cov                              % Outputs fractional coverage volume

toc
```